12-2013

Characterization of the Functional Role and Therapeutic Potential of microRNA miR-125a in Acute Myeloid Leukemia

Melanie Lorraine Ufkin

CHARACTERIZATION OF THE FUNCTIONAL ROLE AND THERAPEUTIC POTENTIAL OF MICRORNA MIR-125A IN ACUTE MYELOID LEUKEMIA

By

Melanie Lorraine Ufkin

B.A. Lawrence University, 2006

A DISSERTATION

Submitted in partial fulfillment of the

Requirements for the Degree of

Doctor of Philosophy

(in Biomedical Sciences)

The Graduate School

University of Maine

December 2013

Advisory Committee:

Pradeep Sathyanarayana, Scientist I, Maine Medical Center Research Institute, Advisor

Robert Friesel, Senior Scientist, Director, Center for Molecular Medicine, Maine Medical Center Research Institute

Lucy Liaw, Senior Scientist, Maine Medical Center Research Institute

Jeong Yoon, Scientist II Maine Medical Center Research Institute

Carol J. Bult, Professor, The Jackson Laboratory

DISSERTATION ACCEPTANCE STATEMENT

On behalf of the Graduate Committee of Melanie Lorraine Ufkin I affirm that this manuscript is the final and accepted dissertation. Signatures of all committee members are on file with the Graduate School at the University of Maine, 42 Stodder Hall, Orono, Maine.

S. Pradeep 12/14/2013

Dr. Pradeep Sathyanarayana Date

LIBRARY RIGHTS STATEMENT

In presenting this dissertation in partial fulfillment of the requirements for an advanced degree at the University of Maine, I agree that the Library shall make it freely available for inspection. I further agree that permission for "fair use" copying of this dissertation for scholarly purpose may be granted by the Librarian. It is understood that any copying or publication of this dissertation for financial gain shall not be allowed without my written permission.

Signature: 

Date: 12-14-13

Characterization of the Functional Role and Therapeutic Potential of microRNA miR-125a in Acute Myeloid Leukemia

By Melanie Lorraine Ufkin

Dissertation Advisor: Dr. Pradeep Sathyanarayana

An Abstract of the Dissertation Presented
in Partial Fulfillment of the Requirements for the
Degree of Doctor of Philosophy
(in Biomedical Sciences)
December 2013

Acute myeloid leukemia (AML) is a heterogeneous disease marked by a highly variable clinical course and response to therapy. The average age of individuals diagnosed with AML is approximately 69 years old. Due to age of the patient and how quickly the disease progresses, many are unable to receive therapy, leading to death between 4 and 12 weeks after diagnosis. More effective and less cytotoxic treatments are crucial for those diagnosed with AML. Therefore my work has been focused on understanding genetic pathways altered within AML to develop new-targeted therapies. Specifically, I have been studying microRNAs (miR), which regulate proteins by degrading the protein messages prior to them becoming functional. MicroRNA-125a (miR-125a) previously was identified as being decreased in cytogenetically normal AML. I have identified that miR-125a is decreased in many subtypes of AML. Correlation of miR-125a to a specific AML subtype was difficult due to the range of molecular and cytogenetic

abnormalities. By ectopically expressing miR-125a, leukemic blasts have decreased cell proliferation, cell cycle progression, and enhanced apoptosis. Through profiling analysis, I have identified Trib2 as a new target of miR-125a though its function has not been characterized. Secondly, I have discovered that the ErbB pathway, a growth promoting pathway, currently known to cause breast and gastric cancer, is enhanced in AML when miR-125a is decreased. As a result of these studies, I have identified a potential new therapeutic, Mubritinib. Currently Mubritinib is being utilized in cancer, such as breast cancer but not yet in blood disorders. From this discovery an additional cancer could be treated with current ErbB inhibitors as a new therapeutic application.

DEDICATION

To my parents, Gary and Cynthia, for their endless support and love to pursue my dreams even during challenging times and to my friends and family who have always stood by and believed in me.

ACKNOWLEDGEMENTS

I would like to thank my mentor Dr. Pradeep Sathyanarayana who accepted me into his laboratory and for his mentorship in both my research training and career as a scientist.

To Dr. Lucy Liaw who played a crucial role in my transition to the Graduate School of Biomedical Sciences and Engineering and guidance throughout my time in the program.

I would like to thank Dr. Sarah Peterson and Dr. Xuehui Yang for their help and expertise for my in vivo studies. Additionally, I would like to thank Dr. Christine Duarte and Dr. Heather Driscoll for their help in bioinformatics analysis.

Thank you to the Graduate School of Biomedical Sciences and Engineering for allowing me to transfer into the program to pursue my goal to complete my doctoral degree.

To my family and friends who supported and provided strength to me throughout this journey.

Thank you to my committee for helping me smoothly transition into the graduate program, training me how to be a critical thinker, and guiding my research throughout my degree.

TABLE OF CONTENTS

LIST OF TABLES

LIST OF FIGURES

ABBREVIATIONS

AGM: aorta-gonad-mesonephros region

ALDH1A3: aldehyde dehydrogenase 1 family, member A3

ALL: acute lymphoblastic leukemia

AML: acute myeloid leukemia

ANOVA: One-way analysis of variance

APAF1: apoptotic protease activator factor 1

APL: acute promyelocytic leukemia

AT: adenine – thymine

BAAL: brain and acute leukemia

BAD: bcl-2 associated protein

BAG: Bcl-2 associated athanogene

BCL2: B cell lymphoma 2

BIR: Baculovirus IAP Repeat

Bmi-1: B lymphoma Mo-MLV insertion region 1 homolog

BP: base pair

BrdU: bromodeoxyuridine

C/EBPα: CCAAT-enhancer-binding proteins alpha alpha

CARD: caspase activation and recruitment domain

CASP: caspase

CBC: complete blood count

CBFbeta: core-binding factor subunit beta

CD10: cluster of differentiation 10

CD11b: cluster of differentiation 11b

CD14: cluster of differentiation 14

CD14: cluster of differentiation 14

CD164: cluster of differentiation 164

CD18: cluster of differentiation 18

CD2: cluster of differentiation 2

CD229/SLAMF3: cluster of differentiation 229 / signaling lymphocyte activation molecular family 3

CD3: cluster of differentiation 3

CD34: cluster of differentiation 34

CD36/SR-B3: cluster of differentiation 36 / scavenger receptor class B, member 3

CD38: cluster of differentiation 38

CD4: cluster of differentiation 4

CD41: cluster of differentiation 41

CD42: cluster of differentiation 42

CD44: cluster of differentiation 44

CD45RA: cluster of differentiation 45 isoform RA

CD48/SLAMF2: cluster of differentiation 48 / signaling lymphocyte activation molecular family 2

CD59: cluster of differentiation 59

CD61: cluster of differentiation 61

CD66: cluster of differentiation

CD68/SR-D1: cluster of differentiation 68 / scavenger receptor class D, member 1

CD69: cluster of differentiation 69

CLL: chronic lymphoblastic leukemia

CLP: common lymphoid progenitor

CML: chronic myeloid leukemia

CMP: common myeloid progenitor

CpG: cytosine – phosphate – guanine

CRACC/SLAMF7: CD2-like receptor-activating cytotoxic cell / signaling lymphocyte activation molecular family 7

CSF: colony-stimulating factor

CXCR1: chemokine (C-X-C motif) receptor 1

DMSO: dimethyl sulfoxide

DNA: deoxyribonucleic acid

DNMT: DNA methyl transferase

DPC: days post conception

E2F: E2 factor

ELKF: erythroid Kruppel like Factor

EMR1: EGF – like module-containing mucin like hormone receptor-like 1

EPO: erythropoietin

ERBB2: v-Erb-B2 avian erythroblastic leukemia viral oncogene

ERG: ETS – related gene

ETO: eight twenty one

FAB: French-American-British

FC GAMMA RIII/CD16: Fc receptor for immune-complexed IgG RIII / cluster of differentiation 16

FDR: false discovery rate

FISH: fluorescence in situ hyrbridization

Flt-3/Flk-2: Fms-like tyrosine kinase 3 / Fetal liver kinase-2

FLT3-ITD: fms-related tyrosine kinase 3 – internal tandem duplicationRUNX

FOG: friends of GATA proteins

G-CSF: granulocyte colony stimulating factor

GAPDH: Glyceraldehyde 3-phosphate dehydrogenase

GATA-1: globin transcription factor 1

GATA-2: globin transcription factor 2

GC: guanine – cytosine

Gfi-1: growth factor independent 1 transcription repressor

GFP: green fluorescent protein

Glycophorin/CD235a: glycophorin/ cluster of differentiation 235a

GM-CSF: granulocyte-monocyte colony stimulating factor

GMP: granulocyte – monocyte progrenitor

H&E: hematoxylin and eosin

H1: histone 1

H2: histone 2

H3: histone 3

H3K27: histone 3 lysine 27

H3K36: histone 3 lysine 36

H3K4: histone 3 lysine 4

H3K79: histone 3 lysine 79

H3K9: histone 3 lysine 9

H4: histone 4

H4K20: histone 4 lysine 20

HDAC: histone deacetylase

HER2: human epidermal growth factor receptor 2

HL60, NB4: human promyelocytic leukemia cells

HOX: homeobox

HSC: hematopoietic stem cells

HSPC: hematopoietic stem and progenitor stems

IL-3Ralpha/CD127: interleukin 3 receptor alpha / cluster of differentiation 127

IL-7R alpha/CD127: interleukin – 7 receptor alpha / cluster of differentiation 127

IMDM: Iscove's Modified Dubecco's Medium

K562: human erythroleukemia cells

KEGG: Kyoto encyclopedia genes and genomes

KG: kilogram

L-Selectin/CD622: l-selectin / cluster of differentiation 622

LAMP/CD107a: lysosomal-associated membrane protein 1 / cluster of differentiation 107a

LB: lysogeny broth

Lmo-2: LIM Domain Only 2 (rhombotin-like 1)

LT-HSC: long-term hematopoietic stem cell

M-CSF: monocyte colony stimulating factor

MAPK: mitogen activated protein kinase

MCL-1: myeloid cell leukemia sequence 1

MDS: myelodysplastic syndrome

MEIS1: meis homeobox 1

MEP: megakaryocyte – erythroid progenitor

MG: milligram

miR-125a: microRNA-125a

miR: microRNA

MLL: myeloid/ lymphoid or mixed lineage

MLLT3: myeloid/lymphoid or mixed lineage leukemia (trihorax homolog)

MOI: multiplicity of infection

MPD: myeloproliferative disorders

MPO: myeloperoxidase

MPP: multi-progenitor cell

MS4A1/CD20: membrane spanning 4 – domains, subfamily A, member 1 / cluster of differentiation 20

MYH11: myosin heavy chain 11

NCAM-1/CD56: neural cell adhesion molecule – 1 / cluster of differentiation 56

NCI: National Cancer Institute

NKp46/NRC1: natural killer cell P46-related protein / NB-LRR required for HR-associated cell death 1

NPM1: nucleophosmin 1

NUP214: nucleoporin 214kDa

PC1: principal component 1

PCR: polymerase chain reaction

PEAR1: platelet endothelial aggregation receptor 1

PEBP2: polyomavirus enhancer binding protein 2

PI: Propidium iodide

PML: promyelocytic leukemia

PSF: penicillin/streptomycin/amphotericin B

RAR alpha: retinoic acid receptor alpha

RNA: ribonucleic acids

RPMI: Roswell Park Memorial Institute

RPN1: ribophorin 1

RT-qPCR: real time – quantitative polymerase chain reaction

RUNX-1 (AML-1): runt-related transcription factor 1

Sca-1: stem cell antigen-1

SCFR/c-kit: stem cell factor receptor

SCL-1 / Tal-1: stem cell leukemia 1 / T-cell acute lymphoblastic leukemia 1

Siglec-2/CD22: sialic acid-binding immunoglobulin-type lectins / cluster of differentiation 22

Singlec-3/CD33: sialic acid binding Ig-like Lectin – 3 / cluster of differentiation of 33

SLAM/CD150: signaling lymphocyte activation molecular / cluster of differentiation 150

TCGA: The Cancer Genome Atlas

Tel: translocation-Ets-leukemia

TNF/TNFR: tumor necrosis factor / tumor necrosis factor receptor

TpoR: thrombopoietin receptor

TRAF: tumor receptor associated factor

Trib2: tribbles pseudokinase 2

UTR: untranslated region

WHO: World Health Organization

WPC: weeks post conception

µg: microgram

SPECIFIC AIMS

Aim 1: Characterizing miR-125a expression and its functional role in acute myeloid leukemia

Hypothesis: miR-125a will be decreased in acute myeloid leukemia and restoration of miR-125a expression will lead to altered cellular function of leukemic blasts.

Aim 2: Characterizing miR-125a's regulation and its mechanism of action to develop novel therapeutics for low miR-125a acute myeloid leukemia

Hypothesis: Targeting miR-125a epigenetically or miR-125a's regulated signaling pathways will result in decreased growth and survival of leukemic blasts.

CHAPTER 1: INTRODUCTION

1.1. Hematopoiesis

Approximately seven to eight percent of a human total body weight is blood, providing nutrients, cells and antigens for immune response, oxygen, clot formation, removal of wastes, and regulating body temperature[1]. Once blood cells differentiate completely they will leave the bone marrow and enter the peripheral blood where each cell type can perform their function. For example once a hematopoietic stem cell (HSC) differentiates into a granulocyte, these cells will leave the bone marrow and enter the peripheral blood where they will function within the immune system. Differentiation of HSC will be discusses more in depth later. Mature red blood cells last approximately 120 days, where as white blood cells last only a few days and platelets last only several hours[2]. Therefore, mature blood cells must continually be replenished. Hematopoiesis describes the process of the maturation of blood cells (hematopoietic cells) from HSC until they become differentiated and functional blood cells[3]. HSC are characterized as having the ability to generate any blood cell when transplanted [3]. The following section will contain a brief description of hematopoiesis development followed by a more in depth discussion of hematopoiesis markers and signaling.

1.1.1. Hematopoietic development

There are several sites of hematopoiesis throughout embryonic development (Figure 1.1.) which has started to be characterized [2]. For example, Bockamp et al developed a transgenic mouse model in which stem cells were labeled and could

be followed throughout the development, providing insight on hematopoietic development [4]. The first sign of hematopoiesis is within the yolk sac three weeks post-gestation[5]. At this stage, studies have demonstrated that the cells are mainly red blood cells (erythrocytes) with a primary function to produce embryonic hemoglobin[5]. Erythrocytes are essential in providing oxygen while the embryo is developing rapidly [2]. Once vasculogenesis and artery specification are initiated in embryonic development, HSC start to develop beyond the yolk sac [2,5]. Within the embryo, the main site becomes the aorta, gonad, mesonephros region (AGM) and the fetal liver until their final place in the bone marrow [2]. There are two waves of hematopoiesis, the primitive wave and the definitive wave. In the primitive wave of hematopoiesis, erythrocytes appear to be the only cell produced. The definitive wave of hematopoiesis initiates once hematopoietic cells are located within embryonic tissues. HSC are developed in addition to myeloid and lymphoid progenitors therefore all blood cells are generated in the definitive wave [2]. Upon reaching the bone marrow, a complex network of hematopoietic cells is developed.

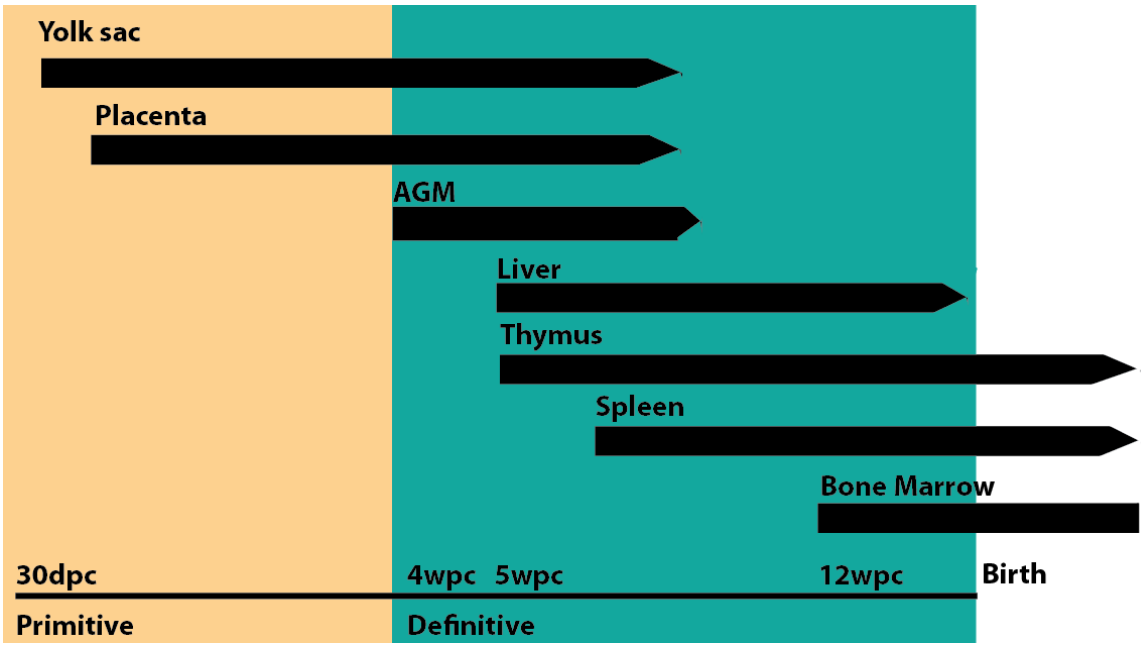

Figure 1.1 Development of the hematopoietic system in humans. This figure is based on Wang et al [6] and Orkin et al [2]. The hematopoietic system has two waves of development, primitive and definitive. This figure illustrates the different sites of hematopoiesis throughout development. AGM: aorta-gonad-mesenephros; DPC: days post conception; WPC: weeks post conception.

1.1.2. Bone marrow niche

Bone marrow is located in the center of both axial and long bones and makes up approximately five percent of the human body weight [7]. Inside the bone marrow there are several components including hematopoietic tissue, adipose cells, and vascular cells [7,6] Capillaries enter and leave the bone marrow creating a circular pattern of blood flow through the bone marrow[6,7]. Though there are many complex networks within the bone marrow niche, the focus will be on the niche that supports HSC.

Current findings demonstrate that HSC are located near the endosteal bone surface while more differentiated cells are located within the center of bone marrow [3] (Figure 1.2.). There are strong data both in vitro and in vivo that

demonstrate a strong role of osteoblasts in supporting hematopoiesis [3,6]. For example, when CD34+ HSC were grown in the presence of osteoblasts, HSC were able to differentiate in addition to having enhanced stem cell maintenance [3]. Additional studies have indicated that osteoblasts are essential in maintaining long-term HSC [3,6].

In addition to osteoblasts contributing to hematopoiesis, another major component of the bone marrow niche is the vascular cells [3,6]. The vascular niche assists in trafficking of the HSC as well as providing nutrition [3,6]. HSC can circulate between the peripheral blood and bone marrow. HSC can be homed to bone marrow from the periphery via the interaction of CXCL-12, found on the cell surface of HSC, and its ligand SDF-1 which is found in the bone marrow [3]. Lastly, adipocytes additionally are contributing to the bone marrow niche by negatively regulating HSC [3,6].

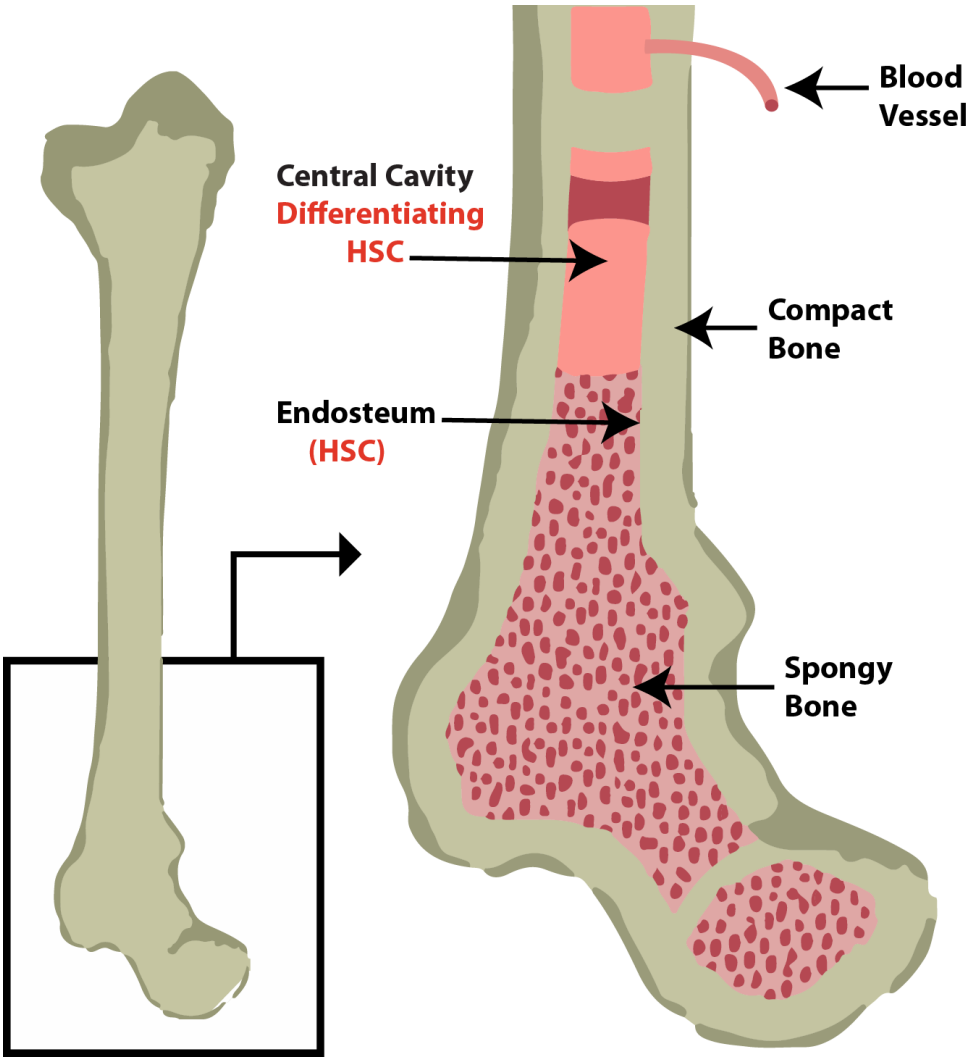

Figure 1.2. The bone marrow niche. Hematopoiesis occurs with the bone marrow prior to entering the peripheral blood stream. HSC are located in the inner bone surface called the endosteum while differentiated blood cells are located within the central cavity. Once developed, mature hematopoietic cells can enter the peripheral blood through blood vessels throughout the bone marrow.

1.1.3. Differentiation of hematopoietic stem cells

The hematopoietic cells must be able to have multi-potency and the ability to self-replicate [8]. Stem cells have the ability to potentially become any type of cell [9]. With the ability to self-replicate, HSC are able to produce daughter cells that are non-differentiated [8] and can be quiescent or self-renewing [10]. By staying in a quiescent state, the stem cells do not become exhausted but can become reactivated when necessary such as with hematopoietic stress [10]. Multi-potent progenitor cells (MPP) can produce multiple cell types but no longer can self-replicate [8]. During hematopoiesis, HSC can differentiate into common myeloid progenitors (CMP) or common lymphoid progenitors (CLP) [8] (Figure 1.3.).

The lymphoid lineage starts with a CLP cell, which is capable of becoming a T-cell, B-cell, or NK cell, which play a role in innate and adaptive immune response. Myeloid lineages initiate from a CMP and can become megakaryocyte-erythroid progenitors (MEP) or granulocyte- macrophage progenitor (GMP). MEP can then receive signals to differentiate into either erythrocytes or megakaryocytes. GMPs have the potential to differentiate into granulocytes (neutrophils, basophils, and eosinophils) or macrophages (Figure 1.3.). Differentiating hematopoietic cells can be identified through cell surface markers and their morphological appearance (Table 1.1.). There are several markers that can identify each cell type and multiple cell surface markers are the best way to identify a specific cellular type. Although this is not an exhaustive list of all the markers for each cell type, it does provide a general view of how each cell has specific markers to differentiate them from one another.

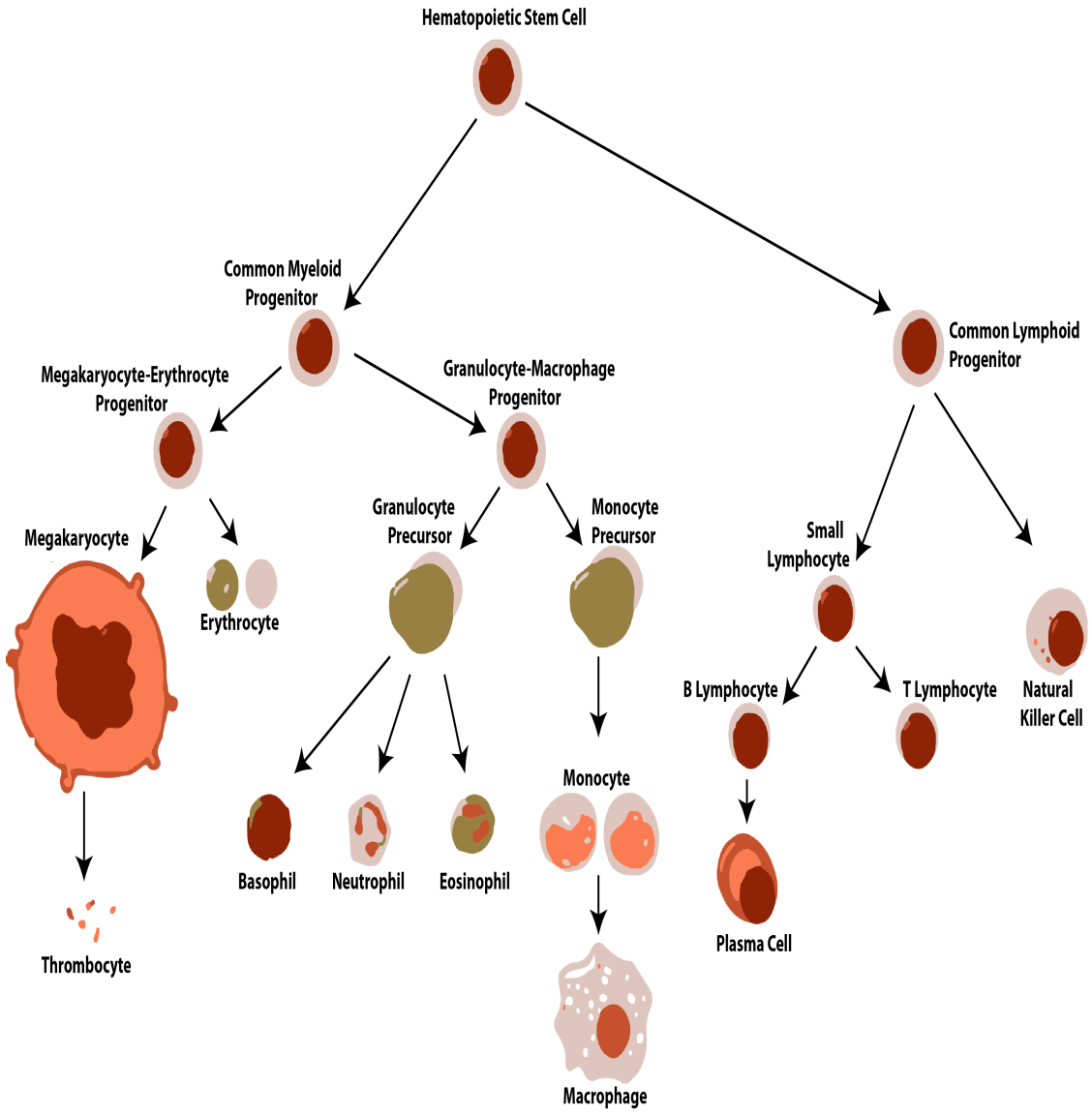

Figure 1.3. An schematic of hematopoietic stem cell differentiation. This figure is based on Dario-becker [11]. This schematic demonstrates HSC differentiation into myeloid and lymphoid lineages.

Cell Type	Marker
Hematopoietic Stem Cell	CD34+, CD38-, Flt-3/Flk-2, Sca-1+, SLAM/CD150, CD48/SLAMF2
Common Myeloid Progenitor	IL-3Ralpha/CD127, CD34, SCFR/c-kit, Flt-3/Flk-2
Granulocyte-macrophage Progenitor Cells	CD34, IL-3 alpha/CD127, CD45RA, CD38
Monocytes	CX3CR1, CD11b, CD14, Singlec-3/CD33
Macrophages	CD14, CD36/SR-B3, CD68/SR-D1, CD163
Granulocytes	CCR3, CD11b, CD13, CD16, CD18
Neutrophils	MPO, CD66, L-Selectin/CD622
Eosinophils	CD44, CD69, EMR1
Basophils	LAMP/CD107a, CD164
Megakaryocyte	CD41, CD42, TpoR
Erythrocytes	Glycophorin/CD235a, CD59
Platelets	CD41, CD61, PEAR1
Common Lymphoid Progenitor	IL-7R alpha/CD127, CD10, Flt-3/Flk-2, CD34
Lymphocytes	CD229/SLAMF3, CRACC/SLAMF7
T cells	CD2, CD3, CD4
B Cells	CD5, CD19, Siglec-2/CD22, MS4A1/CD20
Natural Killer Cells	NCAM-1/CD56, FC gamma RIII/CD16, NKp46/NRC1

Table 1.1. Common cell surface markers of hematopoietic and the myeloid cell lineages. This table is based on information from R&D systems [12]. To specifically identify each specific cell type, combinations of markers can be used.

1.1.4. Signaling in hematopoiesis

Within the bone marrow niche, there are many essential factors that maintain each cell type and induce in differentiation. The main factors controlling and guiding hematopoietic differentiation are transcription factors and cytokines. Transcription factors bind to specific sequences within DNA, controlling transcription either negatively or positively [13]. Cytokines are secreted proteins that induce differentiation or proliferation of blood and the immune system through cell surface receptors [14]. The signaling discussed here will be in reference to myeloid signaling and differentiation, although there are also a different set of factors essential for lymphoid differentiation.

Though this section does not encompass all signaling factors involved in myeloid differentiation, the factors highlighted are commonly disrupted in hematopoietic malignancies resulting in Acute Myeloid Leukemia. There are signals to maintain stem cells until they receive separate signals allowing them to differentiate. For long term HSC (LT-HSC) maintenance, there are a group of factors necessary: Runx-1, SCL/tal-1, Lmo-2, MLL, Tel, Bmi-1, Gfi-1, and GATA-2 [2] (Figure 1.4.). A different combination of factors would guide LT-HSC towards short-term HSC (ST-HSC) and then a second set of factors towards CMP or CLP. CMP, which express both GATA-1 and PU.1 [2,15] (Figure 1.4.) can differentiate into megakaryocyte-erythroid progenitors (MEP) or granulocyte-macrophage progenitor (GMP) depending on which transcription factor is increased. PU.1 drives CMP towards GMP while GATA-1 drives CMP towards the MEP pathway [2,15,16] (Figure 1.4.). C/EBPα additionally aids in production of

GMP from CMP and is also expressed on myeloid cells and granulocytes but not on macrophages [15]. The following section will be a more in depth look at several important regulators of myeloid differentiation.

1.1.4.1. RUNX-1/AML1

RUNX-1/AML1 is a protein part of the core-binding factor (CBF) family of transcription factors that forms a heterodimer with CBF beta [17]. Once in the heterodimer, RUNX-1interacts with the PEBP2 domain in target genes to regulate transcription via its DNA binding domain (Runt) [17-19]. RUNX-1 is important regulator of hematopoiesis through its regulation of many genes such as myeloperoxidase, macrophage CSF receptor, interleukin 3, and neutrophil elastase[20]. RUNX1 interacts with co-factors, such as p300 and CREB binding protein, which promote acetylation of histones of its target genes resulting in increased transcription [20]. Through knockout studies, it has been established that RUNX-1 plays an important role in definitive hematopoiesis and is essential for HSC [20]. When RUNX-1 is disrupted, mice are embryonic lethal at embryonic day 12.5 from massive bleeding in the central nervous system [21]. Primitive hematopoiesis is normal, however definitive hematopoiesis is disrupted. Further, progenitor cells for hematopoiesis are lacking from fetal liver in addition to the lack of HSC in the AGM region [22].

1.1.4.2. PU.1

PU.1 is an important transcription factor for granulocyte and monocyte differentiation [23]. Its role in hematopoiesis is apparent due to the lack of B lymphoid cells and monocytes with decreased neutrophils when PU.1 is knocked out [23]. Similar to RUNX-1, PU.1 binds DNA through a conserved region via its Ets domain [23]. Though it can be an activator of transcription in B cell development, its interaction with GATA-1 decreases its expression pushing hematopoietic cells towards monocyte differentiation and inhibiting development of erythrocytes [23].

1.1.4.3. GATA proteins

The GATA protein family is zinc finger proteins composed of 6 members. GATA 1-3 play a role in hematopoiesis and GATA 4-6 play a role in cardiac development [24]. Recent findings demonstrate that GATA-1 is essential for erythroid and megakaryocyte cell development [24]. GATA-1 has two essential domains necessary for function, a sequence specific DNA binding domain WGATAR motif and region that interacts with its coregulator Friend of GATA-1 (FOG) [24]. To regulate erythropoietic differentiation, GATA-1 interacts and inhibits PU.1 and positively interacts with erythroid Kruppel-like Factor (ELKF) [24,25]. The interaction with FOG allows GATA-1 to regulate its target genes by altering chromatin structure resulting in repression or enhancement of gene expression [24]. Another example of FOG and GATA-1 co-regulation is that this complex can disrupt GATA-2's interaction with its target genes, therefore promoting erythroid differentiation [24]. GATA-2 is necessary in early stages of hematopoiesis and

appears to play a role in HSC maintenance [24]. In studies where GATA-2 is knocked out, mice are anemic and die at approximately embryonic day 10 [24], thus demonstrating how displacement by FOG would push HSC towards differentiation, specifically erythrocytes.

1.1.4.4. C/EBPα

As with the other transcriptional factors discussed, C/EBPα interacts directly with DNA through its leucine zipper domain via a consensus site DNA-binding site [23]. C/EBPα is expressed in granulocyte, monocyte and eosinophil cells as evident from lack of neutrophils and eosinophils when C/EBPα is knocked out [23]. By binding to E2F, C/EBPα inhibitors E2F function causing c-Myc to be decreased resulting in granulocyte differentiation [26].

1.1.4.5. Cytokines

Cytokines, extracellular growth factors, are other key components in normal hematopoiesis signaling [27]. Colony stimulating factors (CSF) promote normal hematopoietic differentiation to specific cell fates. The names of each CSF describe their functional role, since each cytokine stimulates the colony growth of a specific cell type. Thus, Granulocyte-monocyte CSF (GM-CSF) stimulates the colony growth of GMP, monocyte CSF (M-CSF) stimulate the growth of monocytes, and granulocyte CSF (G-CSF) stimulate the growth of granulocytes [28].

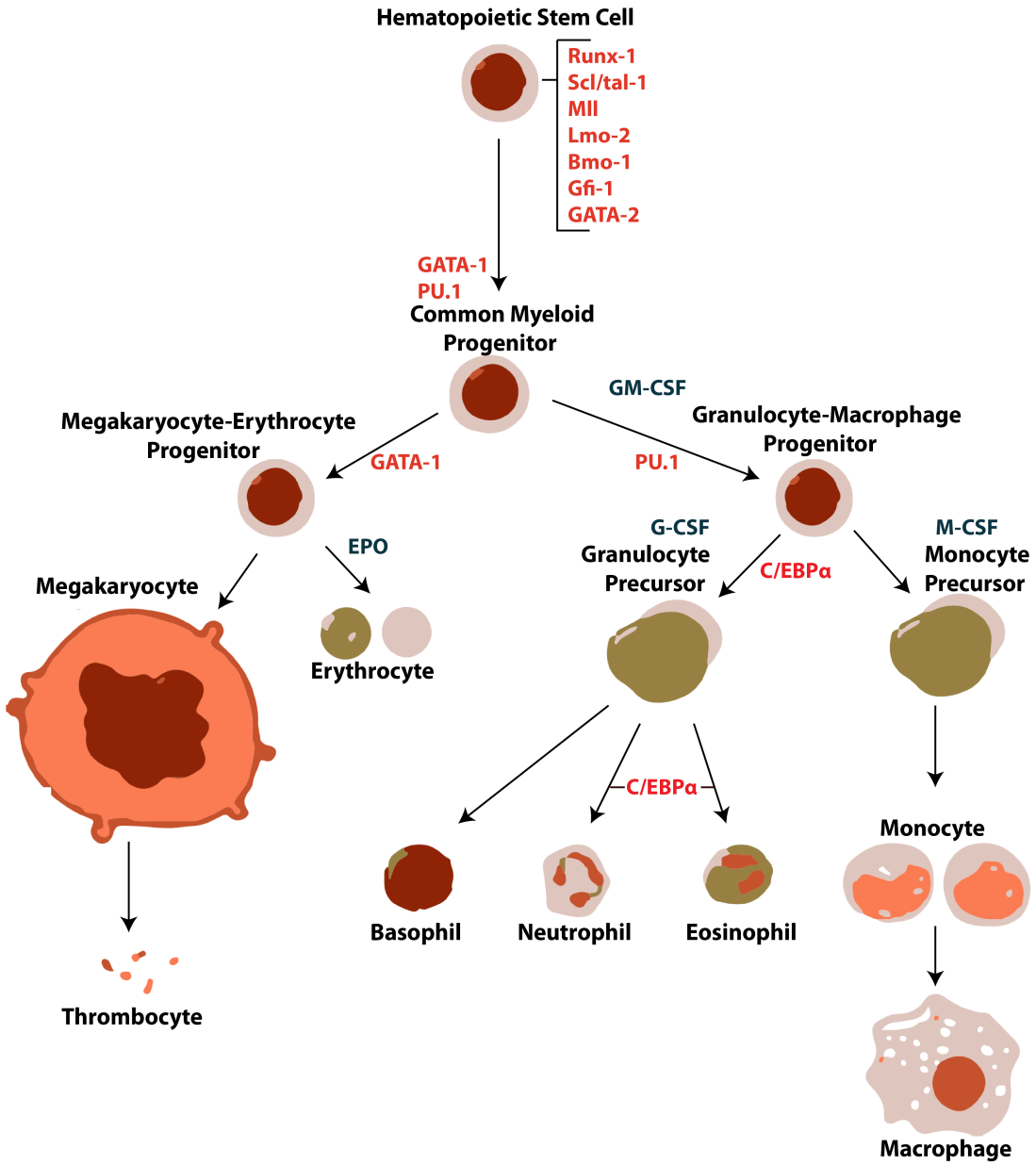

Figure 1.4. An schematic of common signals in myeloid differentiation. This figure is based on information from Dario-Becker [11] and Orkin et al [2]. Transcription factors are in red and cytokines are in blue. RUNX-1 (AML-1): runt-related transcription factor 1; SCL-1 / Tal-1: stem cell leukemia 1 / T-cell acute lymphoblastic leukemia 1; GATA-1: globin transcription factor 1; GATA-2: globin transcription factor 2; MLL: myeloid/ lymphoid or mixed lineage; Lmo-2: LIM Domain Only 2 (rhombotin-like 1); Bmi-1: B lymphoma Mo-MLV insertion region 1 homolog; Gfi-1: growth factor independent 1 transcription repressor; C/EBPα: CCAAT-enhancer-binding proteins alpha alpha; FOG: friends of GATA proteins;GM-CSF: granulocyte-monocyte colony stimulating factor; M-CSF: monocyte colony stimulating factor ; G-CSF: granulocyte colony stimulating factor; EPO: erythropoietin

1.2. Aberrant hematopoiesis

In 2011 it was estimated that 140,310 people living in the United Stated would be diagnosed with leukemia, lymphoma, or myeloma [29]. Leukemia results from uncontrolled accumulation of immature and non-functional blood cells within the bone marrow that invade peripheral blood [30]. Leukemia may be suspected if an individual presents with weight loss, fatigue, fever, night sweats and loss of appetite [31]. Additional symptoms may include infections, feeling cold, dizzy, shortness of breath, excess bruising or headaches [31].

There are two main forms of leukemia: chronic (chronic lymphoblastic leukemia (CLL) and chronic myeloid leukemia (CML)) and acute (acute lymphoblastic leukemia (ALL) and acute myeloid leukemia (AML)) [32]. Chronic leukemias progress slowly and contain functional mature cells that are slowly overtaken by the accumulation of immature cells [32]. Acute leukemia's however progress rapidly and often stop producing differentiated hematopoietic cells[32]. For example, in AML granulocytes, megakaryocytes, macrophages, platelets, or erythrocytes are decreased when myeloid cells accumulate at a progenitor or precursor cell. Chronic and acute leukemia's can affect both lymphoid and myeloid lineages and are classified dependent on the cell type affected [32]. Although diagnosis of any leukemia can devastating, approximately 9% of newly diagnosed individuals (12,950 individuals) will be diagnosed with AML, which has a 23.6% five-year survival rate causing it to be a deadly diagnosis [29]. The average age of an AML patient is approximately 69 years old, although AML can be diagnosed in children and young adults[29].

1.2.1. Diagnosis of acute myeloid leukemia

Diagnosis of AML will first become apparent from the peripheral blood test when white blood cells are increased, red blood cells and platelets are decreased, and lastly an accumulation of leukemic blasts is visible [33]. Below are examples of what normal complete blood counts (CBC) would be as well as a comparison to a leukemic patient. From this example, it is apparent that the patient has extremely heightened white blood cell count with a decrease is both hemoglobin and hematocrit, suggesting the possibility of leukemia from peripheral blood analysis (Table 1.2.).

	Healthy Patient	**Leukemia Patient**
White Blood Cell Count	4,100-9,000 cells/μL	52,000 cells/μL
Red Blood Cell Count	4.10-5.80 million cells/μL	1.13 million cells/μL
Hemoglobin	12.8-17.2 g/dL	5.1 g/dL
Platelet Count	140,000-350,000 μL	173,000 μL
Hematocrit	20.40%	14.10%
Red Blood Cell Distribution	11.4-14.7%	20.40%

Table 1.2. Example of complete blood count results from a healthy and leukemic patient. This table was developed in reference to Shieffer [34] demonstrating an example of peripheral blood results.

To confirm a diagnosis of AML, additional tests are necessary including a blood smear and a bone marrow biopsy/aspirate. A blood smear is utilized to analyze cellular shape and for leukemic blasts. Early progenitor cells are larger in size and contain a nucleus indicating premature cells versus more differentiated cells. If the individual has an abnormal blood sample, then a bone marrow aspirate would be used for both confirmation and classification.

1.2.2. Classification of acute myeloid leukemia

AML is a very cytogenetically and molecularly heterogeneous disease making both its classification and treatment difficult. Classification of AML has changed over the years with increasing knowledge of the disease and development of. In 1976 the first AML classification system was developed entitled the French-American British classification [35] (Table 1.3.). With this system, AML could be classified from morphological and cytochemistry criteria [36]. Depending upon the cell type where differentiation was halted would additionally aid in classification [32]. More recently, the World Health Organization (WHO) developed their own classification for AML, which included cytogenetic and molecular abnormalities in addition to the morphological classifications presented in the FAB classification [35,36] (Table 1.4.). An additional change to AML classification systems with the development of WHO AML classification was the decreased in percent leukemic blasts necessary for diagnosis.

Previously, 30% of cells needed to be considered leukemic blasts, however now it is 20% [35]. By gaining knowledge of the subtype of AML, the patient's risk can also be assessed. An individual can be considered as having poor, intermediate, or favorable prognosis depending on the molecular or cytogenetic abnormalities identified (Table 1.5.).

FAB	Description
MO	Undifferentiated acute myeloblastic leukemia
M1	Acute myeloblastic leukemia with minimal maturation
M2	Acute myeloblastic leukemia with maturation
M3	Acute Promyelocytic leukemia
M4	Acute myelomonocytic leukemia
M5	Acute myelomonocytic leukemia with eosinophilia
M6	Acute erythroid leukemia
M7	Acute megakaryoblastic leukemia

Table 1.3. AML French-American-British classification. This table is based from information provided by Alitheen et al[32].

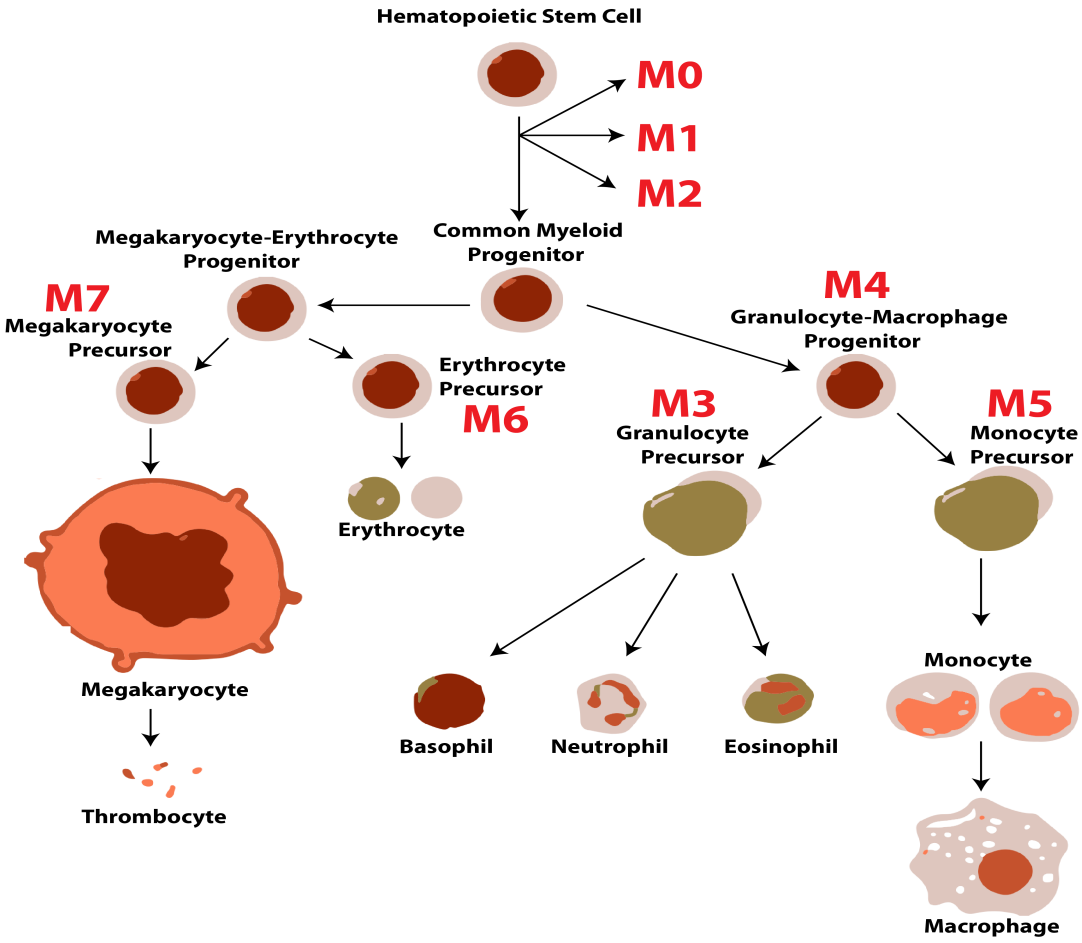

Figure 1.5. Schematic of AML FAB classification within the myeloid lineage. This figure is based on information provided by Dario-Becker [11] and Assouline [37]. Classification is based on morphology for AML FAB Classification. In red denotes the FAB classification and where the myeloid differentiation is halted.

Acute myeloid leukemia with recurrent genetic abnormalities

Acute myeloid leukemia with t (8; 21)(q22; q22), (AML1/ETO)
Acute myeloid leukemia with abnormal bone marrow eosinophils and inv(16)(p13q22) or t(16;16)(p13;q22), (CBFβ/MYH11)
Acute promyelocytic leukemia with t(15;17)(q22;q12), (PML/RARα) and variants
Acute myeloid leukemia with 11q23 (MLL) abnormalities

Acute myeloid leukemia with multilineage dysplasia

Following MDS or MDS/MPD
Without antecedent MDS or MDS/MPD, but with dysplasia in at least 50% of cells in 2 or more myeloid lineages

Acute myeloid leukemia and myelodysplastic syndromes, therapy related

Alkylating agent/radiation–related type
Topoisomerase II inhibitor–related type (some may be lymphoid)
Others

Acute myeloid leukemia, not otherwise categorized
Classify as

Acute myeloid leukemia, minimally differentiated
Acute myeloid leukemia without maturation
Acute myeloid leukemia with maturation
Acute myelomonocytic leukemia
Acute monoblastic/acute monocytic leukemia
Acute erythroid leukemia (erythroid/myeloid and pure erythroleukemia)
Acute megakaryoblastic leukemia
Acute basophilic leukemia
Acute panmyelosis with myelofibrosis
Myeloid sarcoma

Table 1.4. WHO classification of AML. Information from Vardiman et al[35] was used to produce this table. This Table provides categories and description utilized in WHO classification.

Favorable Risk Group

Cytogenetic Analysis	Molecular Analysis
8;21 translocation (FAB M2)	RUNX1-RUNX1T1
15:17 translocation (FAB M3)	PML-RAR alpha
16:16 translocation or inversion 16 (FAB M4)	CBF-beta MYH11
No chromosomal changes	NPM1 or CEBPA mutation without FLT3-ITD

Intermediate Risk Group

Cytogenetic Analysis	Molecular Analysis
No chromosomal changes	
9;11 translocation	MLLT3-MLL
Nondefined chromosomal changes (fewer than 3)	
Trisomy 8	

Poor Risk Group

Cytogenetic Analysis	Molecular Analysis
Deletion of all/part of Chromosome 5 and 7b	
6;9 translocation	DEK-NUP214
Inversion 3 or 3;3 translocation	RPN1-EVI1
v;11q23 translocation	MLL-rearrange
Monsomy 5, del(5q), monosomy 7	
3 or more chromosomal changes (not a recurring translocation or inversion)	
No chromosome changes	FLT3-ITD with/without NPM1 mutation ERG and BAAL overexpression

Table 1.5. AML risk of WHO AML classification categories. Cytogenetic and molecular abnormalities have been correlated to poor, intermediate, and favorable outcome when diagnosed with AML [29]. This table provides the current classifications for each AML prognosis.

1.2.3. Aberrant hematopoietic signaling in acute myeloid leukemia

This section will highlight some of the molecular mechanisms of the common cytogenetic and molecular changes that result in AML within the current FAB and WHO classification systems.

1.2.3.1. RUNX1-RUNX1T1 (AML1-ETO)

This mutation is the result of a translocation (8;21)(q22;q22) that includes the binding domain of RUNX1 and the majority of the ETO protein and accounts for approximately 40% of AML cases [38]. Due to several alternative splice forms of ETO, there are four different forms of the AML1-ETO fusion protein ranging in sizes between 2-8kb [39]. As a result of this fusion gene, downstream genes of RUNX1 are inhibited rather than activated [40]. Studies indicate that the fusion gene product can interact with many factors that are necessary for myeloid differentiation, such as GATA-1 C/EBPα, and PU.1 [41]. As a result of this fusion protein, hematopoietic cells remain as pluripotent stem cells and do not differentiate resulting in AML [42].

1.2.3.2. PML-RAR α

PML normally is expressed in HSC and necessary for erythroid and granulocytic differentiation and is maintained in erythroid differentiation and decreased in granulocyte differentiation [43]. RAR (retinoic acid receptor) alpha-receptor is part of the RAR family [44] and aids in myeloid differentiation [45] specifically granulocyte development [44]. The PML-RAR alpha fusion protein is a result of the

chromosomal translocation (15:17) causing a block in granulocyte differentiation [46]. The block in differentiation is believed to be through suppression of the transcription factor C/EBP alpha [47].

1.2.3.3. CBF-β MYH11

CBF-beta is part of a family of transcription factors composed of RUNX1, RUNX,2 RUNX3, and CBF beta [48]. The alpha subunits (RUNX1-3) dimerize with CBF beta stabilizing its interaction with DNA and regulation of hematopoiesis and differentiation [48]. MYH11 is part of the myosin heavy chain family encoding smooth muscle myosin heavy chain that regulates motor protein in muscle [48,49]. Though this mutation can lead to AML, it cannot solely cause AML and therefore must be in combination with other abnormalities [50]. With the CBF-beta MYH11 fusion protein, the RUNX binding domain is maintained within CBF beta in addition to a RUNX binding domain with the tail of MYH11 [48]. As a result of this fusion protein, interaction with RUNX is enhanced leading to increased RUNX1 transcription rather than transcription inhibition resulting in a block in differentiation [48].

1.2.3.4. NPM1 or CEBPA mutation without FLT3-ITD

Normally NPM1 is a shuttle protein between the nucleus and cytoplasm and plays role in ribosome formation and export and centrosome duplication [51]. Mutations within NPM1 cause it to be increased [52]; however the mutation is normally located with the C-terminal region disrupting the localization of NPM1 to

the cytoplasm [52]. The NPM1 mutation causes several altered cellular functions leading to AML causing cytoplasmic delocalization of nuclear proteins and altered gene expression including increased HOX genes [51]. HOX genes are a family of proteins shown to play a role in HSC and immature progenitors that are decreased upon HSC differentiation [53]. Although the exact function of HOX genes within hematopoiesis is not well defined, it has been established that increased HOX genes in AML results in increased cell cycle proliferation and decreased differentiation [54].

As discussed earlier, CEBP alpha is necessary for granulocytic differentiation within normal hematopoiesis [55]. There are several mechanisms by which CEBP contributes to AML, the first being aberrant methylation of its promoter, secondly a truncated form of CEBP, and sumoylation of CEBP alpha [56]. With the CEBP mutation the AML resembles FAB M1 or M2 [55].

1.2.3.5. MLLT3-MLL and MLL-rearrange

MLL is part of the H3K4 methyltransferase family activating genes by methylating histone 3 on lysine 4 such as HOX genes [57]. There are multiple types of MLL fusion proteins that can result from chromosomal translocation, deletions, or inversions [58] making up to 60 different fusion proteins [57]. Currently, studies suggest that MLL fusion proteins lead to AML via increased expression of HOX and MEIS1 [58]. MEIS1 is another transcription factor that regulates HSC through regulating oxidative metabolism [59]. By enhancing these regulators of HSC via aberrant methylation, HSC differentiation is block resulting in AML [57].

1.2.3.6. DEK-NUP214

DEK regulates global heterochromatin protein [60] that functions by enhancing CEBP alpha promoting myeloid differentiation [61]. NUP214 is a nucleoporin protein that provides a binding site for nuclear export complexes [62]. The mechanism of action for DEK-NUP214 fusion protein within AML is not as well known as other fusion proteins [63]. Studies however currently indicate that DEK-NUP214 enhances eukaryotic translation initiation factor 4E (eIF4E) via phosphorylation [63]. By activating this factor, protein synthesis within myeloid cells is enhanced [63]. In some cases, individuals have a DEK-NUP214 mutation and a FLT3 mutation, leading to both decreased differentiation and enhanced proliferation of myeloid cells [63].

1.2.3.7. FLT3-ITD with and without NPM1 mutation

During hematopoiesis, FLT3 (Fms-like tyrosine kinase 3) is expressed on early progenitors on myeloid and B lymphoid lineages [64]. FLT3 maintains hematopoietic stem cells and progenitors by enhancing anti-apoptotic proteins such as Mcl-1 [65]. In the context of AML, FLT3 has a tandem duplication causing its expression to be increased leading to overexpression of Mcl-1 therefore causing HSC and progenitors (CMP/GMP) to have increased survival [65]. Though it has been established that FLT3-ITD and NPM1 mutations are commonly found together, the mechanism of cooperatively of these two mutations has not been elucidated [66] and that the NPM1 mutation appears to be established prior to FLT3-ITD mutation [67].

1.3. Epigenetic regulation

Epigenetic regulation of gene expression regulates gene expression without changes in the sequence of DNA [68], adding another layer of complexity to transcriptional gene regulation. Epigenetic alterations can be through modifications on chromatin/histone or via DNA methylation [69]. Chromatin packages DNA via histones, H1, H2, H3, and H4 [69]. Approximately 146 base pairs (bp) of DNA are wrapped around each histone complex composed of two copies of histones H2A, H2B, H3, and H4 [69] forming an octamer (nucleosome) [70] (Figure 1.6.). Each histone has a N-terminal tail and H2A and H2B have a C-terminal tail [70] (Figure 1.6.). Histone H1 is considered a linker histone since it interacts with DNA as it enters and leaves the nucleosome [71]. A string of nucleosomes connected by linker H1 and DNA form a 30nm fiber that can be further coiled to form chromatin [72]. There are two main forms of chromatin, heterochromatin and euchromatin [69]. Genes are believed to be inactive within heterochromatin form and active when in euchromatin form [69]. Modifications of histone tails alter chromatin structure [73] and therefore regulate gene expression.

1.3.1 Histone modifications

Each histone has an N-terminal region composed of 19-39 amino acids named histone tails that can be modified via phosphorylation, ubiquination, acetylation, or methylation [69] (Figure 1.6.).

Each of these histone modifications can results in suppression and enhancement of gene expression depending on the specific amino acid it binds

to within each histone [74]. Acetylation within the histone tail results in a more relaxed state of chromatin due to charge neutralization, causing the interaction between DNA and the histones to decrease [75]. By relaxing the chromatin structure, a permissive state for transcription is established. Although it is well known that ubiquination of proteins leads to their proteasomal degradation, the consequences of addition of ubiquitin to histones is less well understood[76]. Current studies indicate that ubiquination can lead to both enhanced and suppressed transcription through its interactions with methylation [76]. Addition of a methyl group on H3K4, H3K36 and H3K79 can enhance transcription, however, when added to H3K9, H3K27 and H4K20 it causes decreased gene transcription [77]. Interestingly, unlike acetylation, the function of histone methylation is currently still being characterized [77]. Histone phosphorylation plays a role in multiple functions, including apoptosis, mitosis, DNA damage, and gene regulation [74,78]. DNA methylation is an additional modification that regulates gene expression.

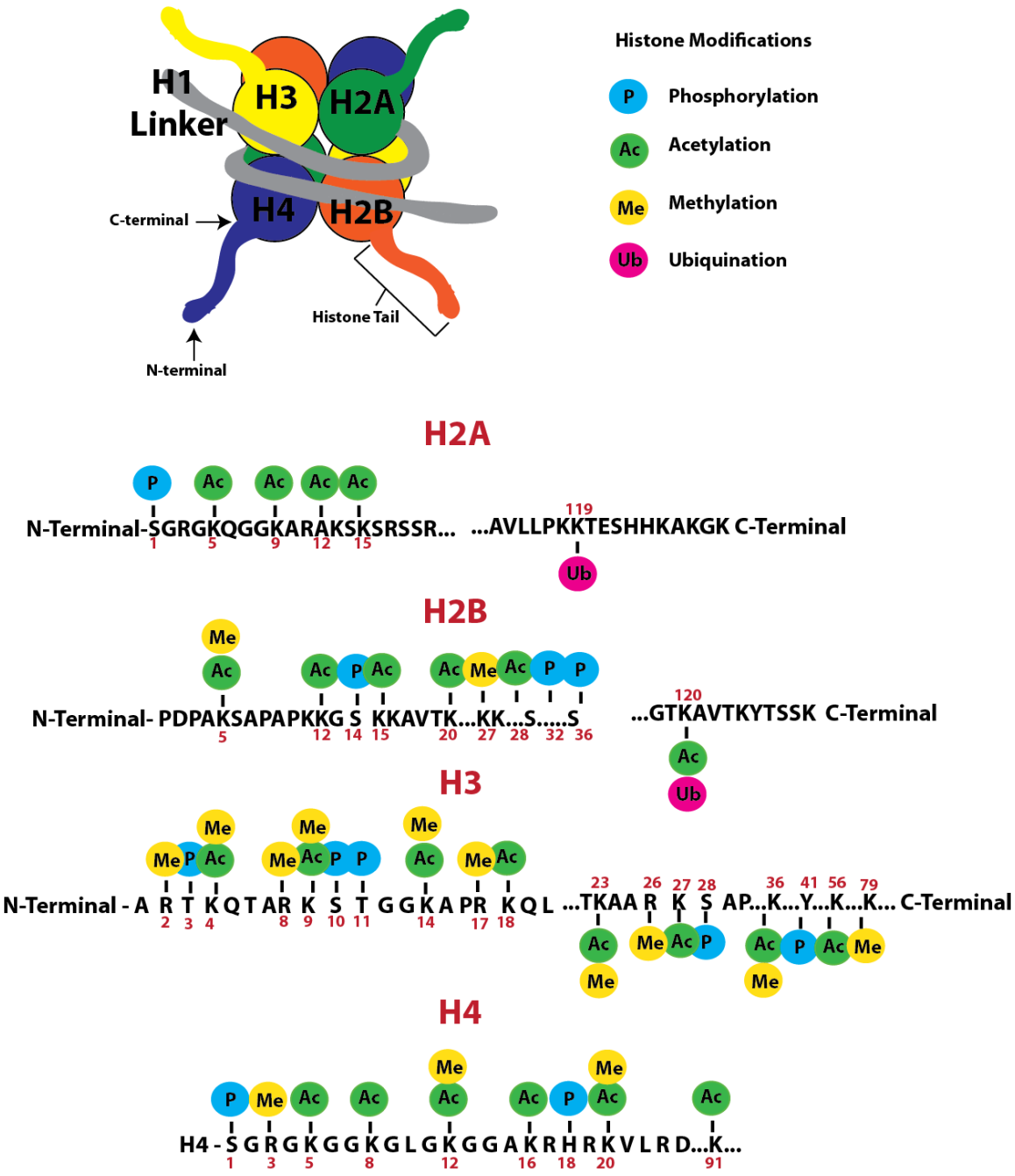

Figure 1.6. Illustration of common histone modifications. This figure is based from information from AMS Biotechnology[79] and Rodriguez-Paredes et al[80]. The nucleosome is composed of two copies of histones H2A, H2B, H3, and H4 (upper left). Nucleosomes are connected via histone H1. Each histone tail can be modified in order to alter chromatin structure (bottom portion). Me: methylation; Ac: Acetylation; P: phosphorylation; and Ub: ubiquination.

1.3.2 DNA methylation

DNA methylation primarily occurs within cytosine and guanine rich regions named CpG islands. Around half of CpG islands are located on transcriptional start sites [81] while the other half is are considered orphan CpG islands since they are in between coding regions [82]. Cytosines are methylated via DNA methyl transferases (DNMTs), which are commonly associated with heterochromatin (compacted chromatin) resulting in decreased gene expression [83]. (Figure 1.7.) One mechanism in which DNA methylation results in gene suppression is via methylated cytosines interaction with co-repressors. Methyl-CpG-binding domain (MBD) proteins interact with methylated cytosines which recruit co-repressors such as histone deacetylases (HDACs) [83,84]. As discussed earlier, histone acetylation results in relaxation of chromatin due to neutralization of the charge on the histone tails disrupting the DNA and histone tail interaction [75]. Therefore, by the removal of histone acetylation, chromatin is compacted resulting in inhibition of gene expression.

Normally, gene expression is regulated by the addition or removal of each epigenetic modulator. However, these epigenetic regulators can become targets within disease causing genes to either be enhanced or suppressed aberrantly due to alterations in histone modifications or DNA methylation.

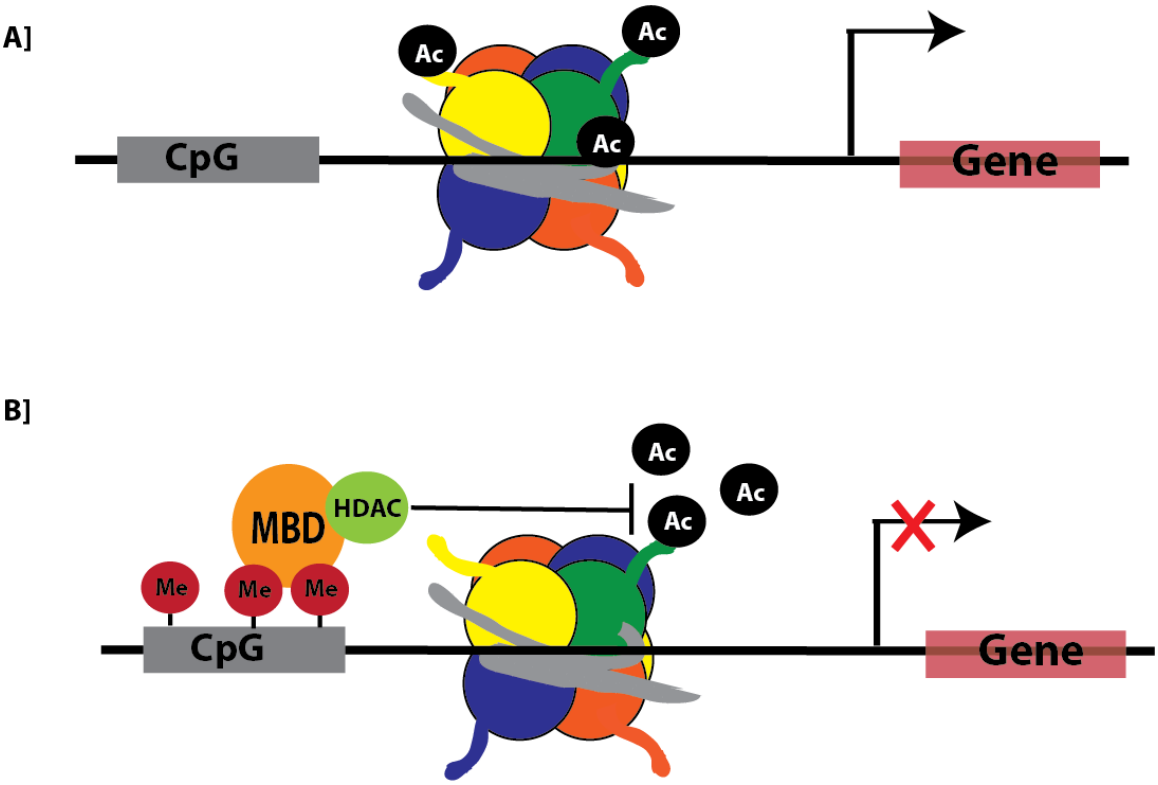

Figure 1.7. DNA methylation regulation of gene expression. A] When CpG islands are unmethylated and histones are acetylated, genes are expressed B] Gene expression can be suppressed by the addition of methyl groups upstream of transcriptional start sites. The addition of methyl groups on cytosines within CpG islands can recruit methyl binding proteins (MBD) and histone deacetylase (HDAC). Recruitment of HDAC results in de-acetylation of histone tails nearby. As a result of DNA methylation and histone de-acetylation genes can be suppressed.

1.4. Altered epigenetic regulation in hematopoietic malignancies

Between 40-49% of AML patients present with normal cytogenetic [85] implying a possible role for abnormal epigenetic regulation in gene silencing. Epigenetic regulation can result in gene silencing without genetic alterations [86] via DNA methylation or histone modifications (methylation or acetylation). Hypermethylation has been linked to AML and could be occurring as a result of overexpression of DNA methyl transferases (DNMT) [87]. Targeting DNA methylation through DNMT inhibitors, like decitabine [88], may permit re-expression of suppressed genes permitting them to act as tumor suppressors. New insights illustrate a play between DNMT and histone deacetylase (HDAC) to suppress gene regulation [89], therefore suggesting both DNMT and HDAC inhibitors may be needed to release gene suppression in AML.

1.5. Techniques utilized in AML classification

1.5.1. Tools for FAB classification

Through the use of Wright-Giesma staining, the myeloid lineages can be dissected through their morphology and cytochemistry [35]. The stain contains both acidic and basic components allowing differential staining of cellular components, such as the cytoplasm, granules, and nucleus [90] (Table 1.6.). Monocytes and lymphocytes have a rounded or kidney shaped nuclei and not much cytoplasm while granulocytes have multi-lobed nucleus and a granular cytoplasm [91]. Below is a table containing the key features of each specific cellular type following wright-giesma staining that is utilized for classifying AML FAB subtypes.

Cell Type	Key Features
Red Blood cells	The cytoplasm has a orange-pink to rose appearance
Lymphocytes	The cytoplasm is light blue while the nucleus is deep blue-violet
Monocytes	The cytoplasm is pale gray-blue while the nucleus is deep bluish-purple
Neutrophils	The cytoplasm is purple-to-lilac, while the nucleus is deep blue-violet and the granules are purple-to-lilac
Eosinophils	The granules are orange to pink
Basophils	The granules are deep blue to violet
Plateles	The central granules are red-purple and surrounded with light blue

Table 1.6. Key staining features for myeloid lineages by Wright-Giesma staining. Information for this table was gathered from Sears [91]. Each cell type can be identified through key features of staining via wright-giesma staining.

1.5.2. Assays for WHO AML classification

For the WHO AML classification system there are additional components beyond morphological and cytochemistry, therefore additional assays are utilized. These assays include karyotyping for detection of chromosomal abnormalities, such as aneuploidy, nondisjunction, and rearrangements [92]. Normally, chromosome 1 is the longest while chromosome 21 is the shortest [92]. The addition of wright or Romanowsky stains results in banding of each chromosome by producing stained (G+bands; AT rich regions) and non-stained regions (G- bands; GC rich regions) [92]. Though these staining may detect chromosomal abnormalities, additional techniques may be necessary. FISH, fluorescence in situ hybridization, can be used to supplement karyotyping to identify difficult cytogenetic abnormalities such as inversions [93]. Through these staining procedures,

chromosomal abnormalities can be utilized to classify AML. When patients have cytogenetically normal AML, it could be due to a molecular abnormality. To identify these there are a range of techniques that can be used depending upon the molecular abnormality. For example, for the NPM1 mutation, the mutation can be detected by western blot, immunohistochemistry, or flow cytometry [51].

1.6. Current treatments for AML

Due to the complexity of AML, treatment is challenging. Sadly, there has not been much change in the treatment strategy for AML over the last 40 years [94]. Currently, two main types of treatments exist which include remission induction therapy and post-remission therapy. Cytarabine (AraC) with a combination of anthracycline is most commonly used for induction therapy at this time [94,95]. Recently, new therapeutics are being developed for AML based upon the genetic pathways that are altered in the pathogenesis of AML[96]. In recent years, microRNAs (miR) have been recognized to regulation normal and malignant biological pathways, including hematopoiesis.

1.7. microRNA

MiRs are non-protein coding ribonucleic acids (RNA) approximately 20-23 nucleotides in length located between genes (intergenic) or between exons within a gene (intronic), which were previously believed to be non-coding regions of deoxynucleic acids (DNA)[97].

1.7.1 Canonical microRNA processing

MiRs are transcribed by RNA Polymerases (II or III) in the nucleus producing the primary-miR (pri-miR) noted for its hairpin structure containing a 5' cap and poly-A tail. They can be transcribed individually or with several other miR called clusters. Drosha and Dicer are two RNase type III enzymes, which process non-coding RNA to small double stranded RNA necessary for miR processing [98]. Following the transcription of the pri-miR, Drosha cleaves the 5'cap and poly-A tail producing a precursor-miR (pre-miR) containing 5' and 3' overhangs. The pre-miR is exported from the nucleus into the cytoplasm by the exportin 5/Ran GTP complex. The pre-miR is separated, producing two single stranded nucleotides known as the mature miR that are named 5p or 3p depending on the strand origin. One strand, often the most thermodynamically unstable strand, becomes functional by integrating with the RNA induced silencing complex (RISC complex where it regulates its target. [99] The RISC complex is still being defined, however argonaute proteins are known to be a central component [100]. Argonaute proteins interact with the miR and guide the RISC complex to target RNA degradation [100]. (Figure 1.8.)

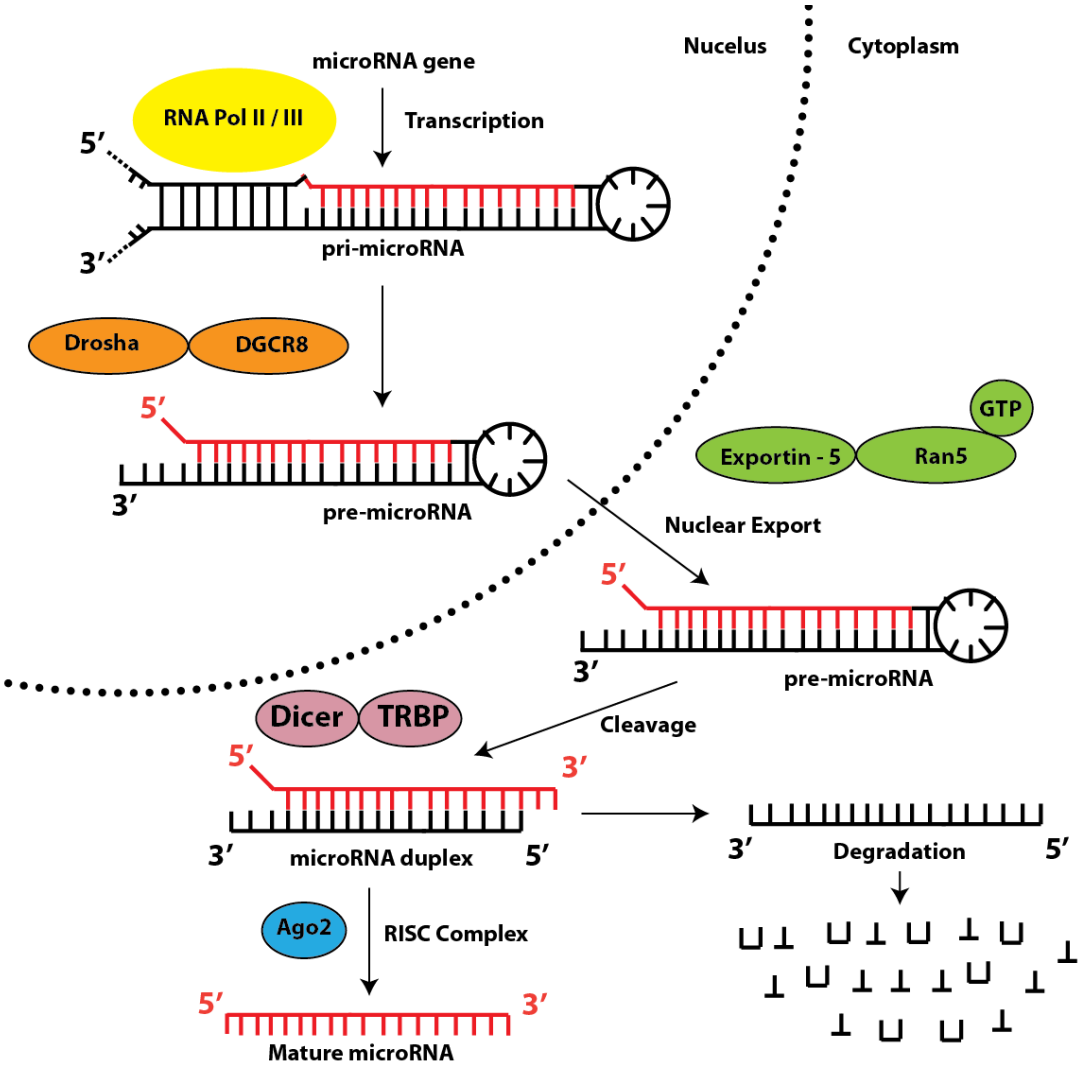

Figure 1.8. Canonical microRNA processing. This figure was developed from Winter et al[99]. MiRs are transcribed by RNA Polymerases (II or III) in the nucleus producing the primary-miR (pri-miR) noted for its hairpin structure containing a 5' cap and poly-A tail. They can be transcribed individually or with several other miR called clusters. Following the transcription of the pri-miR, the Drosha complex cleaves the 5'cap and poly-A tail producing a precursor-miR (pre-miR) containing 5' and 3' overhangs. The pre-miR is exported from the nucleus into the cytoplasm by the exportin 5/Ran GTP complex. The pre-miR is separated, producing two single stranded nucleotides known as the mature miR that are named 5p or 3p depending on the strand origin. One strand, often the most thermodynamically unstable strand becomes functional by integrating with the RISC complex where it regulates its target.

1.7.2 microRNA targeting

One of the most important features for miR target recognition is the nucleotide matching between the miR seed sequence and mRNA. The seed sequence of a miR is defined as the first 2-8 nucleotides within the 5' untranslated region (UTR) region (Figure 1.9.). Currently, there are four main types of matching between the miR seed sequence and mRNA which are defined as follows: 6mer, 7mer-m8, 7mer-A1 site, and 8mer site [101]. A perfect match is considered when there is a Watson-Crick match between a miR and mRNA nucleotides meaning that adenosine (A) pairs with uracil (U) and guanine (G) pairs with cytosine (C) [101]. A 6mer site occurs when there is a perfect match between the miR seed and mRNA, a 7mer-m8 site occurs when there is a perfect seed match in addition to a Watson-Crick match at the 8th nucleotide site, a 7mer-A1 site occurs when there is a perfect seed match in addition to a A across from the miR nucleotide 1, and lastly an 8mer site occurs when there is a perfect seed match in addition to both m8 and A1 as defined earlier [101].

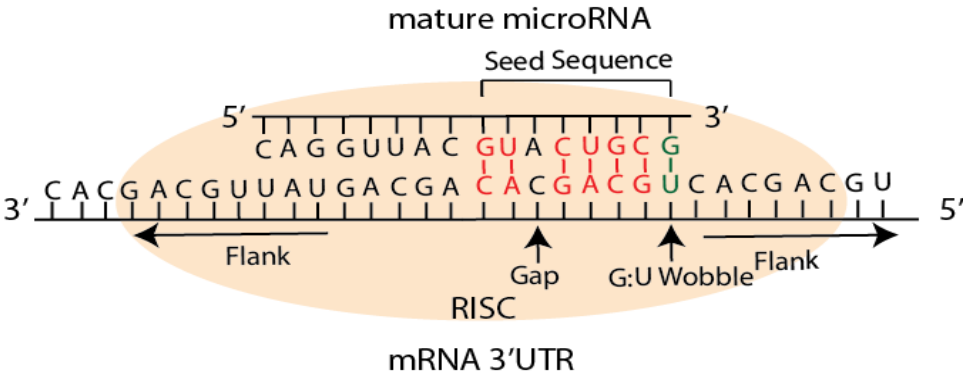

Figure 1.9. Schematic of microRNA targeting. microRNA's interact with the 3'UTR through a semi-complementary sequence. This figure demonstrates the interaction of a microRNA and the 3'UTR of an mRNA and the common terminology utilized surrounding the seed sequence.

In the human genome, there are 1872 precursor microRNAs and 2568 mature microRNAs [102]. The table below demonstrates the current knowledge on the number of identified precursor microRNAs and mature microRNAs for various species (Table 1.7.). In addition to the number of miR, there are approximately 48,360 potentially conserved mRNA target sites [101].

Species Name	Precursor microRNA	Mature microRNA
Xenoturbella bocki	**8**	**8**
Anolis carolinensis	**282**	**416**
Gorilla gorilla	**322**	**317**
Homo sapiens	**1872**	**2568**
Pan paniscus	**88**	**83**
Pongo pygmaeus	**633**	**651**
Pan troglodytes	**655**	**58**
Symphalangus syndactylus	**11**	**10**

Table 1.7. Currently known number of precursor and mature microRNA. Information for this table was gathered from miRbase[102].

Determining a particular miR target is essential to understanding its functional role within biological systems. Due to the numbers of miR and potential target sites it would be very difficult to narrow down potential targets to study experimentally for particular miR, therefore, today several miR databases attempt to computationally predict miR targets to assist in narrowing down targets. As knowledge is gained on the interaction between a miR and its target, new bioinformatics tools are developed to help narrow down potential targets of miRs that often use seed match, free energy, and conservation to identify a particular target.

1.7.3. microRNA in normal and malignant hematopoiesis

There is a complex signaling network for regulating hematopoiesis, including cytokines and transcription factors. miRs are now being discovered that regulate hematopoiesis in these complex networks. From miR expression studies, it has been found that miRs can regulate maintenance and differentiation of cells in hematopoiesis.[103] For example, mir-130, miR-196a and miR-196b are expressed in hematopoietic stem cells and decrease as lymphoid differentiation proceeds [104]. In other cases, miR are being increased when committing to a specific cell type, such as miR-25, miR- 221, and miR-223 are expressed when a stem cell becomes myeloid cells [104]. One-way miR aid in hematopoiesis is by assistance in maintaining the checkpoints within hematopoiesis prior to differentiation.

Several studies, such as one by Garzon et al have demonstrated irregular expression of miR in AML [105]. Another study identified miR-let-7b and miR-let7c, which regulate RAS, to be decreased in AML resulting from t (8; 21) chromosomal translocation [106]. Though these miR's are being illustrated to play vital roles in normal and malignant hematopoiesis, *the functional roles of these miR's need to be elucidated* [103].

1.7.4. miR-125a

In a study where miR expression was analyzed in bone marrow (BM) of newly diagnosed cytogenetically normal AML patients compared to BM of control patients, miR-125a was significantly down regulated [105]. Though miR-125a was not the highlight of Ramsingh et al. article, from the small RNA sequencing within

the study miR-125a expression was decreased in cytogenetically normal AML [107]. Currently, it is known that *miR-125a* is expressed highest in hematopoietic stem and progenitor cells (HSPC) and progressively decreases upon differentiation [108]. Guo et al demonstrated ectopic expression of *miR-125a* in mouse HSPC show an increase in reconstitution of blood lineages in bone marrow transplantations lasting up to five months as well as HSPC self-renewal [108]. Interestingly, ectopic expression of *miR-125a* within common lymphoid progenitors, common myeloid progenitors, granulocyte and macrophage progenitors, and MEP did not result in self-renewal or maintenance of blood lineages. Further analysis illustrated an increase of HSPC to differentiate into myeloid cells and a decrease in lymphoid cells. [108] Within a second study by Gerrits et al, over-expression of miR-125a in mouse HSPC increased competitive advantage and promoted myeloid differentiation, similar to Guo et al. However, unlike Guo et al, miR-125a overexpression did not result in primitive bone marrow maintenance in secondary bone marrow transplants. [109] From these two main studies on the role of miR-125a it is seen that the role of miR-125a in normal hematopoiesis remains inconclusive and undefined in AML.

Furthermore studies have also demonstrated a role for miR-125a in several non-hematopoietic diseases. A recent review by Sun et al highlights the role of miR-125 in solid tumors, hematological malignancies, autoimmune disease, immune system development, and disease pathogenesis[110]. By reading this review, we can gain insight on the potential therapeutic role of miR-125, however it should be noted that when reviewing references many of the points

are in reference to miR-125b's roles. Therefore the role of miR-125a is less well understood.

In another study, ectopic miR-125a expression decreased Mcl-1 resulting in enhanced apoptosis leading to a potential new therapy for short bowel syndrome [111]. In colon cancer, Chen et al demonstrated that decreased miR-125a/b leads to enhanced ALDH1A3 allowing colon tumors to be chemotherapy resistant. Upon overexpressing miR-125a/b, colon tumors had decreased cell survival and increased apoptosis through Mcl-1 and ALDH1A3 [112]. miR-125a is decreased in breast cancer, gastric cancer, and medulloblastoma promoting the progression of the disease [113-115]. Previous findings within breast and gastric cancer demonstrate that re-expression of miR-125a results in decreased cell proliferation, migration, and cell death therefore suggesting that re-expression of miR-125a could be a potential therapeutic [114,115]. Knowing that significantly decreased miR-125a promotes breast cancer, gastric cancer, and medulloblastoma supports the possibility of decreased miR-125a aids in the progression of AML. Therefore within these studies, the functional role of miR-125a was dissected to elucidate if miR-125a could aid in the pathogenesis of AML and if it could be utilized as a new therapeutic for AML.

CHAPTER 2: MATERIALS AND METHODS

2.1. microRNA sequencing

Dr. Daniel C. Link of Washington University, a collaborator, provided the data from his miR sequencing for miR-125a at time of diagnosis and relapse. He provided the following protocol. Bone marrow samples from 30 AML patients and 4 healthy adult volunteers were obtained from a study at Washington University to identify genetic factors contributing to AML initiation and progression. Approval was obtained from the Washington University institutional review board for these studies. Written informed consent was obtained in accordance with the Declaration of Helsinki. Clinical characteristics of the AML patients and a detailed description of the small RNA sequencing protocol and analysis pipeline will be published elsewhere. Briefly, bone marrow was harvested from healthy donor volunteers and CD34+ cells were isolated using the autoMACS purification system. For patients with blast percentages <60% at bone marrow collection, CD34+CD45^{dim} blasts from cryopreserved peripheral blood or bone marrow were sorted directly into Trizol LS. Small RNA sequencing libraries were generated from 500ng of AML patient blast or CD34+ healthy donor bone marrow RNA using the NEB Next Small RNA Library Prep Set (#E6120S); ligation, reverse transcription, and PCR amplification steps were performed according to manufacturer's protocol. Following cDNA amplification, isolation of transcripts representing RNA 15-75 nucleotides in length was performed using the Caliper Lab Chip fractionation system. All cDNA libraries were sequenced on the Illumina GAIIX platform and subsequent reads were aligned to the human

genome. Sequence reads corresponding to miRNAs were identified using genomic coordinates from miRBase (v19). Expression values for specific miRNAs were normalized by dividing the average sequence read depth for that miRNA by the total number of sequence reads for all miRNAs and then multiplying by 1 million.

2.2. Statistical analysis

GraphPad Prism 6 was utilized to graph and determine significance. T.Test (parametric test, unpaired test) or one-way ANOVA (no matching or pairing) was used to determine significance.

2.3. National Cancer Institute the Cancer Genome Atlas Data Portal Analysis

Data files were downloaded from: https://tcga-data.nci.nih.gov/tcga/. Files were downloaded from Data Matrix for LAML level 3 for miRNASeq and Clinical Data.

The following types of data were downloaded for AML samples:

miRNASeq Data Files for miR-125a analysis:

27d3c98a-153d-478f-8a5e-725a82d350d9

2/miRNASeq/BCGSC__IlluminaGA_miRNASeq/Level_3

For analysis, mirna_quantification.txt were used in script.

Clinical Data Files:

51fe2f4f-2417-4379-80c9-18f122915a96/Clinical/Biotab/clinical_patient_laml.txt

Each patient has a unique barcode, for example: "TCGA-AB-2803-03A-01T-0734-13." These barcodes are used to identify individual patients. When comparing sequencing for miR in correlation to clinical information, the barcode is needed to analyze this information within the same patient. Detailed information about sequencing data can be found within the METADATA folder in each of the sequencing data files listed above.

R program was downloaded from R.app GUI 1.53 (6451 Leopard build 32-bit), S. Urbanek & H.-J. Bibiko, © R Foundation for Statistical Computing, 2012. To extract miR-125a information, and correlate it to clinical information, script to run on R was written (below).

To use the R script on another computer, the path for each file needs to be changed to the appropriate location. R script can be altered to look at any miR desired by changing the name of the miR within the R script (below).

For AML samples, data for a healthy control was unavailable. Therefore, comparison to a healthy control was not possible. In cases where statistics was completed, GraphPad Prism 6 was utilized to graph and determine significance. T.Test (parametric test, unpaired test) or one-way ANOVA (no matching or pairing) was used to determine significance.

The R script is as follows:

```
rm(list=ls())
library(survival)
# miRNA data
path = "~/Documents/Bioinformatics Final Project/27d3c98a-153d-478f-8a5e-
725a82d350d9 2/miRNASeq/BCGSC__IlluminaGA_miRNASeq/Level_3//"
files = list.files(path)
nsample = length(files)/2
sample_id = array("",dim=c(nsample))
my_miRNA = "hsa-mir-125a"
isoforms = NULL
mirna = NULL
for (i in 1:nsample) {
# read isoform sample
filenum = (i-1)*2 + 1
file =
read.delim(file=paste(path,files[filenum],sep=""),header=T,stringsAsFactors=F)
parse = strsplit(files[filenum],split="_")[[1]]
sample_id[i] = parse[6]
type = parse[8]
if (type != "isoform") print("error")
pull = file[file$miRNA_ID==my_miRNA,]
isoforms = rbind(isoforms,pull)
filenum = (i-1)*2 + 2
file =
read.delim(file=paste(path,files[filenum],sep=""),header=T,stringsAsFactors=F)
parse = strsplit(files[filenum],split="_")[[1]]
if (parse[6] != sample_id[i]) print("error")
type = parse[8]
if (type != "mirna") print("error")
pull2 = file[file$miRNA_ID==my_miRNA,]
mirna = rbind(mirna,pull2)
}
mirna$id2 = substring(mirna$barcode,1,12)
# clinical data
path = "~/Documents/Bioinformatics Final Project/51fe2f4f-2417-4379-80c9-
18f122915a96/Clinical/Biotab/"
my_file = "clinical_patient_laml.txt"
file =
read.delim(file=paste(path,my_file,sep=""),header=T,stringsAsFactors=F,na.strin
gs=c("NA","[Not Available]","[Not Applicable]"))
id = file$bcr_patient_barcode
survival = file$days_to_death
alive = file$vital_status
age_diag = file$age_at_initial_pathologic_diagnosis
```

```
age = file$days_to_birth/365
followup = file$days_to_last_followup
new_file =
data.frame(id,survival,alive,age_diag,age,followup,stringsAsFactors=F)
merged = merge(mirna,new_file,by.x="id2",by.y="id")
merged$time = merged$survival
living = which(merged$alive=="LIVING")
merged$time[living] = merged$followup[living]
merged$event = 1
merged$event[living] = 0
mergedNonMiss = merged[!is.na(merged$time),]
survObj = Surv(mergedNonMiss$time,mergedNonMiss$event)
mirna_level = mergedNonMiss$reads_per_million_miRNA_mapped
hi = as.numeric(mirna_level>median(mirna_level))
mergedNonMiss$hi_mirna = hi
fit <- survfit(Surv(time, event) ~ hi, data=mergedNonMiss, type="kaplan-meier")
plot(fit,col=c("red","blue"))
survdiff(Surv(time, event) ~ hi_mirna,data=mergedNonMiss)
model = coxph(survObj~mirna_level,data=mergedNonMiss)
#write.table(mergedNonMiss,file="~/Documents/Bioinformatics Final
Project/miRNA.txt",sep="\t",row.names=F,col.names=T,quote=F)
# methylation
path = "~/Documents/Bioinformatics Final Project/f933c567-d118-4823-b051-
dabb7c592497/DNA_Methylation/JHU_USC__HumanMethylation27/Level_3//"
files = list.files(path)
results = array(NA,dim=c(length(files),2))
for (i in 1:length(files)) {
  file = read.delim(file=paste(path,files[i],sep=""),header=T,stringsAsFactors=F)
  id2 = file$barcode
  beta_value = file$beta.value
  results[i,1]=id2[1]
  results[i,2]=mean(beta_value, na.rm=T)
}
names(results) = c("id2","mean_beta_value")
# merged with clinical
mergedClinical = merge(results,new_file,by.x="id2",by.y="id")
merged = mergedClinical
merged$time = merged$survival
living = which(merged$alive=="LIVING")
merged$time[living] = merged$followup[living]
merged$event = 1
merged$event[living] = 0
mergedNonMiss = merged[!is.na(merged$time),]
#write.table(mergedNonMiss,file="~/Documents/Bioinformatics Final
Project/miRNAGenes2.txt",sep="\t",row.names=F,col.names=T,quote=F)
# merge with remaining clinical data
```

```
path = "~/Documents/Bioinformatics Final Project/51fe2f4f-2417-4379-80c9-
18f122915a96/Clinical/Biotab/"
my_file = "clinical_patient_laml.txt"
file =
read.delim(file=paste(path,my_file,sep=""),header=T,stringsAsFactors=F,na.strin
gs=c("NA","[Not Available]","[Not Applicable]"))
mergedClinicalNonMiss =
merge(mergedNonMiss,file,by.x="id2",by.y="bcr_patient_barcode")
write.table(mergedClinicalNonMiss,file="~/Documents/Bioinformatics Final
Project/combinedresults4-18.txt",sep="\t",row.names=F,col.names=T,quote=F)
```

2.4. Cell culture

NB4 cells were cultured in Roswell Park Memorial Institute -1640 (RPMI-1640) with L-Glutamine (Lonza #12-702F) with 10% fetal bovine serum (FBS; Thermo Scientific SH30071.03) and 1X penicillin/ streptomycin/ amphotericin B (PSF; Calbiochem #516104). MV4-11 and K562 were cultured in Iscove's Modified Dubecco's Medium (IMDM) with Hepes and L-Glutamine (Lonza #12-722F) with 10% fetal bovine serum and 1X PSF. HL60 cells were grown in IMDM with Hepes and L-Glutamine with 20% fetal bovine serum and 1X PSF.

2.5. Transfection

For transfection, NB4 cells were transfected with mimic or hairpin inhibitor miR-125a using protocol suggested for Amaxa. Amaxa Cell Line Nucelofactor Kit V was suggested for transfection of NB4 cells. $1x10^6$ NB4 cells per condition were spun down and resuspended in 100uL of Nucleofactor Solution V composed of nucleofactor solution mixed with the supplement provided at a 4.5:1 ratio. 0.2nM of miRIDIAN Mimic hsa-miR-125a-5p (Thermo Scientific #C-300624-05-0005), miRIDIAN Hairpin Inhibitor hsa-miR-125a-5p (Thermo Scientific # IH-300624-06-0005), or control (Thermo Scientific # CN-001000-01) were then added to

mixture containing NB4 cells and nucleofactor solution. Mixture was transferred to cuvette provided and ran on Amaxa program X-001. Warmed RPMI media was immediately added and cells were plated into a 12-well plate.

2.6. Lentiviral transduction

NB4 cells were transduced with SMARTchoice human lentiviral (Figure 2.1.) hsa-miR-125a shMIMIC lentiviral particles (Thermo Scientific #V1SMHS_000872). miR-125a-5p lentivirus particles at a multiplicity of infection (MOI) between 10 and 15 were added to the NB4 cells at 37°C. For controls, SMARTchoice Human Lentiviral shMIMIC CAG/TurboGreen fluorescent protein (GFP; Thermo Scientific #VSH6185) were used at similar MOIs.

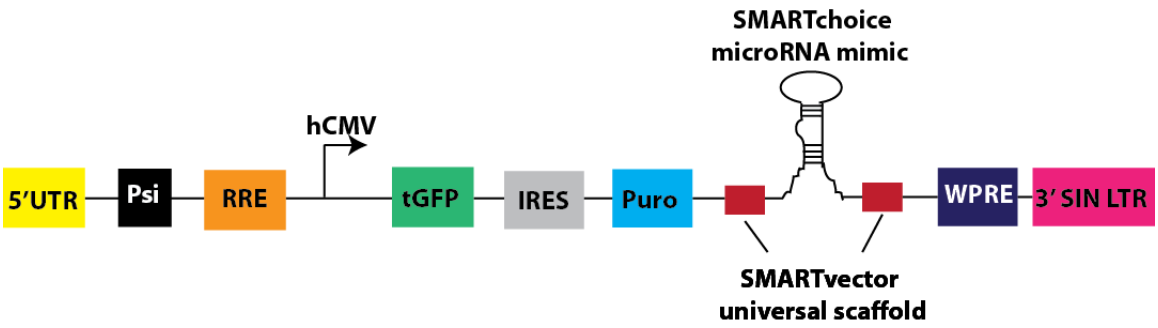

5'LTR: 5' Long Terminal Repeat - control center for retroviral gene expression
Psi: Psi Packaging sequence - viral genome packaging using lentiviral packaging systems
tGFP: TurboGFP - visual tracking of transduction and expression
IRES: Internal Ribosomal Entry Site - translation initiation in middle of mRNA sequence
Puro: Puromycin resistance
SMART vector universal scaffold: Universal primary miR context - mature miR embedded
WPRE: Woodchuck Hepatitis Post-Transcriptional Regulatory Element - enhances transgene expression in target cells
3' SIN LTR: 3" Self-inactivating Long Terminal Repeat - increased biosafety

Figure 2.1. SMARTchoice human lentiviral construct design for shMIMIC and TubroGreen control.

The cells were infected for 15 hours and then recovered in culture medium. Following puromycin selection for 8 weeks (final concentration 2µg puromycin) high transduction and expression of miR-125a-5p was confirmed by analysis of mature miR-125a expression using RT-qPCR and GFP expression on flow cytometry.

2.7 Inhibitors

NB4 cells were pre-treated with Decitabine (Selleck Chemicals #S1200) or dimethyl sulfoxide (DMSO) for control 24 hours before miR isolation or DNA isolation. Prior to selecting 10µM of Decitabine, a concentration curve was tested via analysis of miR-125a expression in response to Decitabine[116]. A range of Mubritinib concentration was first tested using the MTT proliferation assay based on Nagasawa et al findings [117]. After analysis, 0.5µM of Mubritinib was found to be effective and was used for the remaining experiments. NB4 cells or HL60 cells were pre-treated with Mubritinib (Selleck Chemicals #S2216) or DMSO for control 24 hours before miR isolation, MTT assay, and BrdU. NB4 cells were pre-treated with Mubritinib for 96 hours prior to Cd11b and Annexin-V analysis.

2.8. miRNA isolation and RT-qPCR

miRNA was isolated from cell lines using miRNeasy Mini Kit (Qiagen) following the manufacturer's instructions. For analysis of mature miR-125a, cDNA was made utilizing RT^2 miRNA First Strand Kit (SA Bioscience # 331401). cDNA was

made from CD34+ (Stem Cell Technologies #RNA-BM003C) and CD33+(Stem Cell Technologies #RNA-BM006C) RNA obtained from Stem Cell Technologies using the RT^2 miRNA First Strand Kit (SA Bioscience # 331401). Primers used in mature miR-125a analysis were hsa-miR-125a-5p (Qiagen #MPH00022A-200) and RNU-6 (Qiagen# MPH01653A-200). For analysis of precursor miR, cDNA was made utilizing the miSCRIPT RT II Kit (Qiagen # 218160). Primers used for analysis of precursor miR-125a were Hs_mir_125_1_PR (Qiagen# MP00000455), Hs_RNU6_2_1 (Qiagen miSCRIPT PCR Starter Kit # 218193), and 10X miSCRIPT Universal Primer (Qiagen miSCRIPT PCR Starter Kit# 218193). For Trib2 analysis, the following primers were used: Trib2 (Qiagen #PPH12973A-200) and GAPDH (Qiagen #PPH00150E-200). Sequences are not provided, as they are proprietary. Results were normalized to the RNU-6 or GAPDH (sets to 1) values using the 2(-Delta Delta C(T)) method [118].

2.9. Protein isolation and western blots

Protein was isolated from NB4 cells following pre-treatment with Mubritinib using RIPA buffer (0.05M Tris, 0.15M NaCl, 0.85% Triton X-100, 0.05% SDS, phosphatase inhibitor, and protease inhibitor). Cells were spun down and resuspended in 200µL of the above RIPA buffer followed by rotation for 30 minutes at 4°C. Samples were then sonicated for 30 seconds and then spun down for 10,000 rpm at 4°C for 15 minutes. 10 µL of the supernatant was transferred to a new tube for quantification. The remaining of the supernatant was transferred to a new tube and loading dye was added containing DTT.

Samples were then heated for 5 minutes at 95°C. Afterwards samples were either used immediately or stored at -20°C until needed. Following isolation, lysates were quantified by bichonic acid (BCA) assay kit (Thermo Scientific #23225). With this kit, albumin is provided in order to make a standard curve (0 mg/mL to 2 mg/mL) where OD (absorbance) is the X-axis and protein concentration (mg/mL) is the Y-axis. Using the equation of y = mx + b, where m is the slope and b is the y-intercept samples can be quantified. By taking the OD for each protein lysate, each sample can be quantified using the standard curve. 20-30µg of protein lysate was ran on a 10% Ready Gel Tris-HCL (Bio Rad #161-1155). A semi-dry transfer system was used for transfer of protein onto a nylon membrane. Following transfer, membranes were blocked for 1-hour in 1X SignalLOCK blocking solution (KPL #50-58-00). After 3 5-minutes washes with Tris-Saline Buffer with Tween-20 (TBST) membranes were soaked in primary antibodies. Primary antibodies were used at a concentration of 1:1000 diluted in 0.05X SignalLOCK blocking solution (KPL #50-58-00) and TBST. Prior to the addition of secondary antibodies, membranes were soaked in TBST for 3 5-minutes washes. Appropriate secondary antibodies were used at a concentration of 1:5000 in 0.025X SignalLOCK blocking solution and TBST. For Western blots, the following antibodies from Cell Signaling were used: HER2/ErbB2 (2165), P-HER2/ErbB2 (Y1221/1222) (#2243), AKT1 (#2938), P-AKT1 (S473) (#4058), p44/42 MAPK (#4695), P-p44/42 MAPK (T202/Y204) (#4370), and β-tubulin (#2128S). Blots were visualized using HyGLO Quick Spray (Denville Scientific #E2400). β-tubulin was used as a control to indicate equal loading of protein.

2.10. Bisulfite sequencing

NB4 cells were pre-treated with 10μM of Decitabine for 24 hours before DNA isolation using QIAamp DNA Mini Kit (Qiagen #51304) following the manufacturer's instructions. Isolated DNA was bisulfite converted following the manufacturer's instructions provided within the EpiTect Plus DNA Bisulfite Kit (Qiagen #59124). Upon completion of bisulfite converting DNA, samples were amplified using several primer sets surrounding upstream CpG islands from Gatto et al's work [119] and EpiMark Hot Start Taq DNA Polymerase (NE Biolabs #M04905). For the large CpG island one primer set as follows was used: Forward 5'-ATAGATGTGTAGAGATAGAAGGGAGGATAG-3' and Reverse 5'-AAACTAACCCAAATCCAAAAAAAA-3'. For the small CpG island nested PCR was utilized using the following primers: Forward (Outside) 5'-GAGAAAAGGGTTAGAGGTTTGGA-3', Reverse (Outside) 5'-CCACAAAAACACAACAAAAATAAAA-3', Forward (Inside) 5'-GTTTTTGATGAGGAAGGGGTTGAG-3', and Reverse (Inside) 5'-TTCCTCCCAAAATCCCTAAAACAAC-3'. To ensure the PCR was successful and products were the proper size, PCR products were analyzed on a 2% agarose gels. Following successful PCR amplification, PCR products were cloned using TOPO TA cloning kit for sequencing (Invitrogen #K4575-02). DNA was isolated using QIAamp DNA mini kit (Qiagen #51304) from several colonies grown in LB containing ampicillin. Samples were then sequenced and methylation status was determined.

2.11. MTT assay

Transduced NB4 cells or NB4 cells pre-treated for 24 hours with Mubritinib were analyzed for cell proliferation following the instruction manual provided within the Vybrant MTT Cell Proliferation Assay Kit (Invitrogen #V13154). Prior to starting, two solutions must be prepared, 12mM MTT (component A) stock solution and 0.01 M HCL-SDS (component B). For assays analyzed at 48 or 72 hours after cell plating, cells were plated at 10,000 cells per well. For assays analyzed at 24 hours, cells were plated at 50,000 cells per well. At time of analysis, cells are spun down and resuspended in media without supplements. As a control, wells containing only media were used. 10uL of the 12mM MTT stock solution is then added to each well and incubated for 4 hours at 37C. After the 4 hours incubation period, 100uL of 0.01 M HCL-SDS was added to each well followed by another 4-hour incubation period at 37C. Although the protocol states you can read samples as late as 16 hours post the addition of 0.01 M HCL-SDS, the sensitivity of the assay decreases with increased time. Therefore, samples were read at 4 hours post the addition of 0.01 M HCL-SDS at 570nm. Controls indicated no background noise and therefore raw optical density (OD, absorbance) samples were graphed representing cell proliferation.

2.12. Flow cytometry

Flow cytometry analyses were performed using FACS Calibur (BD Biosciences) for each of the following analyses.

2.12.1. Cell cycle analysis (BrdU)

Cell cycle progression of cells was conducted following the manufacturer's instructions included within the FITC BrdU Flow Kit (BD Pharmingen #51-2354AK). All solutions used within the following protocol were included within this kit. All centrifugation steps were completed at 2000rpm for 5 minutes. Prior to flow cytometry analysis, cells were pulsed with BrdU. For a control, samples containing no BrdU are used. From experimental testing, shorter pulses were more effective for identifying differences in cell cycle progression. After pulsing with BrdU was complete, cells were spun down and resuspended in 100 µL of BD Cytofix/Cytoperm buffer. Samples were then incubated on ice for 30 minutes. Cells were spun down and washed with 1mL of 1X BD Perm/Wash buffer. Supernatant is discarded and cells are resuspended in 100µL of BD Cytoperm Plus Buffer. Samples were then incubated on ice for 10 minutes. Cells were spun down and washed with 1mL of 1X BD Perm/Wash buffer. Supernatant is discarded and cells are resuspended in 100µL of BD Cytofix/ Cytoperm buffer and then incubated on ice for 5 minutes. Cells were spun down and washed with 1mL of 1X BD Perm/Wash buffer. Supernatant is discarded and cells are resuspended in 30 µg of DNase and incubated at 37°C for 1 hour. Cells were spun down and washed with 1mL of 1X BD Perm/Wash buffer. Supernatant is

discarded and cells are resuspended in 50 µL of BD Perm/Wash buffer containing anti-BrdU fluorescent antibody at a 1:50 ratio. Cells were then incubated for 20 minutes at room temperature wrapped in tin foil. Cells were spun down and washed with 1mL of 1X BD Perm/Wash buffer. Following this, cells were resuspended in 20 µL of 7-AAD followed by the addition of 1mL of staining buffer (1XDPBS with 3%FBS). Samples were then analyzed by flow cytometry.

2.12.2. Cell death analysis (annexin-V co-stained with PI)

For cell death analysis, cells were stained with APC Annexin-V (BD Pharmingen #550474) and Propidium Iodide (Invitrogen #P3566). All centrifugation steps were completed at 2000rpm for 5 minutes. Prior to staining, cells were washed twice with PBS and then resuspended in 1X annexin-V binding buffer (BD Bioscience #556454). Following the washes, cells were resuspended in 5 µL of APC Annexin-V and 5 µL of PI. There were three controls for this experiment, one sample stained only with Annexin-V, one sample stained only with PI, and one with no stain. Samples were gently vortexed and then incubated for 15 minutes at room temperature in tin foil. After incubation, 400µL of annexin-V binding buffer was added. Samples were then analyzed on flow cytometry.

2.12.3. Differentiation analysis (CD11b)

Prior to staining with CD11b, cells were washed in 500 µL of PBS. All centrifugation steps were completed at 2000rpm for 5 minutes. Cells were resuspended in 200 µL of PBS and 5 µL PE CD11b (BD Bioscience #561689). For a control, one sample contained no CD11b staining. Samples were incubated at room temperature for 30 minutes in tin foil. Following incubation, cells were spun down and resuspended in 500 µL of PBS and analyzed by flow cytometry.

2.12.4. ErbB2 protein analysis

Prior to staining with ErbB2, cells were washed in 500 µL of PBS. All centrifugation steps were completed at 2000rpm for 5 minutes. Several controls were used for this experiment. One sample had ErbB2 and rabbit IgG, a second sample had only secondary antibody, and lastly one sample had no staining. Cells were resuspended in 200 µL of PBS and 2 µL of ErbB2 (Cell Signaling #2165) and 1.5 µL of rabbit IgG, whole molecule (Jackson ImmunoResearch #011-000-003). Samples were incubated for 1-hour at 4°C rotating. Cells were then spun down and resuspended in 200 µL of PBS and 1 µL of secondary antibody (anti-rabbit Alexa Fluor 647; Cell Signaling #4414). Samples are then incubated for 20 minutes in tin foil at 4°C rotating. Following this incubation, cells are spun down and resuspended in 500 µL of PBS and analyzed by flow cytometry.

2.13. Gene expression profiling using microarrays

Three independent samples of RNA were isolated from NB4-GFP and NB4-miR-125a. Samples were sent to Vermont Genetics Network for profiling. The Vermont Genetics Network provided the following protocol.

Amplification of cDNA using the Ovation® Pico WTA System V2 from NuGEN: An RNA input of 50ng was used to generate cDNA through the First Strand and Second Strand synthesis reactions of the Ovation® Pico WTA System V2 from NuGEN. The cDNA samples were then purified using an Agencourt® RNAClean® XP magnetic bead protocol. Following purification, samples were amplified using SPIA reagents from the Ovation® Pico WTA System V2 from NuGEN. A final cDNA purification is performed using an Agencourt® RNAClean® XP magnetic bead protocol. Sample concentrations were determined using a 33ug/mL/A260 constant on a Nanodrop 1000 Spectrophotometer.

Fragmentation and Biotin Labeling using the Encore® Biotin Module from NuGEN: Approximately 4ug of cDNA generated using the Ovation® Pico WTA System V2 was fragmented and labeled using the Encore® Biotin Module from NuGEN. Efficiency of the biotin labeling reaction was verified using NeutrAvidin (10mg/mL) with a gel-shift assay.

Hybridization, Staining, and Scanning Arrays: Samples were injected into arrays and placed in the Affymetrix Genechip® Hybridization Oven 640 at 45° C and 60 RPM for 16-18 hours overnight. Arrays were stained using the Affymetrix Genechip® Fluidics Station 450 and scanned with the Affymetrix Genechip® Scanner 3000.

2.14. Bioinformatics analysis for gene expression profiling

Data Analysis: Raw data in the form of six Affymetrix CEL files (three experimental and three control) were imported into the Exon Workflow in Partek Genomics Suite version 6.6 (Partek, St Louis, MO, USA, www.partek.com). Background correction, quantile normalization, log2 transformation, and probe set summarization were performed using default settings for the Robust Multichip Average (RMA). Principal component analysis (PCA) was implemented with default settings as part of the quality control of the data.

Differential expression between two groups of NB4 cell lines, miR 125a (experimental) and GFP (control) was predicted at both the gene-level (probe sets summarized into transcript clusters/genes) and at the exon-level (alternative splicing analysis). One-way analysis of variance (ANOVA) was used to compare the individual gene expression data with respect to NB4 cell line, miR 125a versus GFP control. Multiple comparison correction was performed using Benjamini-Hochberg false discovery rate (FDR). Differentially expressed genes were defined based on an absolute fold change >1.5 in combination with an unadjusted $p<0.05$. Input for a hierarchical clustering analysis at the gene level utilized the set of genes that met these criteria. Alternative splice variants were defined by an absolute fold change >1.5 and a FDR of 0.05.

In addition differential expression at the individual gene or exon level, we examined differential expression of functional groups using GO-ANOVA and Pathway-ANOVA as implemented in Partek. Pathway-ANOVA uses the KEGG database, and GO-ANOVA the GO database, to find not only differentially

regulated functional groups or pathways, but also functional groups, which are "disrupted" in only a few genes. Disrupted functional groups do not necessarily exhibit differential expression as well. Both GO- and Pathway-ANOVA are performed on the normalized data directly without any filtering. The parameters for the Pathway-ANOVA were configured such that only pathways with more than two genes and fewer than 2000 genes are considered in the analysis.

2.15. Luciferase reporter assay

Wild type (GeneCopoeia # HmiT055404-MT01) and mutant (GeneCopoeia # CS-HmiT055404-MT01-01) 3'UTR luciferase reporter constructs in pEZX-MT01 vector (GeneCopoeia) (Figure 2.2.) containing both hLUC and hRLUC for Trib2 was generated. For mutant Trib2, two bases in the seed sequence were made: UCAGGGA to UCCAGGA. GeneCopoeia made constructs after mutant sequences were provided through their customized products. The night prior to transfection, 1.2 x10^5 HeLa cells/ well were plated in 500 µL of media in a 24 well plate. The next day, media was aspirated and washed with PBS. 400 µL antibiotic free media was added. In one tube, a 500ng of wildtype or mutant Trib2 were mixed with 0.1nM of miRIDIAN Mimic hsa-miR-125a (Thermo Scientific #C-300624-05-0005). In a second tube, 2 µL of Dharmafect Duo (ThermoScientific) with 83 µL of serum-free media were mixed. These two mixtures were incubated for 5 minutes prior to mixing them. After this incubation, tubes were mixed followed by a 20-minute incubation. Upon completion of this incubation, mixture was added drop wise into HeLa cells. Cells were then incubated at 37°C for 48

hours prior to reading samples. Luciferase and renilla expression was analyzed using a dual luciferase kit following manufacturer instructions (Promega). All solutions were provided by dual luciferase kit. For this analysis, media was aspirated and 100 µL of 1X PLB was added to each well. Plate was rocked for 15 minutes at room temperature for lysis of cells. For reading luciferase, 100 µL of LAR II was added to a vial prior to reading samples. When ready to read samples, 20 µL of lysate was added to LAR II followed by reading sample on luminometer. Immediately following this reading, 100 µL of Stop & Glo was added. Sample was quickly mixed via vortex and read on the luminometer. To normalize samples, luciferase expression was divided by renilla expression for each sample.

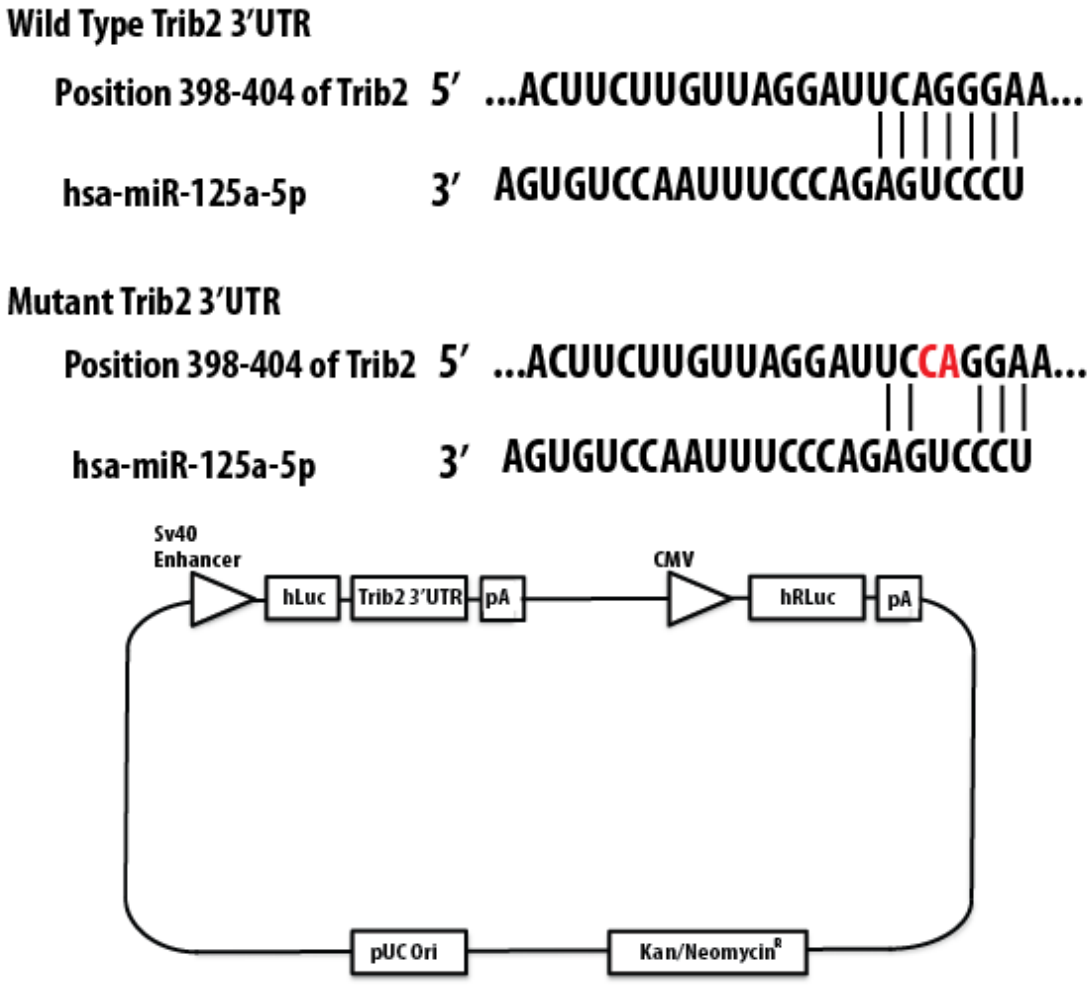

Figure 2.2. Construct for wildtype and mutant Trib2 3'UTR. Lines connecting nucleotides in seed sequences demonstrate interaction between miR-125 and Trib2. Bases in red in mutant Trib2 represent base pairs changed to disrupt interaction between mIR-125a and Trib2. hLuc represents humanized firefly luciferase; Trib2 3'UTR represents sequence for Trib2 3'UTR; pA represents poly A tail; CMV represent the promoter; hRLuc represents humanized renilla luciferase; pUC represent the origin of replication, and Kan/Neomycin represent antibiotic selection.

2.16. NB4 human leukemic xenograft model and histology

Prior to initiation of studies, experiments were approved by IACUC. For NB4-GFP and NB4-mimic miR-125a studies, $5x10^6$ cells in PBS were subcutaneously injected into the left flank of six 5-6 week old female mice per cell type of NOD.CB17-Prkdc scid/J mice (Jackson Laboratory #001303). For Mubritinib studies $3x10^6$ NB4 cells were subcutaneously injected into the left flank of twenty-four 5-6 week old female NOD.CB17-Prkdc scid/J mice (Jackson Laboratory #001303). Mice were randomized for treatment with Mubritinib or vehicle prior to start of experiment. Seven mice from the Mubritinib group and ten mice from the vehicle group formed tumors and progressed to the treatment stage. The remaining seven mice that were monitored throughout the study but never developed tumors and therefore were not included in treatments. Two treatments of 20miligram/ kilogram (mg/kg) Mubritinib or vehicle (DMSO) was given on the first day as a loading dose followed by daily treatment of 20mg/kg of Mubritinib or vehicle via oral gavage. The final two tumor measurements and the tumor collection were performed in a blinded manner. For both studies, tumor measurements were conducted throughout the course of study and tumor volume was calculated by the following equation: tumor volume = (AxB^2) x ½ where A equals the longer dimension and B equals the shorter dimension.
At time of tumor excision, mouse weight, tumor weight, and tumor volume were collected blindly. Excised tumors were placed into approximately 20X the tumor volume in 10% neutral buffered formaldehyde for at least 24 hours. Larger tumors were left in 10% neutral buffered formaldehyde for approximately 36

hours to allow for proper fixation. Tumors were then transferred to 70% alcohol prior to being paraffin embedded. After tumors were paraffin embedded, they were sectioned and stained for hematoxylin and eosin (H&E), Ki-67, and caspase-3 in accordance with standard immunohistochemistry protocols by the MMCRI histology core. The following protocols for H&E, Ki-67 (1:250), and caspase-3 (1:50) were provided by the MMCRI histology core for processing of the above samples.

Section Deparaffinization-Rehydration (Run down) Procedure

Purpose: To rehydrate slide sections in preparation for staining.

Principle: Paraffin is dissolved in clearing agent then a series of decreasing strengths of alcohol and finally water rehydrates the tissue.

Fixative: Various fixatives used prior to paraffin infiltration.

Equipment: Run down table containing clearing agent and alcohol containers located under the hood.

Technique: Paraffin sections are cut at 4 to 5 um.

Quality Control: As indicated for specific staining procedure.

Reagents: Clearing agent (Ex. Xylene) and ethyl alcohol.

Procedure:

NOTE: With the beginning of each station, slides should be dipped 10 to 20 times.

NOTE: Between each station, lift slides from previous station and let drain till no more solution runs off.

1. Clearing agent for 10 min.
2. Clearing agent for 10 min.
3. Clearing agent for 10 min.
4. 100% ethyl alcohol for 2 min.

5. 100% ethyl alcohol for 2 min.
6. 95 % ethyl alcohol for 1 min.
7. Wash in running tap water for 5 min.
8. Keep slides in distilled water until ready to stain.

H&E Procedure (Regressive Method)

Purpose: To differentially stain tissue sections for microscopic structural observation.

Principle: Hematoxylin is a natural dye from the heartwood of a logwood tree and in its oxidized state is called hematein, a weak anionic (negatively charged) dye. When combined with a metallic mordant, it gains a strong affinity for nuclei. In regressive staining methods, the tissue is overstained and then differentiated leaving the desired element emphasized. In this procedure, a weak solution of acetic acid is used to differentiate the nuclear staining to provide detailed chromatin patterns. Formaldehyde and some other fixatives increase tissue basophilia (the ability to uptake cationic dyes). Eosin is a sodium salt and at a pH < 6.0 develops a net positive charge on the protein creating an affinity for the negatively charged tissue.

Fixative: neutral buffered formalin, Carnoy's, Bouins and various others.

Equipment: Run down/up table containing clearing agent and alcohol containers and H&E staining setup.

Technique: Paraffin sections are cut at 4 to 5 um.

Quality Control: Most any tissue type will demonstrate good differentiation of H&E staining.

Reagents:
Hematoxylin III – Richard Alan #7231

Bluing Agent – Richard Alan #7301
Alternative Bluing Agents – 0.25% Ammonia Water OR 0.5% Lithium Carbonate

5% Acetic Acid	100 ml	250 ml
Glacial Acetic Acid	5 ml	25 ml
DdH2O	95 ml	225 ml

Eosin Y – Richard Alan #7111

Procedure:

1. Deparaffinize and rehydrate sections according to run down procedure.
2. Rinse well in tap water.
3. Place slides in Hematoxylin for 5 min. (**NOTE**: Tissues are most venerable to lifting off slides at this point.)
4. Wash gently in tap water until water runs clear.
5. Differentiate in 5% Acetic Acid for 1 min.
6. Wash in tap water.
7. Blue in Bluing Agent for 2 min. (**NOTE**: Nuclear stain changes from violet to bluish color.)
8. Wash in tap water.
9. Place in 95% ethanol for 1 min.
10. Stain in Eosin Y for 2 min.
11. Rinse in two changes of 95% ethanol for 30 seconds each.
12. Dehydrate in three changes of 100% ethanol, clear and mount with synthetic resin. (Ex. Permount@).

Results: Nuclei . . . . . blue
Cytoplasm, other structures . . . . . variations of pink
Erythrocytes, collagen and muscle cytoplasm should stain three different shades of pink.

Reference: Carson, Freida, Histotechnology, A Self-Instructional Text, pg 93-105

IHC Caspase-3 and Ki-67 Antibody- Purified (ABC Kit from Vector)

Purpose: To detect antigens at the cellular level in tissue sections using avidin/biotin complex signal amplification.

Fixative: formalin

Equipment: Steamer, incubation chamber, pipets.

Technique: 5 um sections (2 slides- one for antibody, one for negative control IgG)

Quality Control: same as for Tunel stain, small intestine, skin, thymus and testes from 4-wk old mice
(2 slides- one for antibody, one for negative control IgG)

Reagents:
For the following, see "Buffer Solutions" document:
1x Tris buffered saline pH 7.6 with 0.05% Tween (TBS-T working)
1x PBS pH 7.2
PBS with 3% H_20_2 – make fresh
PBS with 0.05% Tween 20 (PBS-T)
DAB working – make fresh

10x Target Retrieval Buffer (Dako S1699, dilute 1:10. An alternative is Citrate Buffer.)

Citrate Buffer pH 6.0
Stock Sol A – 0.1M Citric Acid monohydrate (FW 210.14) 2.1 g
ddH20 100 ml

Stock Sol B – 0.1M Sodium Citrate Tribasic dihydrate (FW 294.1) 14.7 g
ddH20 500 ml

10x Citrate Buffer pH 6.0 (0.1M, stored at 4°C)
Sol A 90 ml
Sol B 410 ml
pH to 6.0 with NaOH

10mM Sodium Citrate Buffer Working with 0.05% Tween 20 (make fresh)
10x Citrate Buffer pH 6.0 25 ml
ddH20 225 ml
Tween 20 0.125 ml

1% Bovine Serum Albumin (BSA Stock, stored at -20°C)
Bovine Serum Albumin 0.5 g
PBS 50 ml
Let stand for 10-15 min to dissolve BSA, gently mix and freeze in 10 ml aliquots.

2% - 5% Normal Goat Serum Blocking Buffer
Normal Goat Serum 0.2 – 0.5 ml
1% BSA 10 ml

Vector A/B blocking kit (SP2001)

Vector ABC kit (Avidin/Biotin Complex amplification reagent, PK6100, prepare 30 min before use)

PBS 1ml
Sol A 20 ul
Sol B 20 ul

Primary Antibody- Rabbit polyclonal Cleaved Caspase-3 antibody for human, mouse and rat.

(Cell Signaling 9664L, 300ul size received in 50% glycerin, stored at -20°C, **NO dilution factor adjustment needed for glycerin.**)

Negative Control- ChromPure Rabbit IgG, whole molecule

(Jackson 011-000-003, approx. 11 mg/ml, stored at -20°C)

Secondary Antibody- Biotin-SP-conjugated Goat Anti-Rabbit IgG (H&L)

(Jackson 111-065-144 mouse absorbed, approx 1.4 mg/ml, stored at -20°C)

Gill Hematoxylin or Methyl Green Solution – see "IHC Nuclear Counterstain" document

Procedure:

1. Deparaffinize sections down to 100% ethanol according to run down procedure (**For Frozen sections, see Note 4.)**
2. Remove from 100% ethanol and let slides dry completely.
3. Encircle tissue with PapPen, lay slide flat and allow to dry for several minutes.
4. Pre-warm the antigen retrieval steamer by filling it with distilled water to fill line, plugging it in and turning the steamer timer past 45 min.
5. Wash slides in running tap water and rinse in distilled water.
6. Antigen retrieve formalin-fixed tissue by putting the slides in a rack and placing the rack in 250 ml of working 10 mM Citrate Buffer in a staining dish. Once steam is escaping, place the uncovered buffer dish in the holder of the steamer, place cover on steamer and steam for 30 min. (NOTE: For white coplin jars, steam 25 min. If steamer is cold, antigen retrieve slides for pre-warm time plus 30 min.)
7. After steamer has shut off, place staining dish on counter to cool for 20 min.
8. Wash in tap water and then rinse in distilled water.

9. Rinse 2 x 5 min in TBS-T.
10. Block slides with normal goat serum blocking buffer for 30 min.
11. Wash slides in TBS-T buffer 2 x 5 min.
12. Biotin block with Vector A/B blocking kit as follows
    a. Avidin (1-3 drops to cover tissue) for 15 min
    b. Wash slides in TBS-T 5 min.
    c. Biotin (1-3 drops to cover tissue) for 15 min
13. Wash slides in TBS-T buffer 2 x 5 min.
14. Incubate with primary antibody Caspase-3 diluted 1:50 or Ki-67 diluted 1:250 in blocking buffer (**see Note 1**) **ON at 4°C**. (**NOTE**: Dilute Neg control IgG to same concentration in ug/ml. May require an intermediate dilution step of 1:100 first before acquiring final dilution concentration.)
15. Wash slides in TBS-T buffer 4 x 15 min on a gentle rotator.
16. Incubate with secondary antibody diluted in PBS 1:500 (**see Note 1)** for 30 min. (**NOTE**: Make ABC reagent.)
17. Wash slides in TBS-T buffer 3 x 5 min.
18. Block endogenous peroxidase with 3% H_2O_2 in PBS for 15 min. **(For Frozen Sections use 0.3% H_2O_2 in 0.1% NaAzide in PBS for 15 min)**
19. Wash slides in TBS-T buffer 2 x 5 min.
20. Incubate with ABC amplification reagent for 30 min.
21. Wash slides in TBS-T buffer 4 x 5 min. (save last wash buffer)
22. Incubate slides in working DAB for 2-10 min. **Check every min after 2 min.**
23. Wash slides in tap water.
24. Counterstain in Gill Hematoxylin for 30 to 90 sec.
25. Wash in tap water for 1 min.
26. Blue in saved last wash buffer from previous steps for 1 min.
27. Wash in tap water for 1 min.
28. Dehydrate, clear and mount with synthetic resin. (Ex. Permount@).

Results: Nuclei . . . . . blue (or green if blue if Methyl Green was used)

Antigen sites . . . . . brown

Non-specific sites . . . . . light brown to brown

Notes:

1. Antibodies stored diluted 50% with glycerol must have dilutions doubled. Example, a 1:100 dilution would require a 2:100 mixture.
2. For cell surface/membrane antigen targets, do NOT include detergent (ie. Tween 20) in diluents or wash buffers as this may cause stripping or alteration of cell surface antigens.
3. Other chromogenic or fluorescence visualization options are available with the purchase and substitution of the appropriate streptavidin conjugate in place of the SA-HRP. SA-AP can be used with alkaline phosphatase chromogenic substrates such as BCIP/NBT. There are several SA-fluorophores available like SA-Fluorescein, SA-Texa Red and SA-Coumarin.
4. For Frozen sections, warm at 60°C for 10 min, dDH2O for 30 min, 60°C for 10 min, then PapPen.

Background:

Caspase-3 (CPP-32, Apoptain, Yama, SCA-1) is a critical executioner of apoptosis, as it is either partially or totally responsible for the proteolytic cleavage of many key proteins such as the nuclear enzyme poly (ADP-ribose) polymerase (PARP) (1). Activation of caspase-3 requires proteolytic processing of its inactive zymogen into activated p17 and p12 fragments. Cleavage of caspase-3 requires aspartic acid at the P1 position (2).

Reference:

1. Vector ABC kit (PK6100) package insert.
2. Vector A/B blocking kit (SP2001) package insert.
3. IHC World at www.ihcworld.com.
4. Cell Signaling Caspase-3 antibody specification sheet 9664L.

CHAPTER 3: DECREASED MIR-125A PROVIDES A SURVIVAL AND PROLIFERATIVE ADVANTAGE TO LEUKEMIC BLASTS

3.1. Characterizing miR-125a expression in clinical samples

Previously it was shown that miR-125a was decreased in cytogenetically normal AML, however, additional AML subtypes were not analyzed in the study. Studies indicate that miR-125a effects HSC self - renewal and maintenance whereas remaining of the cluster, miR-99b and miR-let7e, do not have a functional role in hematopoiesis. Originally, miR was isolated from 58 paraffin embedded samples. The quality of the miR however was not good for many of the samples, therefore, 34 samples were used in analyzing miR-99b, miR-let7e, and miR-125a (Appendix A; Figures A.1., A.2., and A.3.). Due to the lack of amount of miR available for each sample, many of samples were run in duplicate and therefore statistics was not conducted. Since miR-125a was the focus of this work, samples were ran in three independent experiments in order to establish miR-125a's expression level in AML (Figure 3.1.). miR-125a expression from paraffin embedded bone marrow, the entire miR-125a cluster was decreased although they were not always decreased in the same sample Appendix A; Figures A.1., A.2., and A.3.). Sixty two percent of patient samples were decreased in miR-99b, seventy one percent had decreased miR-Let7e, and forty one percent had decreased miR-125a expression.

Due to the lack of clinical information provided with paraffin embedded tissue samples, classification of a specific AML FAB that represented low miR-

125a expression was not possible. From samples where classification was provided, FAB M5 had the most samples with low miR-125a, however many of the samples had unknown classification (Figure A.3.D). From this analysis it was gained that miR-125a expression as well as its cluster were decreased beyond cytogenetically normal AML however its classification remained inconclusive.

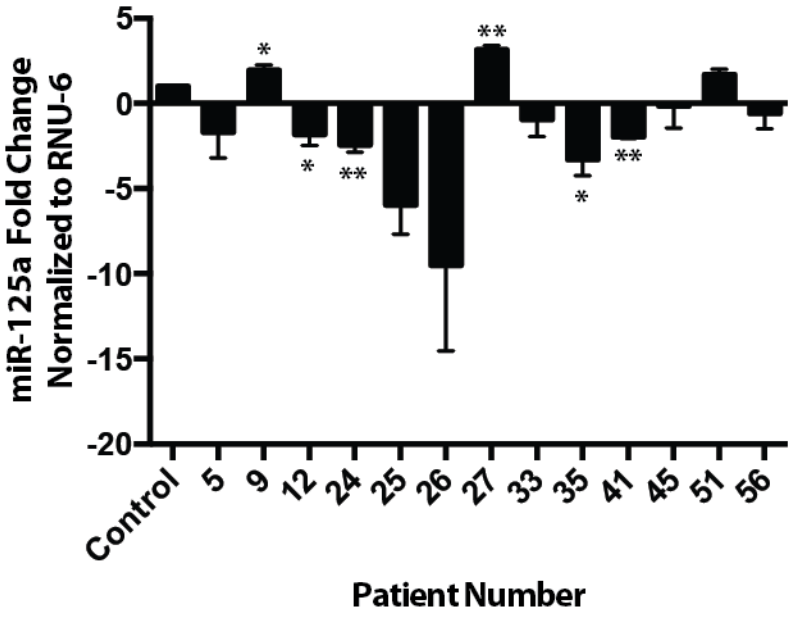

Figure 3.1. miR-125a expression is significantly decreased in AML from paraffin embedded bone marrow samples. miR-125a expression in paraffin embedded bone marrow samples from AML patients and healthy CD34+ (HSC) samples (control). Results are means +/- SD and * p-value = <0.05.

To further study miR-125a expression in AML, small RNA sequencing results from clinical patients samples were analyzed at both time of diagnosis and relapse in collaboration with Dr. Daniel Link (Figure 3.2. A). These results demonstrated that at both time of diagnosis and relapse miR-125a was significantly decreased in comparison to healthy CD34+ controls for all AML FAB

classifications. Similar to results from paraffin embedded bone marrow samples, multiple AML FAB subtypes demonstrated low miR-125a expression. Though miR-125a expression is decreased at both diagnosis and relapse, there is a trend that its expression is lowest at diagnosis and slightly increased at relapse with exception the FAB M2. Further, miR-125a expression is lowest at FAB M5 and highest in FAB M3 (Figure 3.2. B). The majority of the samples are significantly decreased, however for some subtypes there were only one sample and therefore statistical significance analysis could not be completed (FAB M0 at diagnosis and relapse; M3 at relapse).

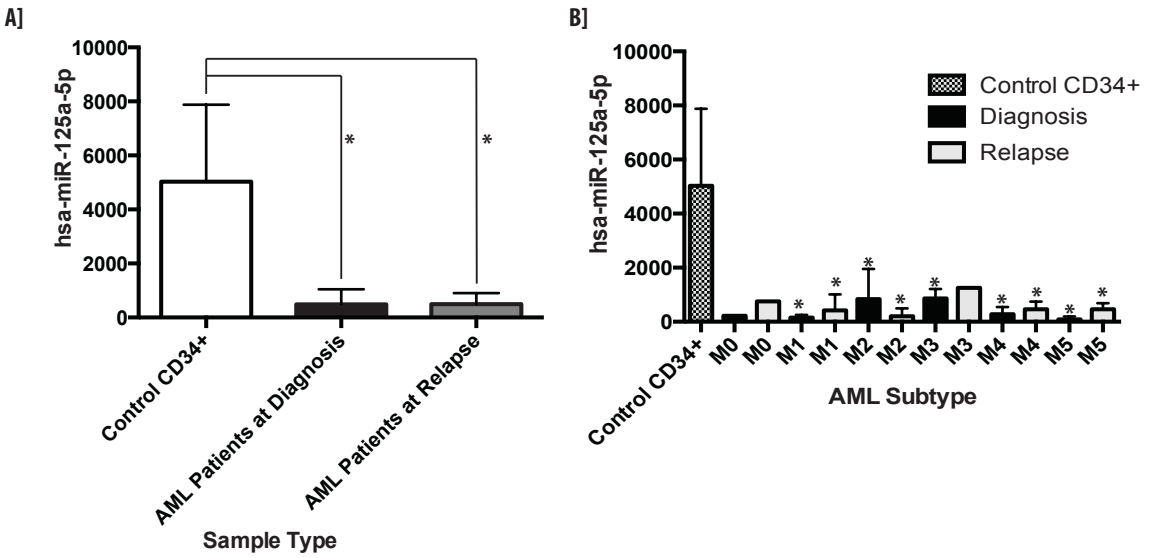

Figure 3.2. Small RNA sequencing of miR-125a reveals miR-125a expression is decreased at both time of diagnosis and relapse. A] Normalized small RNA sequencing miR-125a-5p expression levels from clinical AML samples at time of diagnosis and their correlated relapse values (for some) in comparison to healthy control bone marrow CD34+ cells. Expression values of miR-125-5p were normalized to the total number of miR reads in that sample. B] French-American-British AML subtype classification of clinical AML samples and their corresponding normalized small RNA sequencing miR-125a-5p expression level. P-values calculated for each subtype in comparison to control CD34+ sample. Results are means +/- SD and * p-value = <0.05.

miR-125a expression analysis from paraffin embedded bone marrow and small RNA sequencing from AML clinical samples it is established that miR-125a expression is decreased in multiple AML subtypes. To understand miR-125a expression in relation to clinical data, miR-125a expression was analyzed from samples on the National Cancer Institute Cancer Genome Atlas Data Portal (TCGA) (Figure 3.3.). For this analysis, clinical information and miR expession information were downloded. The clinical file downloaded contained eight separate files whereas the miR expression file contained three hundred and seventy four miR expression files. Within the miR files downloaded, two types of files were donwloaded: isoform quantification and miR quantification. Each miR quantification file contained aproximately seven hundred and six miR expression results. To assist with analyzing miR-125a expression and its relation to clinical data for each patient R code was written allowing this information combined into one data file.

From miR-125a expression analysis, the majority of the patient samples had between 1 and 250 reads per million as visible in the histogram (Figure 3.3.. A and B). No difference between miR-125a expression and gender or age of diagnosis was found (Figure 3.3. C and D). Though a significant difference appears between ethnicity, there was only one patient within the Hispanic or Latino group (Figure 3.3. E). AML FAB classification of miR-125a expression revealed that subtype M5 has the lowest miR-125a expression. To further dissect low miR-125a classification in AML, cytogenetic and molecular abnormalities were analyzed, however due to the complexity of the disease, no specific

classification could be identified (Tables 3.1. and 3.2.). Many of the patients had their own unique molecular and cytogenetic abnormality (Tables 3.1. and 3.2.). miR-125a expression was most decreased in favorable and intermediate AML prognostic. Low miR-125a was associated with decreased survival (Figure 3.4. A and B). Although the TCGA is useful for analysis of miR-125a expression and correlation to clinical samples, at this time a healthy control was not available.

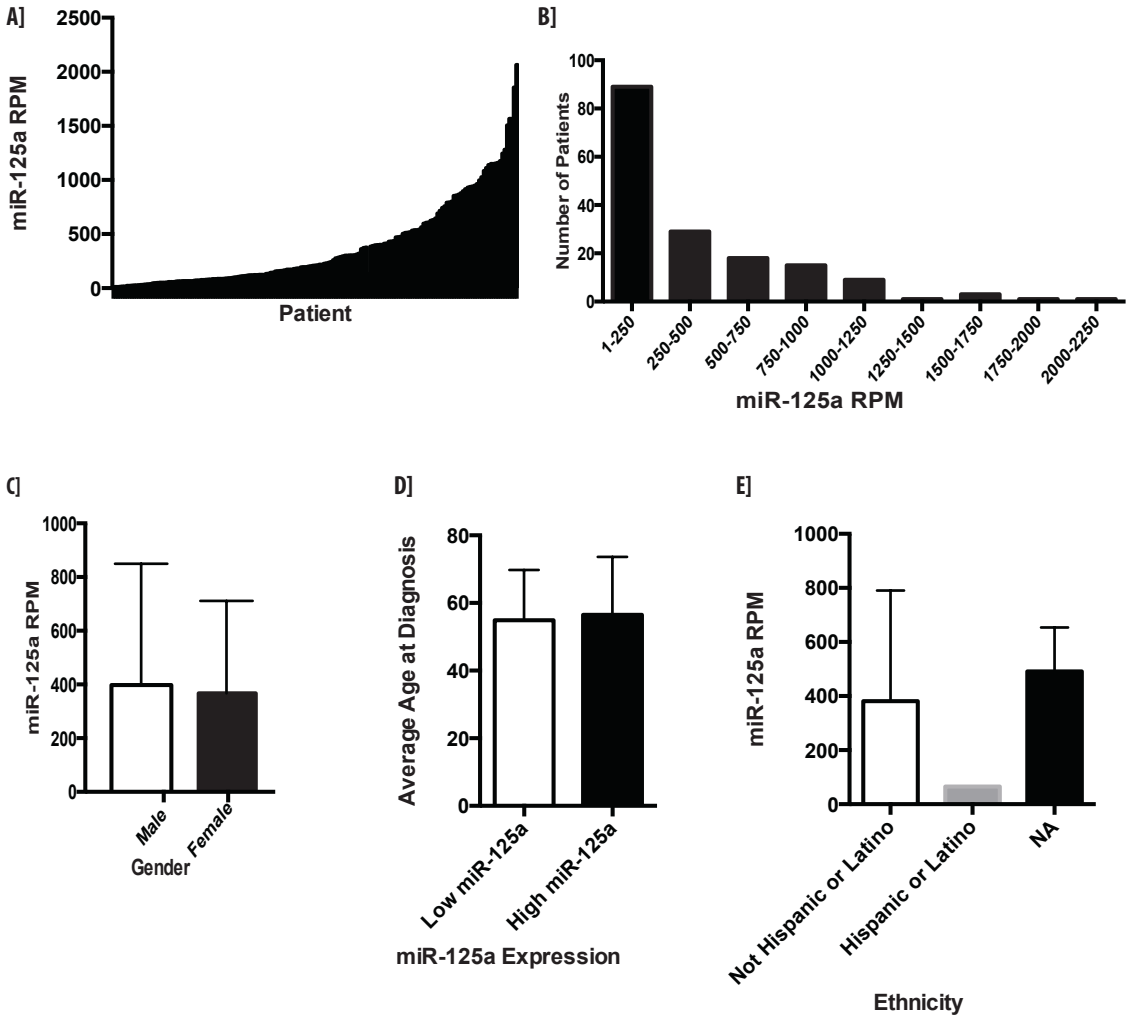

Figure 3.3. miR-125a analysis in clinical patient samples from the National Cancer Institute Cancer Genome Atlas Data Portal. A] miR-125a expression in clinical patients revealed a large range of miR-125a expression in AML B] Histogram of miR-125a expression from clinical samples C] miR-125a expression correlated to gender. miR-125a expression was sorted from lowest to highest. Samples above the median were considered high miR-125a expression and samples below the median were considered low miR-125a expression. Results are means +/- SD and are not significant. D] miR-125a expression correlated to age of diagnosis. Results are means +/- SD and are not significant. E] miR-125a expression correlated to ethnicity. NA refers to non-applicable since information was not provided. Results are means +/- SD and are not significant.

Cytogenetic Abnormality	Average miR-125a Expression	Number of Patients
Normal|del (7q) / 7q-|t (9;11)	49.624066	1
Normal|t (9;11)	64.877377	1
Normal|Complex (greater than or equal to 3 distinct abnormalities)|Trisomy 8	75.427722	1
inv (16)	130.169189	4
Normal|t (8;21)	157.602973	1
Complex (greater than or equal to 3 distinct abnormalities)|t (15;17)	178.950872	1
del (5q) / 5q-|del (7q) / 7q-	235.658872	1
Normal|inv (16)	256.431326	5
Normal	261.506684	88
del (7q) / 7q-	295.44962	1
t (8;21)	331.202216	6
del (5q) / 5q-	361.337313	1
NA	363.608544	16
(blank)	397.971651	1
Normal|t (15;17)	399.425442	4
Normal|del (5q) / 5q-|del (7q) / 7q-	400.347925	1
Complex (greater than or equal to 3 distinct abnormalities)|del (5q) / 5q-	429.130049	3
Normal|del (7q) / 7q-|Trisomy 8|t (15;17)	431.808151	1
t (15;17)	443.139113	7
Normal|del (7q) / 7q-	518.40224	4
Complex (greater than or equal to 3 distinct abnormalities)|del (5q) / 5q-|del (7q) / 7q-|Trisomy 8	566.75145	2
Complex (greater than or equal to 3 distinct abnormalities)|del (5q) / 5q-|Trisomy 8	638.594193	2
Trisomy 8|t (15;17)	689.651542	1
Trisomy 8	775.12554	5
Normal|Trisomy 8	798.711805	3
Normal|Complex (greater than or equal to 3 distinct abnormalities)|del (7q) / 7q-	817.849251	2
Complex (greater than or equal to 3 distinct abnormalities)	833.390703	3
Complex (greater than or equal to 3 distinct abnormalities)|del (7q) / 7q-|Trisomy 8	896.020853	1
Complex (greater than or equal to 3 distinct abnormalities)|del (5q) / 5q-|del (7q) / 7q-	925.71156	4
Normal|Complex (greater than or equal to 3 distinct abnormalities)	1138.63934	1
Normal|Complex (greater than or equal to 3 distinct abnormalities)|del (7q) / 7q-|Trisomy 8	1176.15985	1
Complex (greater than or equal to 3 distinct abnormalities)|Trisomy 8	1507.23168	2

Table 3.1. Cytogenetic abnormality of AML patients relationship to miR-125a expression and number of individuals with each cytogenetic classification from TCGA. Though 50% of samples are cytogenetically normal, the majority of the remaining 50% of samples have a unique cytogenetic signature. These data indicate the complexity in classifiying low miR-125a expression.

Molecular Abnormality	Average miR-125a Expression	Number of Patients
BCR-ABL Negative|FLT3 Mutation Negative|IDH1 R132 Negative|IDH1 R140 Negative|IDH1 R172 Negative|Activating RAS Negative|NPMc Negative	413.668501	3
BCR-ABL Negative|FLT3 Mutation Negative|IDH1 R132 Negative|IDH1 R140 Positive|IDH1 R172 Negative|Activating RAS Negative|NPMc Negative	939.898322	1
BCR-ABL Negative|FLT3 Mutation Negative|IDH1 R132 Positive|IDH1 R140 Negative|IDH1 R172 Negative|Activating RAS Negative|NPMc Negative	606.735113	1
BCR-ABL Negative|FLT3 Mutation Positive|IDH1 R132 Negative|IDH1 R140 Negative|IDH1 R172 Negative|Activating RAS Negative|NPMc Negative	87.331091	1
BCR-ABL Negative|FLT3 Mutation Positive|IDH1 R132 Negative|IDH1 R140 Negative|IDH1 R172 Negative|Activating RAS Negative|NPMc Positive	21.973298	2
BCR-ABL Negative|FLT3 Mutation Positive|IDH1 R132 Positive|IDH1 R140 Negative|IDH1 R172 Negative|Activating RAS Negative|NPMc Positive	714.776776	1

Table 3.2. Molecular abnormality of AML patients relationship to miR-125a expression and number of individuals with each cytogenetic classification in TCGA analysis. Results show that there is a large range of molecular abnormalities and further that many samples had their own molecular signature. These data indicate the complexity in classifiying low miR-125a expression.

Table 3.2 Continued

Molecular Abnormality	Average miR-125a Expression	Number of Patients
BCR-ABL Negative|PML-RAR Negative|FLT3 Mutation Positive|IDH1 R132 Negative|IDH1 R140 Negative|IDH1 R172 Negative|Activating RAS Negative|NPMc Negative	11.269757	1
BCR-ABL Negative|PML-RAR Not Tested|FLT3 Mutation Negative|IDH1 R132 Positive|IDH1 R140 Negative|IDH1 R172 Negative|Activating RAS Negative|NPMc Negative	158.711775	1
BCR-ABL Negative|PML-RAR Not Tested|FLT3 Mutation Positive|IDH1 R132 Negative|IDH1 R140 Negative|IDH1 R172 Negative|Activating RAS Negative|NPMc Negative	375.393539	1
FLT3 Mutation Negative|IDH1 R132 Negative|IDH1 R140 Negative|IDH1 R172 Negative|Activating RAS Negative|NPMc Negative	425.494478	69
FLT3 Mutation Negative|IDH1 R132 Negative|IDH1 R140 Negative|IDH1 R172 Negative|Activating RAS Negative|NPMc Positive	151.2115465	13
FLT3 Mutation Negative|IDH1 R132 Negative|IDH1 R140 Negative|IDH1 R172 Negative|Activating RAS Positive|NPMc Negative	564.471039	6
FLT3 Mutation Negative|IDH1 R132 Negative|IDH1 R140 Negative|IDH1 R172 Negative|Activating RAS Positive|NPMc Positive	99.961302	1

Table 3.2 Continued

Molecular Abnormality	Average miR-125a Expression	Number of Patients
FLT3 Mutation Negative|IDH1 R132 Negative|IDH1 R140 Negative|IDH1 R172 Positive|Activating RAS Negative|NPMc Negative	1148.336868	1
FLT3 Mutation Negative|IDH1 R132 Negative|IDH1 R140 Positive|IDH1 R172 Negative|Activating RAS Negative|NPMc Negative	489.5893413	6
FLT3 Mutation Negative|IDH1 R132 Negative|IDH1 R140 Positive|IDH1 R172 Negative|Activating RAS Negative|NPMc Positive	132.9821933	3
FLT3 Mutation Negative|IDH1 R132 Positive|IDH1 R140 Negative|IDH1 R172 Negative|Activating RAS Negative|NPMc Negative	997.6591697	3
FLT3 Mutation Negative|IDH1 R132 Positive|IDH1 R140 Negative|IDH1 R172 Negative|Activating RAS Negative|NPMc Positive	366.8583073	3
FLT3 Mutation Negative|IDH1 R132 Positive|IDH1 R140 Negative|IDH1 R172 Negative|Activating RAS Positive|NPMc Positive	1152.467473	1
FLT3 Mutation Negative|IDH1 R132 Positive|IDH1 R140 Negative|IDH1 R172 Positive|Activating RAS Negative|NPMc Negative	2062.910544	1
FLT3 Mutation Negative|IDH1 R140 Negative|IDH1 R172 Negative|Activating RAS Negative|NPMc Negative	689.651542	1

Table 3.2 Continued

Molecular Abnormality	Average miR-125a Expression	Number of Patients
FLT3 Mutation Positive|IDH1 R132 Negative|IDH1 R140 Negative|IDH1 R172 Negative|Activating RAS Negative|NPMc Negative	295.6991016	20
FLT3 Mutation Positive|IDH1 R132 Negative|IDH1 R140 Negative|IDH1 R172 Negative|Activating RAS Negative|NPMc Positive	124.3150081	11
FLT3 Mutation Positive|IDH1 R132 Negative|IDH1 R140 Negative|IDH1 R172 Negative|Activating RAS Positive|NPMc Positive	303.918176	1
FLT3 Mutation Positive|IDH1 R132 Negative|IDH1 R140 Positive|IDH1 R172 Negative|Activating RAS Negative|NPMc Positive	531.734441	1
FLT3 Mutation Positive|IDH1 R132 Positive|IDH1 R140 Negative|IDH1 R172 Negative|Activating RAS Negative|NPMc Negative	996.566893	1
FLT3 Mutation Positive|IDH1 R132 Positive|IDH1 R140 Negative|IDH1 R172 Negative|Activating RAS Negative|NPMc Positive	58.199115	3
FLT3 Mutation Positive|IDH1 R132 Positive|IDH1 R140 Negative|IDH1 R172 Negative|Activating RAS Positive|NPMc Positive	37.215471	1
IDH1 R132 Negative	1565.164232	1
IDH1 R132 Negative|IDH1 R140 Negative|IDH1 R172 Negative|Activating RAS Negative|NPMc Negative	205.283883	2

Table 3.2 Continued

Molecular Abnormality	Average miR-125a Expression	Number of Patients
IDH1 R132 Negative|IDH1 R140 Positive|IDH1 R172 Negative|Activating RAS Negative|NPMc Negative	475.069037	1
null	191.285305	2
PML-RAR Negative|FLT3 Mutation Negative|IDH1 R132 Positive|IDH1 R140 Negative|IDH1 R172 Negative|Activating RAS Negative|NPMc Negative	91.903859	1
PML-RAR Negative|FLT3 Mutation Positive|IDH1 R132 Negative|IDH1 R140 Negative|IDH1 R172 Negative|Activating RAS Negative|NPMc Negative	194.570025	1
PML-RAR Negative|FLT3 Mutation Positive|IDH1 R132 Negative|IDH1 R140 Negative|IDH1 R172 Negative|Activating RAS Negative|NPMc Positive	414.581356	1
PML-RAR Positive|FLT3 Mutation Negative|IDH1 R132 Negative|IDH1 R140 Negative|IDH1 R172 Negative|Activating RAS Negative|NPMc Negative	162.232349	2
PML-RAR Positive|FLT3 Mutation Positive|IDH1 R132 Negative|IDH1 R140 Negative|IDH1 R172 Negative|Activating RAS Negative|NPMc Negative	450.591169	2
PML-RAR Positive|IDH1 R132 Negative|IDH1 R140 Not Tested|IDH1 R172 Not Tested|Activating RAS Negative|NPMc Negative	384.012339	1

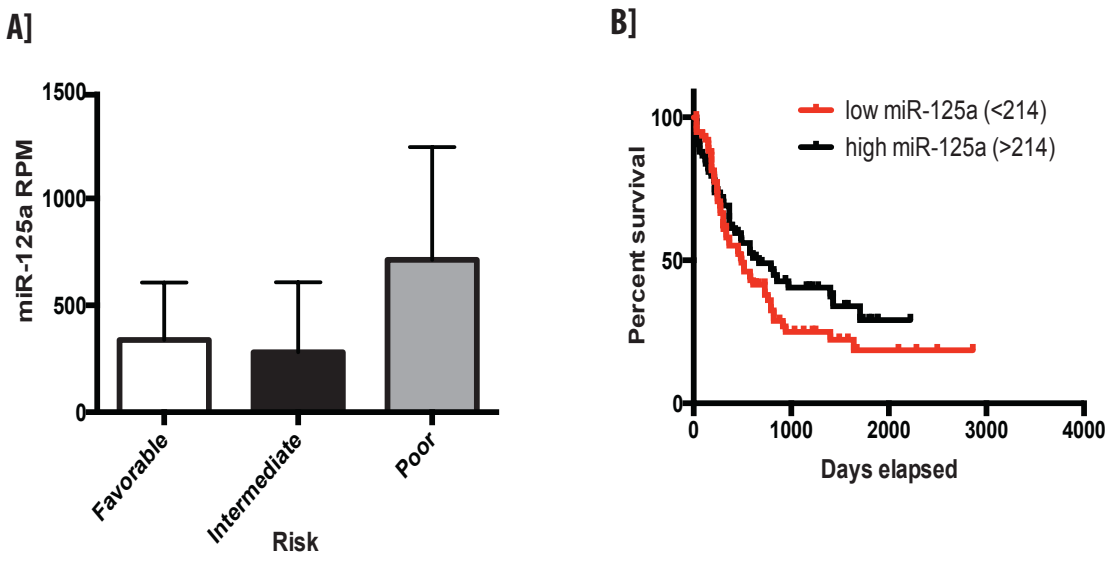

Figure 3.4. Decreased miR-125a is associated with decreased survival. A] Prognostic risk and their correlating miR-125a expression level (RPM) B] Kaplan-Meier Survival Curve of low miR-125a expression (RPM) and high miR-125a expression (RPM). miR-125a expression was sorted from lowest to highest. Samples above the median were considered high miR-125a expression and samples below the median were considered low miR-125a expression. Results are mean +/- SD and are not statistically significant.

3.2. Restored miR-125a expression causes decreased cell proliferation, cell cycle progression, and enhanced apoptosis

Several leukemic cell lines were screened in order to determine miR-125a expression status. MV4-11 (Biphenotypic B Myelomonocytic Leukemia), K562 (Chronic Myeloid Leukemia, mimics acute erythroleukemia), and HL60 (Acute Promyelocytic Leukemia) had decreased miR-125a expression in comparison to healthy CD34+ (HSC) or CD33+ cells (Myeloid Progenitors). (Figure 3.7. A). MV4-11 cells were isolated from a 10 year old male and contain the FLT3 mutation and several cytogenetic abnormalities ((48, XY, t(4;11)(q21:q23), +8, +19)). K562 cells are from a 53-year-old female and contain the t(9;22)(q34;q11)

resulting in the BCR-ABL fusion protein. HL60 cells are from 36-year-old female and contain several molecular abnormalities (C-myc, NRAS, and p53 mutation). Lastly, NB4 cells are from a 20-year-old female containing the t (15;17) resulting in the PML-RAR alpha. miR-125a expression was most significantly decreased in human acute promyelocytic leukemia (APL) NB4 cells in comparison to either CD34+ (HSC) or CD33+ cells (Myeloid Progenitors) (Figure 3.5. A). Using the TCGA data, miR-125a expression was analyzed in samples containing PML-RAR alpha mutation (Figure 3.5. B and C). Though no difference was seen in patients with PML-RAR alpha mutation and those without this mutation, an in depth look at samples with PML-RAR alpha demonstrate complex heterogeneity (Figure 3.5. A and B). Therefore, no conclusion can be made on the effects of PML-RAR alpha mutation and miR-125a expression. Due to the significant decrease of miR-125a in NB4 cells, these cells were used to identify the effects of restoring miR-125a expression within AML.

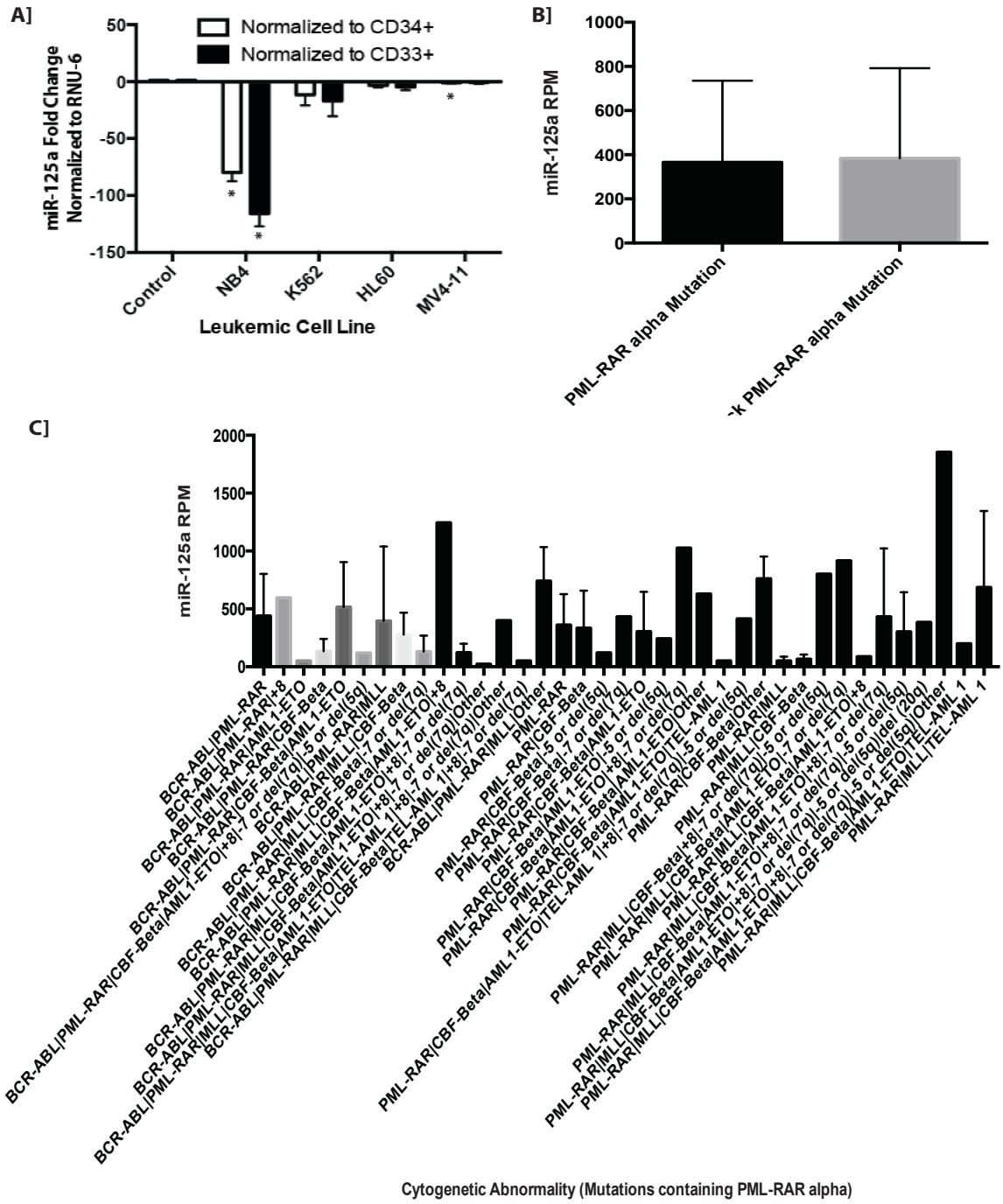

Figure 3.5. miR-125a expression analysis in leukemic cell lines reveals NB4 with PML-RAR alpha as most significantly decreased miR-125a. A] Mature miR-125a expression in bone marrow derived CD34+ and CD33+ cells and leukemic cell lines measured by RT-qPCR B] miR-125a expression within AML containing PML-RAR alpha and AML not containing PML-RAR alpha C] Breakdown of miR-125a expression in correlation to molecular mutations that contain PML-RAR alpha. Results are means +/- SD and * p-value = <0.05.

To elucidate the role of miR-125a in NB4 cells, NB4 cells were transfected with control (scramble), mimic miR-125a or hairpin inhibitor of miR-125a. Transcript level of miR-125a was not completed for transfection experiments since these experiments were used to identify if increasing or decreasing miR-125a expression would result in alterations of NB4 cells. To ensure that the process of transfection does not affect cell viability and cell number, the effect of shock alone and the transfection mixture was analyzed. Cell number and viability were accessed via Moxi. At 24, 48, and 72 hours post transfection shock or transfection mixture were not affected (Figure B.1.A and B). Since the effect of miR-125a AML was not known, several biological assays were tested, including apoptosis, differentiation, and cell cycle. Apoptosis increased with mimic miR-125a at both 72 and 96 hours post transfection although some apoptosis was visible at 96 hours post transfection with hairpin inhibitor miR-125a NB4 cells (Figure B.2. A). Analysis of differentiation through Cd11b expression analysis demonstrated no effect between hairpin inhibitor and mimic miR-125a (Figure B.2. B). The effect of miR-125a on cell cycle progression was analyzed via BrdU incorporation. To determine optimal amount of time for BrdU pulsing, a range of time points were tested (3, 6, 24, 48, and 72 hours). The shorter time pulses of 3 and 6 hours offered differences between hairpin inhibitor and mimic miR-125a and suggested that mimic miR-125a may lead to decreased S-phase (Figure B.2. C and D).

Out of the biological assays studied enhanced apoptosis due to mimic miR-125a was the most dramatic, therefore an apoptosis array was conducted.

These results however were inconclusive due to the poor quality of RNA from transfected cells. Due to these inconclusive results, NB4 cells were transduced with GFP or mimic miR-125a since transfection results in transient expression and may not be an effective way to screen for potential targets and altered cellular function. Though transduction of NB4 cells were described in methods, the protocol will be briefly described here. NB4 cells were transduced with SMARTchoice human lentiviral hsa-miR-125a shMIMIC lentiviral particles. For a control, NB4 cells were transduced with SMARTchoice Human Lentiviral shMIMIC CAG/TurboGreen fluorescent protein (GFP). Puromycin selection for 8 weeks (final concentration 2µg puromycin) was used prior to analysis of stably transduced cells.

After selection of cells that were transduced with miR-125a was over expressed in NB4 cells. Confirmation that cells were properly transduced is seen through both GFP positive expression (Figure 3.6. A) and miR-125a fold change (Figure 3.10. B). Analysis of cell proliferation via an MTT assay revealed a decrease in cell proliferation in response to overexpression of miR-125a (Figure 3.6. C). Cells started to accumulate at the G0/G1 stage causing a decrease in both the S-phase and G2/M phase when miR-125a was overexpressed (Figure 3.6. D). Cell death analysis via co-staining of PI and Annexin-V by flow cytometry resulted in increased apoptosis as visualized by Annexin-V positive cells (Figure 3.6. E) when miR-125a is overexpressed.

Although, K562 and MV4-11 cells did not ectopically express miR-125a at the fold change as NB4 cells, restoring miR-125a expression in additional lines that do not have significantly decreased miR-125a expression results in increased cell proliferation rather than decreased cell proliferation. This outcome may be due to the variation in cytogenetic or molecular abnormalities for these cells lines.

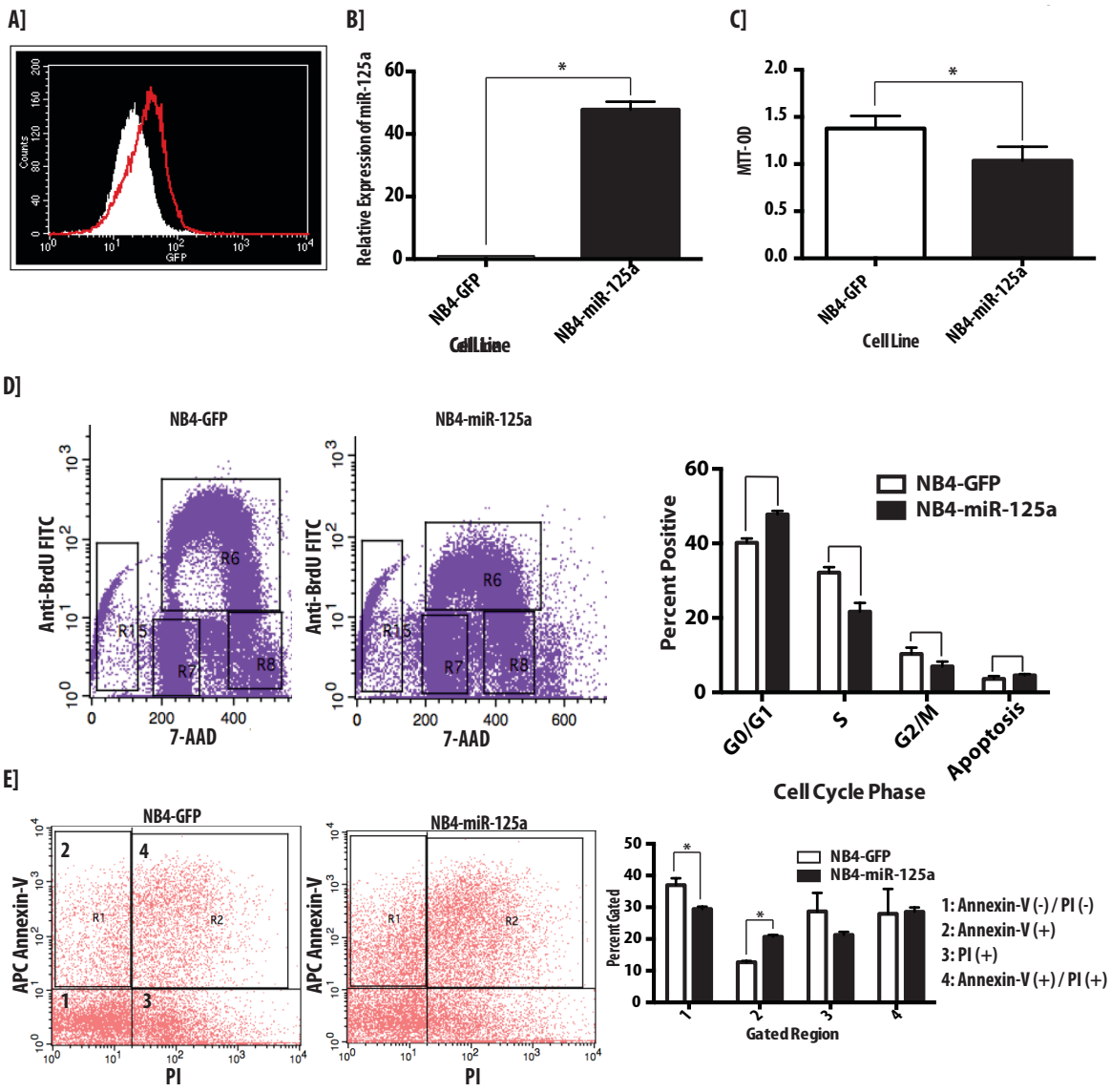

Figure 3.6. Overexpression of miR-125a in NB4 cells results in decreased cell proliferation, cell cycle progression, and apoptosis. A] Histogram of GFP expression of GFP or shMIMIC miR-125a lentivirus transduced NB4 cells from Flow Cytometry Analysis. White represents NB4-miR-125a and red line represents NB4-GFP.B] Mature miR-125a expression of NB4 cells transduced with GFP or shMIMIC miR-125a lentivirus measured by RT-qPCR. C] Proliferation analysis of transduced NB4 cells as measured by MTT assay. Transduced NB4 cells or NB4 cells pre-treated for 24 hours with Mubritinib prior to analysis. D] Representative image of cell cycle progression of NB4 transduced cells measured by BrdU flow cytometry assay (left panel). Graphical results represent a series of 6 BrdU pulses of 15-minute increments (0, 15, 30, 45, 60, 75 minutes) (right panel). E] Representative images of cell death analysis of transduced lines via co-staining of Annexin-V and Propidium Iodide (PI) in flow cytometry (left panel). Graphical results represent combined Annexin-V and PI staining (right panel). Results are means +/- SD and * p-value = <0.05.

3.3. Mimic miR-125a humanized xenograft model

To test if ectopic miR-125a expression could affect in vivo tumor growth, a xenograft model was utilized. NB4 cells ($5x10^6$) transduced with GFP control or mimic miR-125a expression were subcutaneously injected into the left flank of NOD.CB17-Prkdc scid/J mice. Prior to xenograft study, ectopic miR-125a expression was confirmed. Tumor measurements throughout the course of the study showed no significant difference (Figure 3.7. A). Interestingly, tumors expressing miR-125a ectopically had a slight increase in tumor size. Upon completion of the study, tumors were collected for histological analysis. Interestingly, H&E analysis showed an increase in holes within the tumor when mIR-125a was ectopically expressed. Consultation with Dr. Michael Jones, a pathologist at Maine Medical Center, revealed that these holes were fat deposits (Figure 3.7. B). Since there was not a significant different in tumor size, only a few tumors for NB4-GFP and NB4-miR-125a were analyzed for histological analysis. Therefore, at this time, Ki-67 and caspase-3 staining were not quantified. Trends however were analyzed to help guide future studies. There was no noticeable difference in proliferation via Ki-67 staining however caspase-3 staining is suggestive of enhanced apoptosis within tumors ectopically expressing miR-125a (Figure 3.7. B).

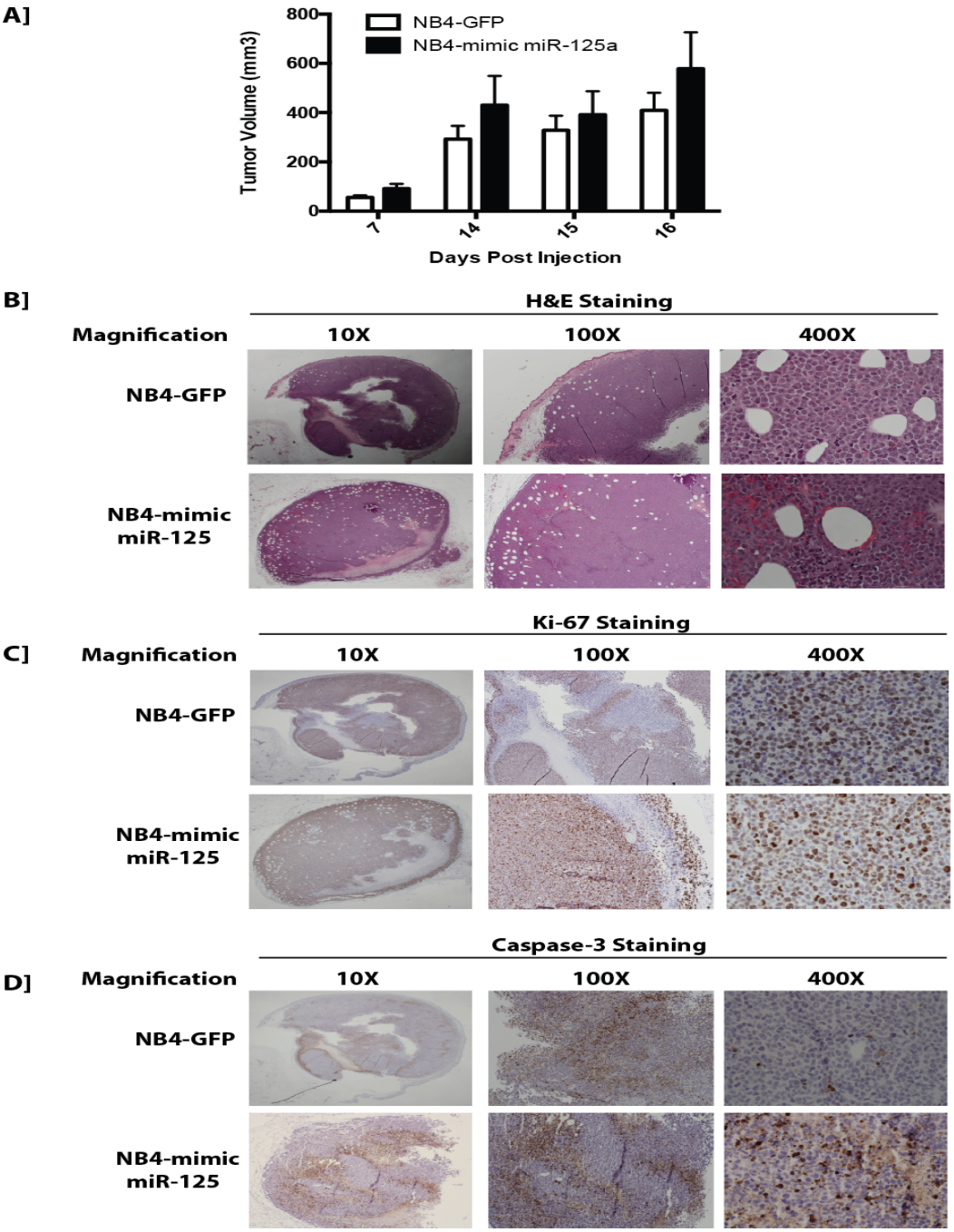

Figure 3.7. Xenograft model of NB4 cells transduced with GFP or mimic miR-125a do not show a significant change in tumor growth. A] Tumor volumes throughout the course of the study of NB4-GFP and NB4-mimic miR-125a tumors. Results are mean +/-SD and are not significant. B] Histological representation of NB4-GFP and NB4-mimic miR-125a tumors stained with H&E C] Histological representation of NB4-GFP and NB4-mimic miR-125a tumors stained with Ki-67 for proliferation analysis D] Histological representation of NB4-GFP and NB4-mimic miR-125a tumors stained with caspase-3 for apoptosis analysis.

CHAPTER 4: RESTORATION OF EPIGENETICALLY SILENCED MIR-125A TARGETS TRIB2 AND REVEALS ERBB2 INHIBITION AS A POTENTIAL NEW THERAPEUTIC FOR MIR-125A LOW AML

4.1. miR-125a is epigenetically silenced in AML

Although pharmacological miR mimics are being developed for treatments, utilization of pharmacological mimic miR as therapy is still in development. Therefore gaining insight to the molecular basis of miR-125a's silencing is a viable alternative approach to re-express miR-125a in patients who have decreased miR-125a expression.

When considering the molecular mechanisms of miR-125a silencing there are several possible mechanisms leading to suppression of a miR, including microRNA processing [120-122], transcriptional [123], or post-transcriptional [124,125] regulation. Within the context of AML aberrant methylation has been correlated to decreased gene expression [86,89]. When analyzing the upstream region of miR-125a using PubMed's Gene/Epigenomics Tool, several CpG islands upstream were identified (Figure 4.1.); therefore, miR-125a expression was analyzed in response to a de-methylating agent, decitabine. Mature miR-125a expression increased with increasing amounts of decitabine treatment after 24 hours (Figure 4.1. A) and slightly decreases by 48 hours (data not shown). If miR-125a is transcriptionally expressed, precursor miR-125a should additionally increase in response to decitabine. Correlating to increased mature miR-125a expression, precursor miR-125a expression was further found to increase significantly in

response to decitabine treatment at 24 hours (Figure 4.1. B). Global methylation analysis demonstrated that decitabine resulted in decreased methylation of NB4 cells (Figure 4.1. C). To confirm that increased precursor and mature miR-125a expression was a result of decreased methylation of upstream CpG island methylation bisulfite sequencing was performed. Analysis of a portion of the large CpG Island revealed a decrease of fifty-six percent (Figure 4.1. D). Alterations of the small CpG islands were not visible at the decitabine concentration and time point analyzed (data not shown). Combined results from bisulfite sequencing and miR-125a expression in response to decitabine treatment indicate that miR-125a is transcriptionally suppressed by methylation. Although miR-125a expression is restored by decitabine treatment, decitabine is resulted in global de-methylation within NB4 cells and therefore, present work was focused on defining miR-125a's role and potential target when re-expressed in AML.

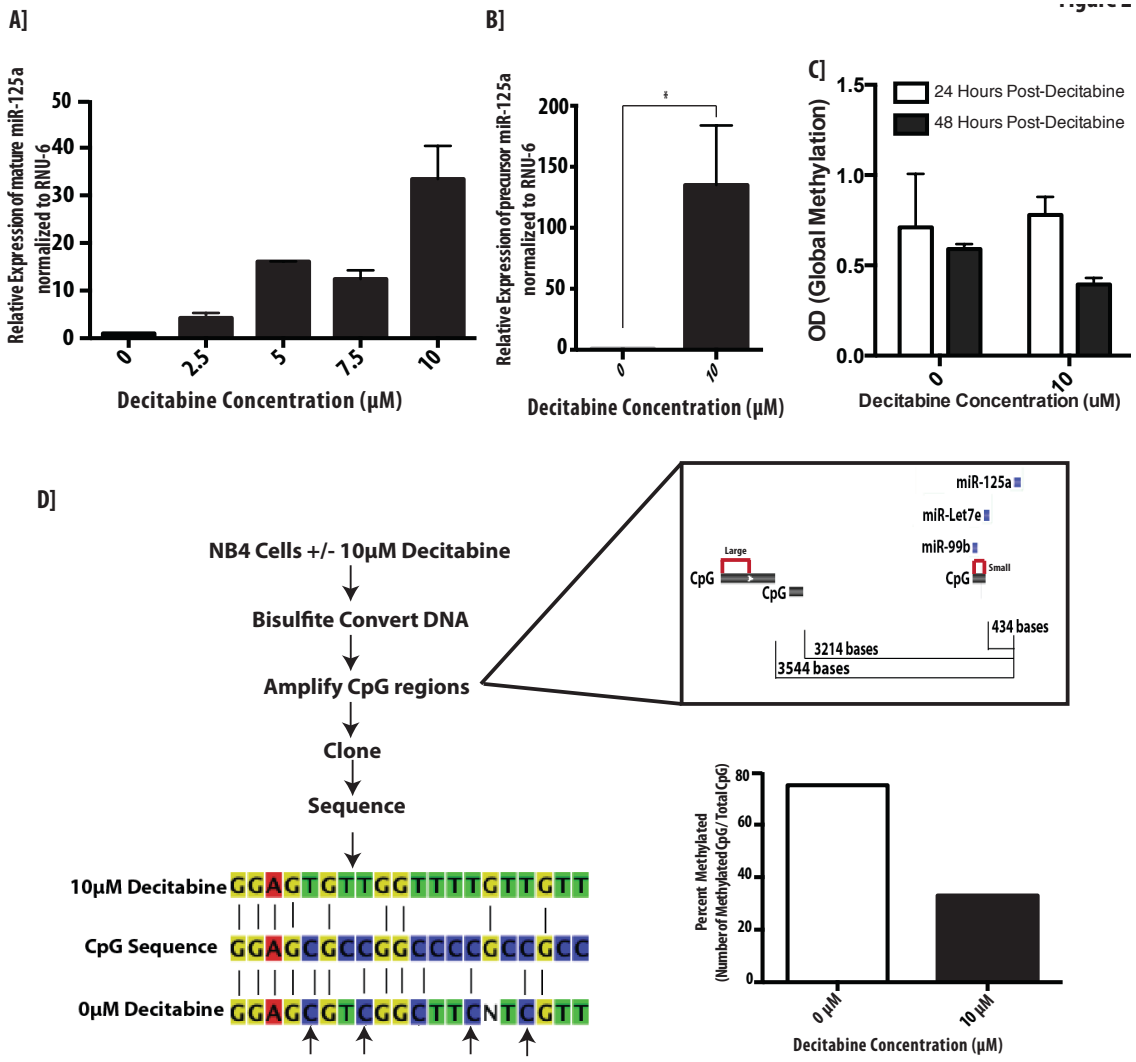

Figure 4.1. Decreased miR-125a expression due to aberrant methylation. A] Mature miR-125a expression 24 hours post-Decitabine treatments (0-10μM) measured by RT-qPCR B] Precursor miR-125a expression 24 hours post-Decitabine treatment (10μM) measured by RT-qPCR. C] Global methylation of NB4 cells 24 and 48 hours post- Decitabine treatment (10μM) measured by methylflash methylated DNA kit. D] Experimental design for bisulfite sequencing 24 hours post-Decitabine treatment and representative images of sequencing results. Location of upstream CpG islands in relation to miR-125a locus found using PubMed's Gene/Epigenomics Tool. Regions outlined by red lines represent CpG islands analyzed in bisulfite sequencing. Arrows point to CpG islands de-methylated with Decitabine treatment. Percent methylation of large CpG island located at -3544 bp upstream of miR-125a locus. Results are means +/- SEM and *p-value = <0.05

4.2. Ectopic expression of miR-125a leads to significant alterations in biological pathways in NB4 cells

To better understand the effects of ectopic miR-125a on NB4 cells transduced cells lines were profiled. Three independent samples of RNA were isolated from NB4-GFP and NB4-miR-125a. Samples were sent to Vermont Genetics Network for profiling. Quality of RNA was confirmed prior to analysis. For detailed methods of profiling and bioinformatics analysis please see methods (2.13. and 2.14.)

RNA expression profiling demonstrated significant changes in biological processes enlightening us on the impact of miR-125a's role in AML. ANOVA results from the gene-level analysis include 812 genes differentially expressed between miR-125a and GFP control groups ($p \leq 0.05$; fold change $\geq |1.5|$) (Figure 4.2. B, Table C.1. A and B). Of these 812 genes, 449 genes were downregulated (Figure 4.3. B, Table A.1. A) and 363 probe sets were upregulated (Figure 4.2. B, Table C.1. B). A three-dimensional scatter plot from a principal component analysis clearly identifies distinct molecular phenotypes in miR-125a samples and shows no significant outliers in the study set (Figure 4.2. A). The first principal component (PC1) correlates with our single biological factor, NB4 cell line (Figure C.1.).

A hierarchical clustering map generated from these 812 significant differentially expressed genes revealed two distinct expression patterns (Figure 4.2 A). miR-125a samples lower half of the map and GFP samples in the upper half of the map (genes with increased expression are shown in red and genes

with decreased expression in green). The 363 probes/genes in the upper right quadrant of the cluster map are genes that show higher levels of expression in miR-125a samples relative to GFP control samples. The 449 probes/genes left upper quadrant are genes that exhibit lower expression levels in miR-125a samples relative to GFP control samples. Results from the exon-level ANOVA include 2830 alternative spliced genes and 3980 genes that are differentially expressed ($p \leq 0.05$). Of these, 694 are alternatively spliced and differentially expressed (Figure 4.2. C, Table C.2. A and B). Pathway ANOVA recovered 262 KEGG functional groups that were either significantly differentially expressed and/or disrupted in a few genes as a result of treatment ($p \leq 0.05$ for both differential expression and disruption) (Table 4.1). GO ANOVA yielded 1685 differentially expressed and 3838 disrupted GO categories ($p \leq 0.05$) (Figure 4.2. D-E). At this time, altered genes have not been verified by RT-qPCR and will be part of future directions.

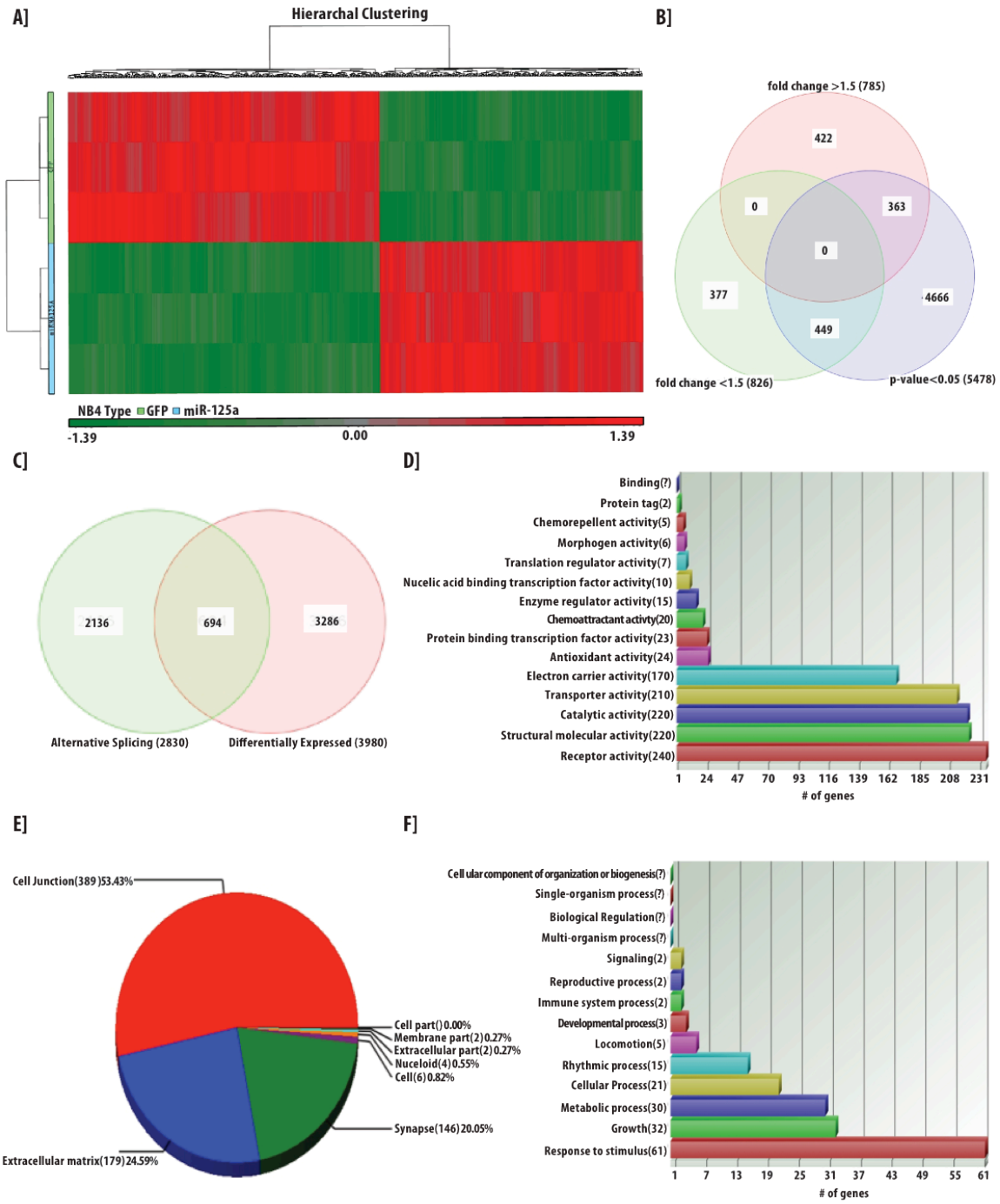

Figure 4.2. Ectopic expression of miR-125a leads to significant alterations in biological pathways in NB4 cells. A-F] Analysis of GFP and shMIMIC miR-125a lentiviral transduced NB4 cells profiled on the Affymetrix Human Gene 2.0ST Array. A] Heat map representing genes significantly differentially expressed >1.5 fold change or < 1.5 fold change between GFP and shMIMIC miR-125a lentiviral transduced NB4 cells. Subgroups within blue color represent miR-125a shMIMIC-NB4 cells while green subgroups represent GFP-NB4 cells. Green represents decreased gene expression while red represents increased gene

expression. B] Venn diagram representing total number of genes significantly regulated and break down of genes significantly increased or decreased by >1.5 fold or <1/5 fold. C] Venn diagram representing total number of genes differentially expressed in comparison to alternatively spliced genes. D] Bar graph representing KEGG molecular function groups and the number of genes within each functional group E] Pie graph representing percentages of KEGG cellular components F] Bar graph representing KEGG biological process group and the number of genes within each functional group.

4.3. Identifying a miR-125a target in NB4 cells

Previously, overexpression of miR-125a in human medulloblastoma led to cell growth arrest and apoptosis[113]. Further, similar ectopic expressions in gastric cancer cells led to inhibition of proliferation [114]. Likewise, overexpression of miR-125a in breast cancer cells led to decreased anchorage dependent growth [115]. Within the context of the gastric cancer and breast cancer studies, it was identified that miR-125a regulates these cellular functions through Erbb2 and ErbB3, which were validated through 3'UTR luciferase assays. Erbb2 mRNA and protein levels were decreased when miR-125a is overexpressed in NB4 cells (Figure 4.3.). Although ErbB2 appeared to be a potential target, it was not found to be a significantly altered gene within profiling.

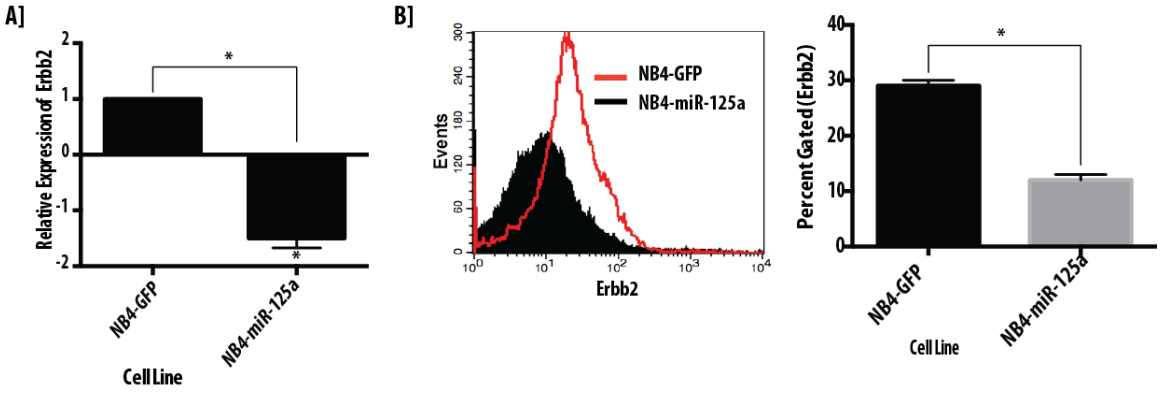

Figure 4.3: miR-125a decreases ErbB2 in NB4 cells. A] Erbb2 expression in transduced cells as measured by RT-qPCR. B] Histogram represents Erbb2 protein expression in transduced NB4 cells as measured by flow cytometry (left panel). Graphical results represent combined results for Erbb2 protein expression (right panel). Error bars represent SEM and *p-value = <0.05.

Since ErbB2 was not altered within profiling, a new potential target was investigated. From profiling results, Trib2 was significant decreased (p=0.0003, Table C.1. A) when miR-125a expression was restored in NB4 cells and is a predicted target within TargetScan. Trib2 has been implicated in AML in several contexts. Keeshan et al demonstrated that increased Trib2 resulted in inhibition of C/EBPα causing decreased cell differentiation [126]. In an additional study, Trib2 was found to interact with HoxA9 to aid in the progression of AML [127]. Therefore, if miR-125a targets Trib2 it may inhibit pathogenesis of AML. Analysis of alternative splicing revealed specific exons that were decreased within Trib2 in comparison to NB4-GFP cells (Figure 4.4. A). RT-qPCR confirmed that Trib2 was significantly decreased in miR-125a overexpressing cells (Figure 4.4. B). Therefore, 3'UTR luciferase of Trib2 was tested to confirm Trib2 as a target of miR-125a since it is not currently been demonstrated as a target. Wild type and mutant 3'UTR luciferase reporter constructs in pEZX-MT01 vector

(GeneCopoeia) containing both hLUC and hRLUC for Trib2 was generated. For the mutant Trib2, two bases were changed to disrupt the seed match between miR-125a and Trib2 (Figure 4.4.C). Constructs were co-transfected with miRIDIAN Mimic hsa-miR-125a in HeLa cells using Dharmafect Duo. 48 hours post transfection; luciferase assays were performed (Figure 4.4.C). Luciferase expression was normalized to renilla expression prior to determining percent activity. The wildtype Trib2 3'UTR percent activity was significantly decreased when compared to the percent activity of the mutated Trib2 3'UTR (Figure 4.4. C and D). Thus, for the first time Trib2 is confirmed experimentally as a target of miR-125a. Additional cell lines ectopically expressing miR-125a showed decreased Trib2 further suggesting that miR-125a targets Trib2 in AML. Analysis of Trib2 protein was attempted; however there currently is no good antibody for Trib2. Therefore, at this time we were not able to analyze if miR-125a affected Trib2 protein levels.

Though Trib2 has been demonstrated as being overexpressed in AML, pathway analysis revealed significant alterations in biological pathways in NB4 cells overexpressing miR-125a, leading us to study altered pathways further.

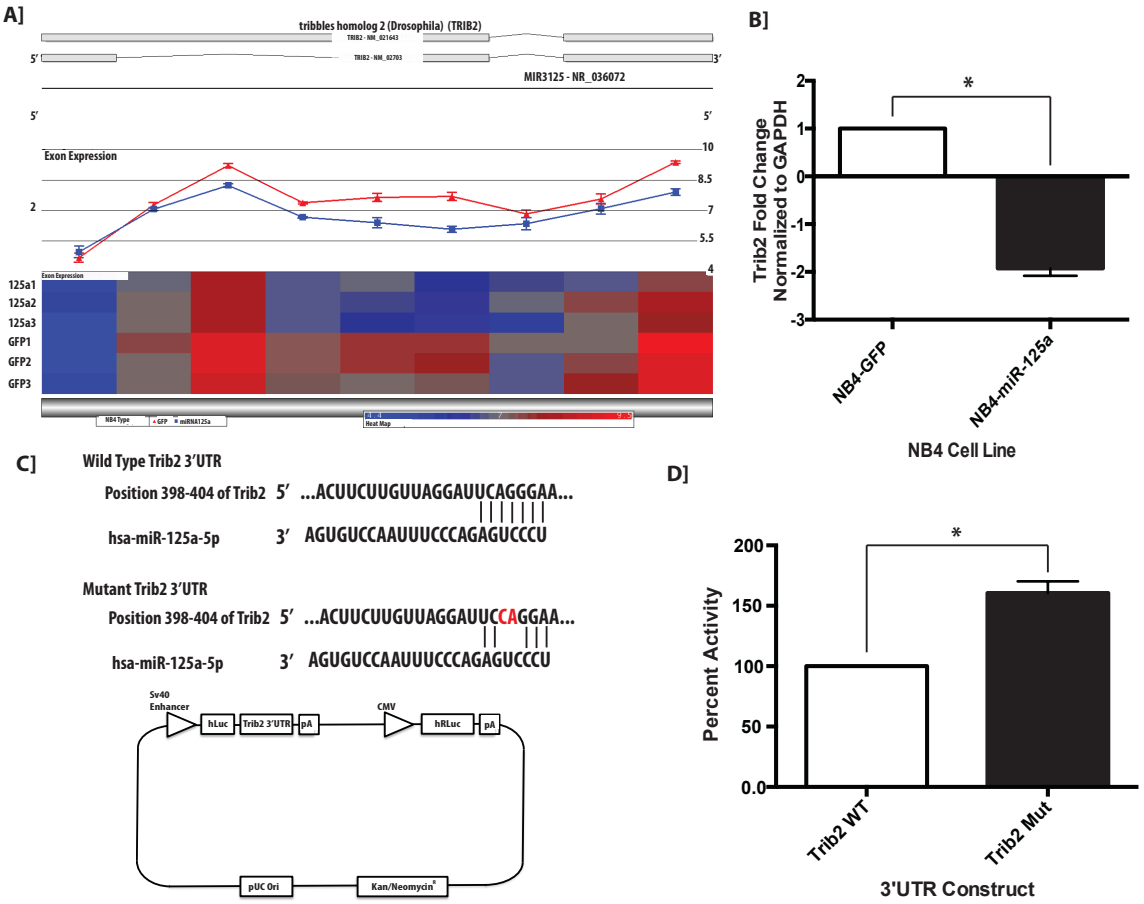

Figure 4.4. miR-125a targets Trib2. A] Image demonstrating individual probes within alternative splice analysis of Trib2 gene of profiling results descried earlier. Red line represents GFP-NB4 cells and blue line represents miR-125a shMIMIC-NB4 cells. Within heat map generated, blue represents decreased expression while red represents increased expression. B] Trib2 expression quantified by RT-qPCR of GFP-NB4 cells and miR-125a shMIMIC-NB4 cells. C] Diagram of Trib2 3'UTR interaction with miR-125a seed sequence (Top) Diagram of mutated Trib2 3'UTR interaction with miR-125a seed sequence (Middle) Diagram of plasmid used for 3'UTR luciferase experiment. D] Percent activity of luciferase expression normalized by renilla luciferase expression of wildtype Trib2 3'UTR and mutant Trib2 3'UTR. Results are means +/- SD and * p-value = <0.05.

4.4. Targeting ErbB pathway reveals potential new therapeutic for AML

When conducting ANOVA pathway analysis, the ErbB pathway was significantly decreased ($p = 0.004$, Figure 4.5; Table 4.1.). The ErbB pathway is a family of tyrosine kinase containing the epidermal growth factor receptor (EGFR), ErbB2 receptor, ErbB3 receptor, and ErbB4 receptor [128]. Once ligands bind, the ErbB receptors either homodimerize or heterodimerize activating downstream effectors, such as MAPK and PI3K/AKT[128]. Activation of the ErbB pathway can affect proliferation, cell migration, metabolism and survival [128]. Overexpression of miR-125a in human medulloblastoma led to cell growth arrest and apoptosis[113]. Further, similar ectopic expression in gastric cancer cells led to inhibition of proliferation [114]. Likewise, overexpression of miR-125a in breast cancer cells led to decreased anchorage-dependent growth [115]. In the context of the gastric cancer and breast cancer studies, it was identified that miR-125a regulates these cellular functions through Erbb2, which were validated through 3'UTR luciferase assays. In visualizing the ErbB pathway within KEGG pathway analysis, there is a visible decrease in several ErbB receptors (ErbB-1, ErbB-3, EGFR) and many of the downstream effectors (MTOR, CAMK2G, CBL, CDKN1B, SOS2, PRKCB, PLCG2, PRKCA, MAP2K27, AKT2, CRKL, MAPK1, PIK3CA, HBEGF, BRAF, ABL1, and ARAF). (Figure 4.5.; Table 4.2.). Although ErbB2 did not show a significant decreased within profiling results, enhanced ErbB pathway has been correlated to decreased miR-125a and plays roles in proliferation and survival and is commonly altered within cancer [114,115,129]. Mubritinib (TAK-165), previously shown to be a selective inhibitor of ErbB2 phosphorylation was tested [117]. An

apparent decrease in cell proliferation of NB4 cells was observed upon Mubritinib treatments (Figure 4.6. A). Strikingly, Mubritinib treatment of NB4 cells resulted in almost complete inhibition of G1- S-phase transition (Figure 4.6. B). HL60 cells, which have more miR-125a expression, remained unaffected at 24 hours post treatment (Figure 4.6. B). There was a significant increase in cell death as visible by co-staining of Annexin-V and Propidium Iodide (PI) with Mubritinib treatment (Figure 4.6. C). CD11b expression was increased significantly on NB4 cells treated with Mubritinib 96 hour's post-Mubritinib treatment representing enhanced differentiation of NB4 cells (Figure 4.6.D).

Cell proliferation and apoptosis effects through inhibition of ErbB2 phosphorylation by Mubritinib have been previously suggested to be via decreased phosphorylation of its downstream effectors AKT and MAPK [117]. To examine if Mubritinib was acting through these pathways within NB4 cells, phospho- and total- protein levels were analyzed. Mubritinib treatment highly decreased Erbb2 phosphorylation in NB4 cells (Figure 4.6.E). Furthermore Mubritinib decreased phospho-AKT and phospho-MAPK whereas total protein levels were unaffected (Figure 4.6.E). These results indicate that cellular effects observed via Mubritinib in NB4 cells are via ErbB2-AKT-MAPK signaling axis.

Pathway Name	p-value (NB4 Type)	Fold-Change (miRNA125A vs. GFP)
Bladder cancer	3.79E-06	-1.09991
NF-kappa B signaling pathway	3.26E-05	-1.12691
Fatty acid metabolism	5.93E-05	1.05935
Malaria	8.01E-05	-1.1914
Type II diabetes mellitus	0.000126515	-1.12257
Pertussis	0.000157627	-1.08628
Cysteine and methionine metabolism	0.000176294	-1.02217
Chemokine signaling pathway	0.000206517	-1.04851
Chagas disease (American trypanosomiasis)	0.000212817	-1.10865
Fc epsilon RI signaling pathway	0.000334632	-1.11866
Cytokine-cytokine receptor interaction	0.000392066	-1.06844
NOD-like receptor signaling pathway	0.000650311	-1.11599
mTOR signaling pathway	0.000675565	-1.08782
Apoptosis	0.000972475	-1.09752
T cell receptor signaling pathway	0.000975279	-1.07622
Natural killer cell mediated cytotoxicity	0.00107794	-1.06584
Proximal tubule bicarbonate reclamation	0.00108525	1.16931
Ribosome	0.00109747	1.04086
MAPK signaling pathway	0.00137082	-1.01806
RIG-I-like receptor signaling pathway	0.00147865	-1.07387
Steroid biosynthesis	0.00175149	-1.14477
Bile secretion	0.00185034	1.06054
Leishmaniasis	0.00251488	-1.05813
Rheumatoid arthritis	0.0030027	-1.08151
Type I diabetes mellitus	0.00302858	-1.0497
Toll-like receptor signaling pathway	0.00305689	-1.0826
Acute myeloid leukemia	0.00309619	-1.05113
Non-small cell lung cancer	0.00316774	-1.04272
Amyotrophic lateral sclerosis (ALS)	0.00329637	-1.07144
Renin-angiotensin system	0.0036039	1.15374
Hepatitis B	0.00378721	-1.03922
African trypanosomiasis	0.00394907	-1.15914
Parkinson's disease	0.0041834	1.04864
Ubiquinone and other terpenoid-quinone biosynthesis	0.00454412	1.07862

Table 4.1. ANOVA pathway analysis (pathways $p<0.05$). Left column is the pathway analyzed, followed the significance value and fold change.

Table 4.1. continued

Pathway Name	p-value (NB4 Type)	Fold-Change (miRNA125A vs. GFP)
Graft-versus-host disease	0.00459788	-1.04725
ErbB signaling pathway	0.00499906	-1.03138
Adipocytokine signaling pathway	0.00504005	-1.06089
Sulfur relay system	0.00575118	-1.11113
Osteoclast differentiation	0.00579844	-1.07267
Vitamin digestion and absorption	0.00593106	1.04726
TGF-beta signaling pathway	0.00606898	-1.07382
Leukocyte transendothelial migration	0.00613613	-1.02915
Glycosaminoglycan degradation	0.00626005	-1.08668
Neurotrophin signaling pathway	0.00636601	-1.04168
VEGF signaling pathway	0.00683287	-1.04466
Tryptophan metabolism	0.00750665	1.02068
GnRH signaling pathway	0.00825133	-1.02329
Glioma	0.00828954	-1.02511
HTLV-I infection	0.00980975	-1.01708
Hepatitis C	0.010194	-1.02291
Fc gamma R-mediated phagocytosis	0.0108151	-1.04098
Proteoglycans in cancer	0.0116252	-1.03651
Allograft rejection	0.0123793	-1.03868
Synthesis and degradation of ketone bodies	0.0153085	-1.10852
Shigellosis	0.0161043	-1.05636
Huntington's disease	0.0161873	1.04617
Oxidative phosphorylation	0.0181178	1.05222
Purine metabolism	0.0193204	1.02834
Vasopressin-regulated water reabsorption	0.0198173	1.04076
Oocyte meiosis	0.020863	1.04837
Chronic myeloid leukemia	0.0217122	-1.0316
Proteasome	0.0235713	1.05076
Cell cycle	0.0243284	1.05194
Amino sugar and nucleotide sugar metabolism	0.0246317	-1.04404
Fatty acid elongation	0.024808	1.09566
Prion diseases	0.027392	-1.05114
Salmonella infection	0.0281235	-1.04801
B cell receptor signaling pathway	0.0285664	-1.04244

Table 4.1. continued

Pathway Name	p-value (NB4 Type)	Fold-Change (miRNA125A vs. GFP)
Measles	0.0305398	1.0271
D-Glutamine and D-glutamate metabolism	0.0319806	-1.1482
Transcriptional misregulation in cancer	0.0361865	-1.022
Cardiac muscle contraction	0.0377085	1.04049
Terpenoid backbone biosynthesis	0.0385507	-1.08785
Protein processing in endoplasmic reticulum	0.0412914	1.03126
Vitamin B6 metabolism	0.0418627	1.0615
Biosynthesis of unsaturated fatty acids	0.0419772	1.08975
Regulation of autophagy	0.0432117	1.0298
Gastric acid secretion	0.0483952	1.04288
Propanoate metabolism	0.0487645	1.04263
Base excision repair	0.0499038	1.05193
Alcoholism	0.0499877	1.04921
Glycosaminoglycan biosynthesis - keratan sulfate	0.0503016	-1.02947
Collecting duct acid secretion	0.0507922	1.08453

Gene Symbol	Reference Sequence	P-value	Fold Change
PIK3CD	NM_005026	0.122948	-1.15772
MTOR	NM_004958	0.052792	-1.11149
PIK3R3	NM_003629	0.115235	-1.21242
JUN	ENST00000371222	0.350085	-1.07507
NRAS	NM_002524	0.385307	1.06006
SHC1	NM_183001	0.110202	1.10826
ABL2	NM_007314	0.628125	1.05249
AKT3	NM_005465	0.122874	-1.27318
MAPK8	ENST00000374189	0.202705	1.20835
NRG3	NM_001165973	0.0797238	1.21426
CAMK2G	NM_172171	0.0463335	-1.13107
RPS6KB2	NM_003952	0.278068	1.10539
CBL	ENST00000264033	0.0371611	-1.23797
HRAS	NM_005343	0.576894	1.10057
BAD	NM_004322	0.772898	-1.00795
PAK1	NM_001128620	0.54722	-1.03694
CDKN1B	ENST00000228872	0.0464565	1.14887
ERBB3	NM_001982	0.0140526	-1.12733
KRAS	NM_033360	0.187674	1.04004
SOS2	NM_006939	0.0341967	-1.13695
AKT1	ENST00000554581	0.368759	-1.10746
MAP2K1	NM_002755	0.155258	-1.07521
SHC4	NM_203349	0.861554	1.01196
NRG4	NM_138573	0.218196	-1.10691
PRKCB	NM_002738	0.0482713	-1.20566
PLCG2	ENST00000565054	0.0232671	-1.2231
PLCG2	NM_002661	0.298988	-1.08902
MAPK3	NM_001040056	0.263638	-1.05262
MAP2K4	NM_003010	0.623905	-1.09545
ERBB2	ENST00000406381	0.989239	-1.00162
STAT5A	NM_003152	0.154941	-1.26786
RPS6KB1	NM_003161	0.175825	1.12472
PRKCA	NM_002737	0.0256204	-1.25152

Table 4.2. Gene list of each gene's fold change utilized to construct ErbB pathway illustration containing fold change values between GFP-NB4 and miR-125a shMIMIC-NB4 cells. Genes highlighted in yellow represent significantly altered genes ($p<0.05$).

Table 4.2 continued

Gene Symbol	Reference Sequence	P-value	Fold Change
CRK	ENST00000300574	0.719897	1.01992
PIK3R5	NM_001142633	0.0817491	-1.22257
STAT5B	NM_012448	0.642102	1.06914
GRB2	ENST00000392564	0.850791	1.00926
MAP2K7	NM_145185	0.0454646	-1.15879
PIK3R2	ENST00000222254	0.413878	1.09615
PAK4	NM_001014831	0.819766	1.03289
CBLC	NM_012116	0.899317	1.01604
PRKCG	NM_002739	0.62671	1.0471
SHC2	NM_012435	0.737414	-1.03722
MAP2K2	NM_030662	0.0571057	-1.21287
AKT2	NM_001626	0.0269275	-1.10694
NCK2	NM_003581	0.141575	-1.09838
SOS1	ENST00000426016	0.737293	-1.02158
TGFA	NM_003236	0.688632	1.03654
ERBB4	ENST00000342788	0.182996	1.2692
SRC	NM_005417	0.71241	-1.0741
PLCG1	ENST00000244007	0.297561	1.12008
PAK7	ENST00000378429	0.571137	1.09063
CRKL	NM_005207	0.0126195	-1.2582
MAPK1	NM_138957	0.018139	-1.26082
NCK1	ENST00000469404	0.850487	-1.01682
PIK3CA	ENST00000263967	0.000185498	-1.26189
PAK2	NM_002577	0.840668	1.02276
RAF1	NM_002880	0.311351	-1.04936
CBLB	NM_170662	0.0179084	1.20539
GSK3B	NM_002093	0.374066	-1.06806
PIK3CB	ENST00000477593	0.567307	1.03502
EREG	NM_001432	0.586194	1.03711
AREG	NM_001657	0.500317	-1.12689
AREG	NM_001657	0.759343	-1.04915
EGF	NM_001963	0.526452	1.11038
GAB1	NM_207123	0.525871	1.03653
BTC	ENST00000395743	0.817686	-1.03373
MAPK10	NM_138982	0.908831	1.0136
CAMK2D	ENST00000418639	0.185848	-1.1557
PIK3R1	NM_181523	0.0445674	1.1532
NRG2	NM_004883	0.131591	1.07026
HBEGF	ENST00000230990	0.0112012	-1.26203

Table 4.2 continued

Gene Symbol	Reference Sequence	P-value	Fold Change
CAMK2A	NM_015981	0.560326	-1.12702
MAPK9	NM_139068	0.581539	1.03605
CDKN1A	NM_001220778	0.652323	-1.04453
EGFR	ENST00000275493	0.0233013	-1.14634
PIK3CG	ENST00000496166	0.84067	1.01764
CAMK2B	NM_001220	0.749188	1.04522
BRAF	NM_004333	0.0115535	-1.25531
NRG1	NM_001160004	0.43457	1.10912
EIF4EBP1	ENST00000338825	0.439574	1.13303
MYC	NM_002467	0.0439841	-1.14375
PTK2	NM_153831	0.384358	1.0956
ABL1	NM_007313	0.0205418	-1.08524
SHC3	NM_016848	0.0539349	1.15068
ARAF	NM_001654	0.0328007	-1.09334
PAK3	NM_002578	0.194749	1.13903
ELK1	NM_001114123	0.551168	-1.06366

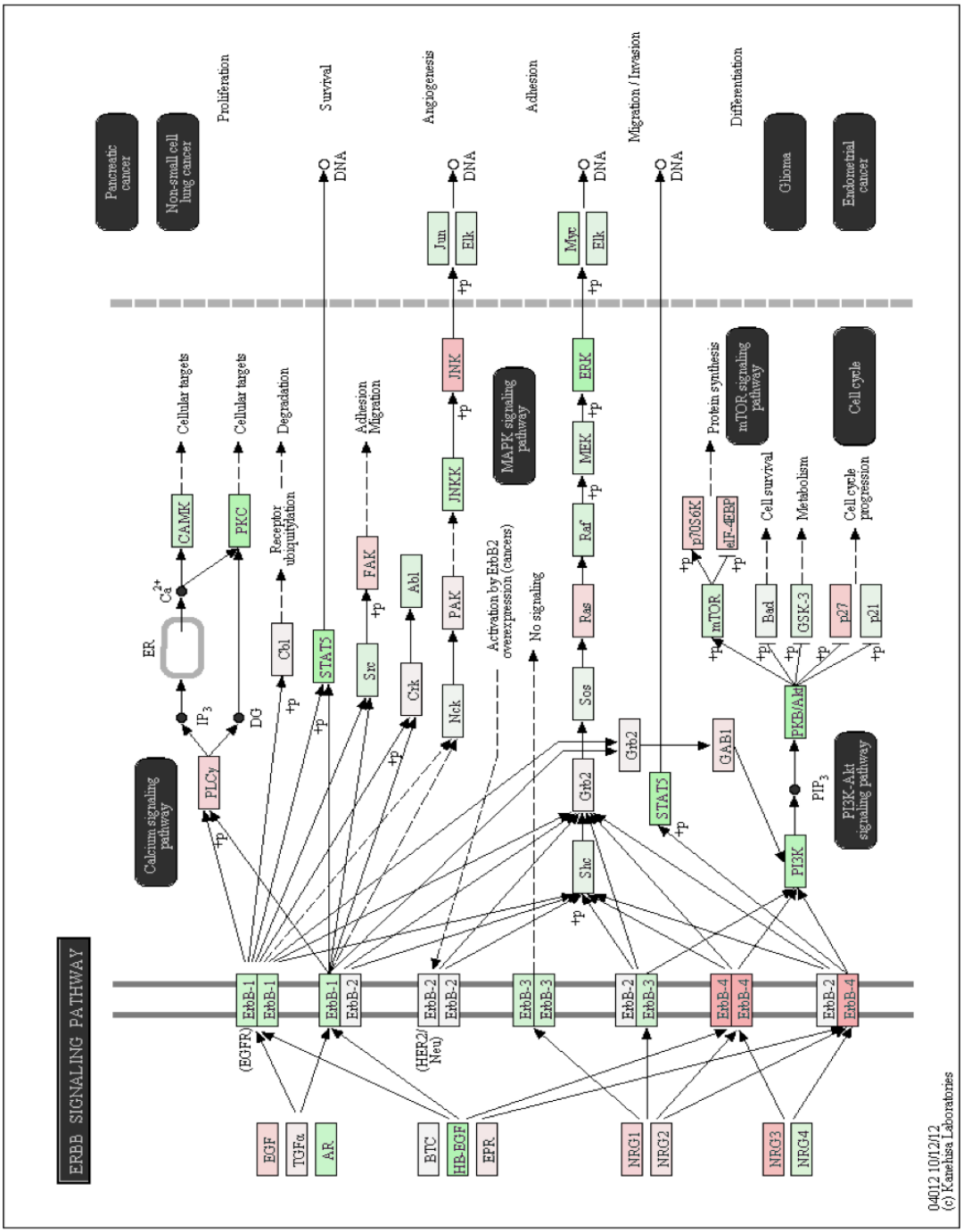

Figure 4.5. Global decrease of ErbB Pathway with ectopic miR-125a expression. Image depicting ErbB pathway of differentially expressed genes through KEGG pathway analysis from profiling described earlier. Green represents decreased fold change, red represents increased fold change, and no color represents no fold change of gene expression between GFP-NB4 cells and miR-125a shMIMIC- NB4 cells.

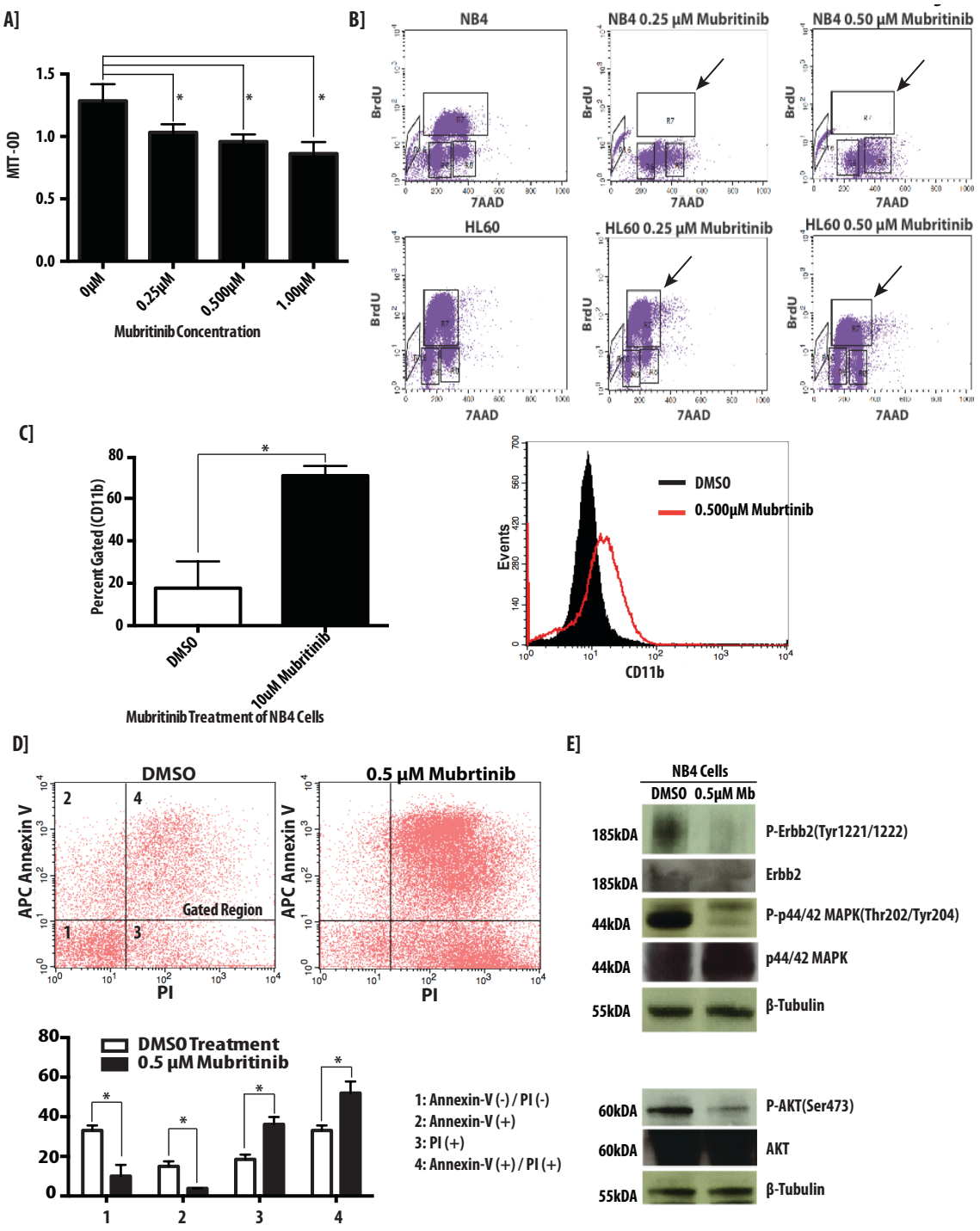

Figure 4.6. Targeting ErbB pathway reveals potential new therapeutic of low miR-125a AML. A] Cell proliferation analysis of NB4 cells 24 hours post-Mubritinib treatments (0-1μM) as measured by MTT proliferation assay as previously described. B] Representative images of cell cycle progression analysis of NB4 and HL60 Acute Promyelocytic Leukemia lines 24 hours post 0.25μM and 0.50μM Mubritinib Treatment measured by BrdU flow cytometry. C] Histogram represents differentiation analysis of NB4 cells 96 hours post Mubritinib treatment

(0.50μM) measured by CD11b+ cells in flow cytometry (left panel). Graphical results represent combined CD11b+ expression by flow cytometry (right panel). D] Representative images of cell death analysis of NB4 cells 24 hours post 0.5μM Mubritinib treatment via co-staining of Annexin-V and Propidium Iodide (PI) in flow cytometry (top panel). Graphical results represent combined Annexin-V and PI staining (bottom panel). E] Protein levels of phosphorylated and total protein of NB4 cells 24 hours post DMSO or 0.50μM Mubritinib treatment via western blot analysis. Results are means +/- SD and * p-value = <0.05.

4.5. Mubritinib inhibits in vivo tumor growth of NB4 human leukemic xenografts

Due to the dramatic effects of Mubritinib treatment of NB4 cells observed in vitro, we tested Mubritinib in an in vivo model of NB4 cells xenograft in NOD-SCID mice (Figure 4.7. A). As previously stated in methods, $3x10^6$ NB4 cells in PBS were subcutaneously injected into the left flank of twenty-four NOD.CB17-Prkdc scid/J mice. Mice were randomized for treatment with Mubritinib or vehicle (DMSO) prior to start of experiment. Seven mice from the Mubritinib group and ten mice from the vehicle group formed tumors and progressed to the treatment stage. Some mice did not develop tumors and therefore were not included for treatments but were monitored for the course of the study. Two treatments of 20mg/kg Mubritinib or vehicle (DMSO) was given on the first day as a loading dose followed by daily treatment of 20mg/kg of Mubritinib or vehicle via oral gavage. Tumor measurements were conducted throughout the course of study and tumor volume was calculated by the following equation: tumor volume = (AxB^2) x ½ where A equals the longer dimension and B equals the shorter dimension. The final two tumor measurements and the tumor collection were performed in a blinded manner. (Figure 4.7.)

Tumors were allowed to grow to approximately 200 mm^3 in size before treated with vehicle or Mubritinib, but upon treatment with Mubritinib a significant effect on tumor growth was visible (Figure 4.7. A and B; Figure 4.8. A). Histopathological analysis revealed that the majority of the Mubritinib treated mice had large areas of necrosis which were identified through consultation by Dr. Volkhard Lindner at Maine Medical Center Research Institute. Interestingly, areas of necrosis lacked Ki-67 (proliferation) staining suggesting further that these cells were necrotic (Figure 4.7. C and Figure 4.8. B). Quantification of Ki-67 staining showed a trend that Mubritinib treated mice had decreased proliferation, however at this time it was not a significant difference (data not shown). Caspase-3 staining for cell death was most prominent surrounding the regions of necrosis (Figure 4.7. C and Figure 4.8. B). Quantification of caspase-3 staining did not show a significant difference between Mubritinib and vehicle treated mice (data not shown). Mice treated with the vehicle (DMSO) also had regions of necrosis, but typically the necrotic regions were not as large as those treated with Mubritinib. These findings therefore suggest that although the tumors may have appeared to be growing at the end there were also massive areas of necrosis and decreased proliferation (Figure 4.8. B). From these findings, inhibition of the ErbB pathway could be a new therapeutic for patients with low miR-125a expression.

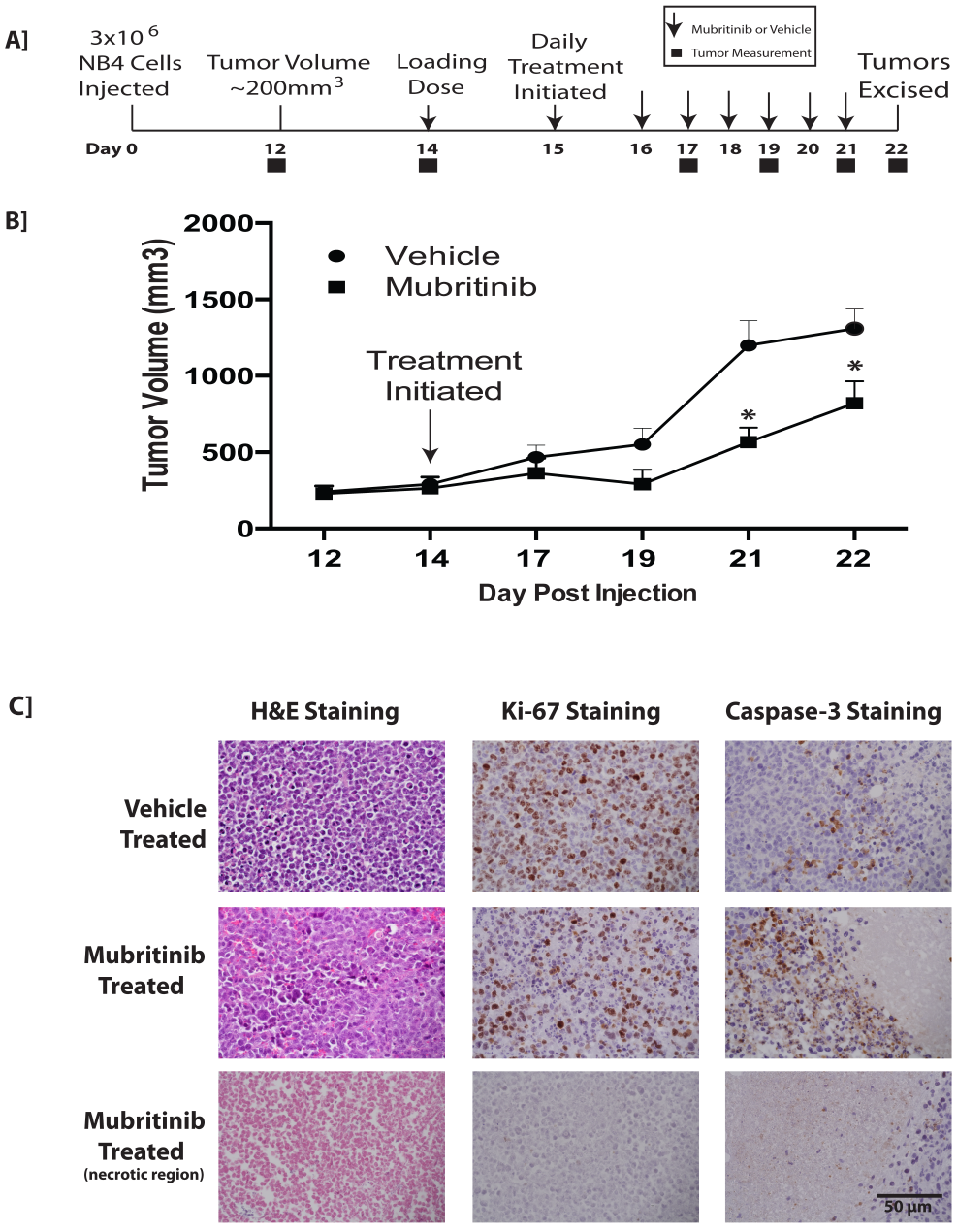

Figure 4.7. Mubritinib inhibits in vivo tumor growth of NB4 human leukemic xenografts. Necrotic region is identified in Figure 4.8. A] Timeline of in vivo NB4 human leukemic xenograft model B] Tumor volumes of Mubritinib and vehicle treated mice C] Histopathological features of human xenografts in Mubritinib treated and vehicle treated mice. Representative fields from H&E, Ki-67, and Caspase-3 staining. Regions of necrosis are defined in Figure 4.8. Results are means +/- SEM and *p-value = <0.05

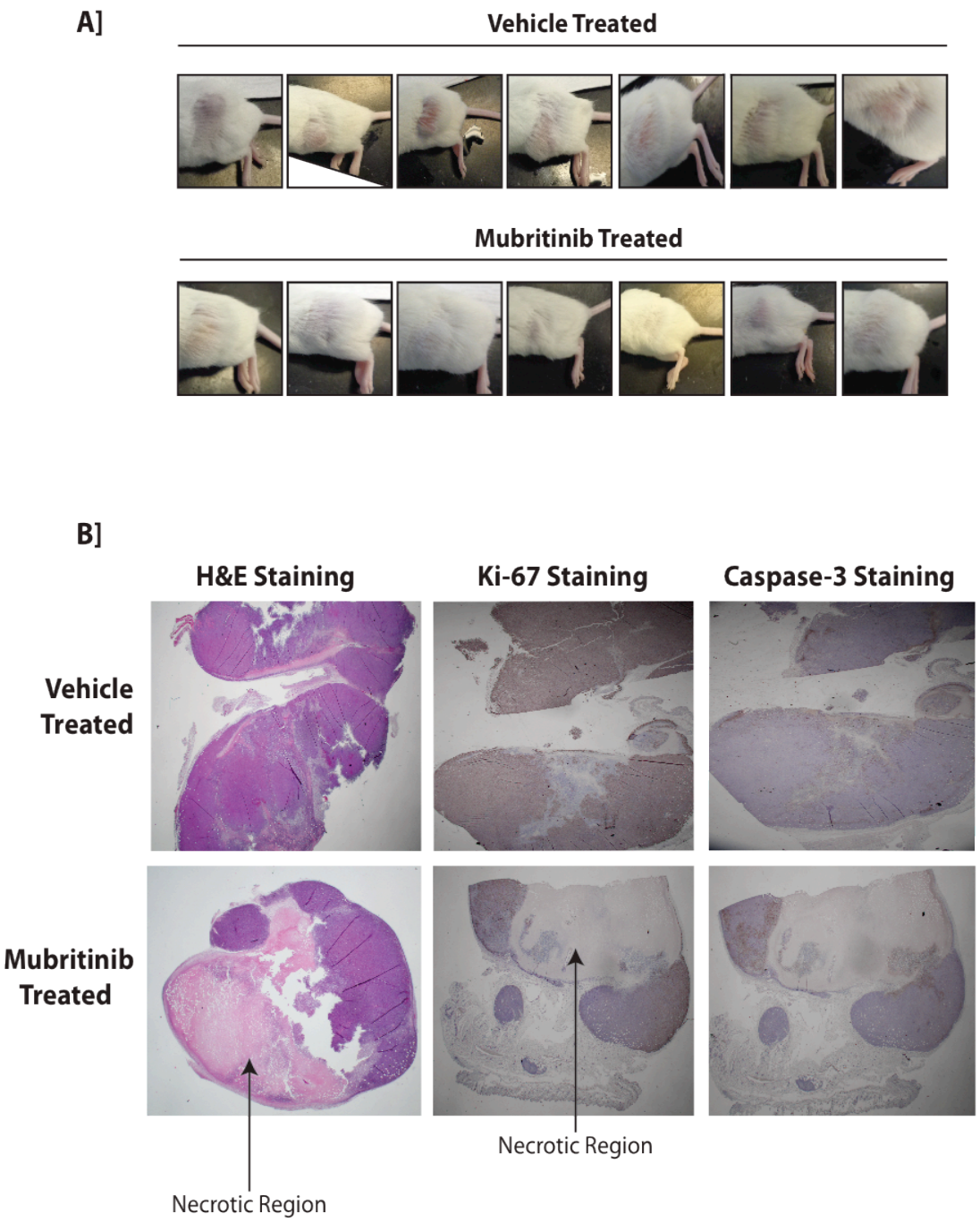

Figure 4.8. Mubritinib induces cell death and inhibition of proliferation in NB4 xenograft in vivo model. A] Images of tumor xenograft B] Representative histological images of vehicle and Mubritinib treated mice and stained with H&E, Ki-67, or caspase-3 (Magnification at 10x)

CHAPTER 5: DISCUSSION

5.1. miR-125a Characterization and Functional Role in AML

This section will summarize the major findings, their potential significance, and potential future experiments from the results presented in Chapter 3.

5.1.1. Major Findings

For the first time, miR-125a expression was analyzed beyond cytogenetically normal AML in addition to its correlation to clinical information and dissection of its functional role within AML. miR-125a expression analysis in clinical patient samples, paraffin embedded bone marrow samples and leukemic cell cultures revealed that miR-125a is decreased beyond cytogenetically normal AML. Although miR-125a is part of a miR cluster containing miR-let7e and miR-99b, previous studies found that miR-125a controlled cellular functions within hematopoiesis in comparison to miR-let7e and miR-99b, which is why I focused on miR125a.

Although we were able to analyze miR-125a expression in paraffin embedded AML samples, there were issues in obtaining quality miR for analysis. Therefore there was a limitation on studies that could be completed using these samples. Further, many of samples lacked AML classification resulting in the inability to classify low miR-125a. Utilizing the NCI TCGA website allowed for miR-125a correlation to clinical information for each AML patient. Since healthy patient information is not provided for AML patients in TCGA, trends were analyzed but final conclusions could not be made at this time. In addition to AML

classification analysis from paraffin embedded bone marrow samples and clinical samples, AML FAB M5 also correlated with low miR-125a expression within data found on the NCI TCGA site. No difference was identified between gender and ethnicity demonstrating that correlating miR-125a to a specific AML subtype would be more beneficial. Although miR-125a expression is decreased within all types of AML risk categories, favorable and intermediate risk had the greatest decrease in miR-125a expression. From Kaplan-Meier survival analysis, there was a trend that miR-125a expression may lead to decreased survival.

Upon confirming that miR-125a was decreased in AML, the effect of miR-125a expression restoration was analyzed. Several leukemic cell lines were analyzed in order to mimic low miR-125a expression *in vitro*. From these studies, NB4 cells that represent FAB subtype M3 and containing t (15; 17) was identified to have the most significantly decreased miR-125a expression. Therefore, NB4 cells were used for functional analysis of over expressed miR-125a expression. From MTT proliferation assays and BrdU incorporation assays, NB4 cells transduced with mimic miR-125a demonstrated decreased proliferation and an increase in G0/G1 stage of the cell cycle. Though there was a significant decrease in cell cycle progression and proliferation, there was not a complete halt in cell cycle progression suggesting additional cellular alterations may be occurring. Interestingly, Cd11b, which marks differentiation, was decreased in comparison to control cells although additional differentiation markers were not analyzed. Apoptosis measured by co-staining with Annexin-V and PI

demonstrated a significant increase. These findings demonstrate leukemic blasts may have an advantage when miR125a is decreased.

Analysis of ectopic miR-125a expression in additional leukemic cell lines demonstrated that miR-125a had a differential effect on cellular function. These differences appear to be related to the starting expression level of miR-125a. Thus, restoration of miR-125a may not be effective unless it is significantly decreased. Interestingly, within a xenograft model of NB4 cells ectopically expressing miR125a there was no significant difference in tumor growth. Histological analyses however were suggestive of increased apoptosis as determined by caspase-3 staining. Proliferation analysis via Ki-67 staining does not appear to show a difference, however staining of Ki-67 ectopically miR-125a expression is lighter than control. For confirmation of these differences more samples would need to be analyzed and quantified. Another model, such as engraftment of miR-125a into the hematopoietic system may be better model to study the effects of ectopic miR-125a in NB4 cells.

5.1.2. Significance and Speculations

Current literature has focused on the role of miR-125a expression in normal hematopoiesis [108,109]. These studies have implicated a role of miR-125a in HSC maintenance via decreased apoptosis by targeting Bak-1[108]. Ectopic expression of miR-125a in more differentiated cells did not result in cell maintenance implicating a cell survival role solely in the HSC stage. Further investigations demonstrated that miR-125a expression was decreased in cytogenetically

normal AML. Other cancers that have identified miR-125a as being decreased have demonstrated that ectopic miR-125a could be a new therapeutic via decreasing proliferation and enhancing apoptosis. As a result of these discoveries, decreased miR-125a within AML appears to provide leukemic blasts a proliferative and survival advantage.

By analyzing miR-125a expression in a range of clinical AML samples in comparison to healthy patients, miR-125a was confirmed to be decreased but further that it was not solely within cytogenetically normal AML. Cytogenetic and molecular abnormalities analysis demonstrated increased complexity to identify an AML classification for low miR-125a. Although miR-125a is known to decrease with HSC differentiation, our results find that miR-125a is significantly decreased in comparison to CD33+ cells, which represents a myeloid blast. Restoration of miR-125a expression in leukemic blasts that showed significantly decreased miR-125a resulted in cell death and proliferation. Previous studies showed ectopic expression of miR-125a in more differentiated myeloid cells did not result in long-term cell maintenance. Therefore my studies of ectopic miR-125a in leukemic blasts in comparison to normal myeloid cells would suggest that miR-125a may play a role in cell maintenance only within HSC. A complication to this speculation is that when ectopic miR-125a expression is increased in leukemic blasts that do not have decreased expression, significant changes in proliferation or apoptosis is not seen. Thus, my results indicate that there is a delicate balance of miR-125a expression needed within hematopoiesis. An alternative explanation to these differences is the variation in cytogenetic and

molecular changes within each leukemic cell line. Consequently the role of miR-125a may not play the same role due to other confounding factors disrupted within each type of leukemia. For example, K562 contain the BCR-ABL fusion protein as a result of the t (9; 22)(q34:q11) chromosomal translocation. HL60 cells have amplification in the c-myc gene with deletion in the p53 gene and a truncation in GM-CSF. NB4 cells harbor the t (15; 17) chromosomal translocation creating the PML-RAR alpha fusion gene. As a result of each of the cytogenetic or molecular alterations, many cellular changes occur explaining why ectopic miR-125a may not have the same functional role within each leukemic cell line tested.

Although there were significant alterations within miR-125a expression *in vitro,* within the *in vivo* xenograft model there were no significant changes. Tumor volume did not show a significant change, however there was enhanced apoptosis within cells ectopically expressing miR-125a. miR-125a expression was not analyzed within this study. If miR-125a expression was not maintained throughout the study, it may explain why there was not a significant different in tumor volume. Further, as mentioned previously and alternative model may be useful is studying the effects of ectopic miR-125a expression. Therefore suggesting that over time it is the potential that the tumors may become necrotic making a significant difference between tumors expressing ectopic miR-125a and GFP. At this time, the results from the in vivo experiment remain inconclusive.

5.1.3.Future Directions

The studies presented within the first aim of this thesis demonstrated that miR-125a expression was decreased in a range of AML subtypes containing mixed molecular and cytogenetic abnormality backgrounds. By restoring miR-125a expression in leukemic blasts that were identified to have decreased miR-125a levels illustrates a potential new therapeutic role for restored miR-125a expression. Though there were several questions answered, additional questions were raised along the way. First, an increase in patient samples is necessary in order to determine if a specific AML subtype classification could correlate to low miR-125a expression. Although clinical information was analyzed and trends were discovered, clinical information for healthy patients was not available therefore significantly altered results could not be identified. In order to understand the effect that miR-125a has on AML, this information would be essential. Analysis of miR-99b and miR-let7e expression demonstrated a decrease in each of these miRs within paraffin embedded samples. Interestingly, the entire cluster was not always decreased within the same samples. Therefore further analysis of this cluster should be conducted.

From in vitro studies, ectopic miR-125a did not have the same effect on each cell line tested. In order to gain insight to how miR-125a is functioning within AML, additional cell lines should be tested with ectopic miR-125a. Further, within these studies, ectopic miR-125a expression was analyzed, however decreased miR-125a was not tested. By testing the effects of both ectopic and decreased miR-125a expression a better understanding of the molecular

mechanism of miR-125a could be dissected. Even though miR-let7e and miR-99b did not show an effect on normal hematopoiesis, the differential expression of these may show that they have a role in malignant hematopoiesis.

Preliminary studies of ectopic miR-125a on tumor growth in vivo were tested however remained inconclusive. Only one concentration of cells was tested for subcutaneous injection for tumor growth. Additional concentrations of cells at the time of injection may reveal a difference in tumor growth. Since histology suggested enhanced apoptosis in tumors expressing ectopic miR-125a, increasing the length of the experiment might demonstrate whether or not ectopic miR-125a can affect tumor growth over a length of time. Secondly, determine if the tumors ectopically expressing miR-125a could become completely necrotic. Lastly, a survival curve would identify if ectopic miR-125a could aid in increased survival.

5.2. Characterizing the regulation of miR-125a silencing and the mechanism of action of miR-125a in AML

This section will summarize the major findings, their potential significance, and potential future experiments from the results presented in Chapter 4.

5.2.1. Major Findings

Although pharmacological mimic miR is being developed for treatments, utilization of pharmacological mimic miR as therapy is still evolving. Therefore gaining insight to the molecular basis of miR-125a's silencing is a viable

alternative approach to re-express miR-125a in patients who have decreased miR-125a expression. When considering the molecular mechanisms of miR-125a silencing there are several possible mechanisms leading to decreased miR expression, including microRNA processing [120-122], transcriptional [123], or post-transcriptional [124,125] regulation. Treatment with a de-methylating agent, decitabine, demonstrated a dose-dependent increase in mature miR-125a expression. Precursor miR-125a expression was significantly increased in response to decitabine corresponding to an increase in mature miR-125a expression. Bisulfite sequencing of the upstream CpG island region demonstrated decreased methylation in response to decitabine confirming that miR-125a expression was increased due to a decrease in methylation. As a result of these findings, decitabine could be a potential new therapeutic for AML containing low miR-125a expression, however it does de-methylate genes in a relatively nonspecific way genome-wide [130,131] which may result in potential off target sites. Therefore studies to identify potential targets and pathways altered with restored miR-125a expression within NB4 cells were pursued.

To elucidate potential targets and pathways alterations due to miR-125a overexpression, profiling was conducted. Among the significant decreased genes were FLT1, MMP-9, IL-32Rα and HIP-1. FLT-1 is increased within myelodysplastic syndrome and associated with poor prognosis [132]. Further, MMP-9 has been demonstrated to play an important role within invasion of malignant myeloblasts [133]. IL-3Rα has several studies linking its overexpression to AML by demonstrating its overexpression results in enhanced blast

proliferation, increased cellularity, and poor prognosis [134]. To combat this, several studies have also demonstrated that inhibition of IL-3Rα may be a new potential therapeutic since inhibition leads to cell death of AML cells [135,136]. Lastly, HIP-1 has been demonstrated within prostate and colon cancer to be overexpressed leading to cell survival, which could be playing similar roles within AML [137]. As with the decreased genes, several increased genes were of interest such as cathepsin-G, EPX, and SPARC. Within one study, the authors demonstrated that re-expression of cathepsin-G within AML can lead to differentiation, growth inhibition and apoptosis of AML1-ETO cells [138]. Although this gene was studied within a specific subtype of AML, cathepsin-G could be furthered analyzed within low miR-125a expressing cells since it was increased significantly and previously decreased within an AML subtype. EPX is known to be a marker of eosinophil [139], suggesting that its increased expression could reflect differentiation of NB4 cells with increased miR-125a expression. Additionally, SPARC has been demonstrated to play a potential role within AML due to its decreased expression [140] and addition of exogenous SPARC leads to growth inhibition of AML cells [140,141]. Though all of these were interesting due to their previous implications within cancer or AML, they are not predicted targets of miR-125a. Therefore, analysis on identifying a potential target of miR-125a within AML became the new aim.

Trib2 has been implicated in AML in several contexts. Keeshan et al demonstrated that increased Trib2 resulted in inhibition of C/EBPα causing decreased cell differentiation [126]. In an additional study, Trib2 was found to

interact with HoxA9 to aid in the progression of AML [127]. Results from RT-qPCR validated our profiling results by demonstrating decreased expression when miR-125a is overexpressed. Lastly, 3'UTR luciferase assays of wild type and mutated Trib2 confirmed Trib2 as a target of miR-125a. Although Trib2 has been implicated in cancer, inhibitors do not currently exist, but a necessity has been demonstrated [142]. Therefore, the focus shifted to identifying a pathway with known inhibitors.

Although a new target was identified for miR-125a, profiling analysis demonstrated a range of systemic alterations was occurring. From ANOVA pathway analysis, the ErbB pathway was significantly altered, such as decreased ErbB receptors (ErbB1 and ErbB3) and downstream effectors (PI3K, AKT, and Stat5). Though the ErbB pathway has been implicated to play a role in epithelial cancers such as breast and gastric cancer [114,115], it has not yet been demonstrated in hematopoietic malignancies. When visualizing fold change values of the ErbB pathway within KEGG pathway analysis, the ErbB pathway appeared to be decreased, suggesting the potential use of ErbB inhibitors for AML with low miR-125a. Several ErbB2 inhibitors have been developed, and we chose to test Mubritinib (TAK-165), which selectively inhibits ErbB2 phosphorylation [117]. Excitingly, through MTT proliferation and BrdU incorporation assays, a profound affect was observed in response to Mubritinib. Unlike NB4 cells transduced with mimic-miR-125a expression, a complete halt in the S-phase was demonstrated. K562, which also has decreased miR-125a expression additionally, demonstrated an affect on the S-phase in response to Mubritinib.

Most strikingly was the lack of affect of the inhibitor on HL60 and MV4-11 cells, which contain more miR-125a expression suggesting that inhibition of the ErbB pathway would be specific for low miR-125a AML. Mubritinib treatment of mimic miR-125a transduced cells demonstrated a synergistic affect of inhibition of proliferation within the first forty-eight hours. By seventy-two hours however, both control and mimic miR-125a transduced NB4 cells have complete inhibition of proliferation demonstrating that the combination of restored miR-125a expression is not necessary to achieve a potential therapeutic advantage. Similar to transduced NB4 cells; enhanced apoptosis was visible in response to Mubritinib. Interestingly, Cd11b was significantly enhanced showing that differentiation was occurring in addition to partial cell death and decreased cell proliferation. An *in vivo* model was next utilized to demonstrate the therapeutic potential of Mubritinib for miR-125a low- AML.

5.2.2. Significance and Speculations

As a result of these novel findings, several insights have been gained. Though decreased miR-125a has been implicated in many cancers, the majority of these studies have not identified the mechanism behind miR-125a's suppression. By characterizing how miR-125a expression is suppressed in AML, restoration of miR-125a could be achieved to decrease cell proliferation, cell cycle progression, and enhance apoptosis of leukemic blasts. Some studies have demonstrated that there are mutations within pri-miR-125a causing decreased mature miR-125a expression. Within these studies, miR-125a was suppressed by aberrant

methylation. Though decitabine was effective in increasing miR-125a expression in NB4 cells, it did not sustain its expression. Multiple treatments of decitabine may be necessary to have sustained miR-125a re-expression. Decitabine treatment within K562 additionally resulted in increased miR-125a expression for 24 hours. HL60 cells however did not have increased miR-125a. Both NB4 and K562 cells had decreased miR-125a while HL60 cells did not, providing more confirmation that miR-125a is suppressed by methylation. Surprisingly, miR-99b and miR-let7e were suppressed by treatment of methylation. Although the promoter of cluster miR-99b, miR-let7e, and miR-125a has not been identified, literature suggests they have a common promoter. These findings imply that the cluster may have different promoters or that there are different factors regulating the cluster that is altered with decitabine treatment. Lastly, it is possible that additional epigenetic modulators, such as an HDAC inhibitor. By the addition of this inhibitor, histones would be both de-methylated and acetylation would be promoted potentially enhancing transcription of miR-125a.

Since decitabine resulted in global de-methylation and did result in a significant effect in cell proliferation and apoptosis, profiling was utilized to identify a target of miR-125a in AML. Previous studies have identified several targets of miR-125a that are enhanced when miR-125a is decreased within cancer such as ErbB2, MMP1, HuR, and Fyn. By targeting these factors, decreased proliferation, migration and enhanced apoptosis occurs within cancer cells demonstrating the therapeutic potential of miR-125a. Interestingly, all of these known targets that correlate with miR-125a and cancer were not

significantly altered genes when miR-125a was ectopically expressed in NB4 cells. Dissecting the results revealed that Trib2 was significantly decreased and a predicted target of miR-125a.

Trib2 has been implicated in AML in several contexts. Keeshan et al demonstrated that increased Trib2 resulted in inhibition of C/EBPα causing decreased cell differentiation [126]. In a additional study, Trib2 was found to interact with HoxA9 to aid in the progression of AML [127]. Results from RT-qPCR validated our profiling results by demonstrating decreased expression when miR-125a is overexpressed. 3'UTR luciferase assays of wild type and mutated Trib2 confirmed Trib2 as a target of miR-125a. Although Trib2 has been implicated in cancer, inhibitors are not developed currently but a necessity has been demonstrated [142]. Therefore, studies shifted on identifying a pathway with known inhibitors that could make advancement in a new therapeutics for low miR-125a AML.

From ANOVA pathway analysis, the ErbB pathway was significantly altered, such as decreased ErbB receptors (ErbB1 and ErbB3) and downstream effectors (PI3K, AKT, and Stat5). Though the ErbB pathway has been highly demonstrated within the context of epithelial cancers such as breast and gastric cancer [114,115], it is just starting to be studied within hematopoietic malignancies. When visualizing fold change values of the ErbB pathway within KEGG pathway analysis, the ErbB pathway appeared to be decreased implicating the potential use of ErbB inhibitors for miR-125a low AML. For targeting the ErbB pathway, ErbB2 inhibitors have been well developed, therefore we tested Mubritinib (TAK-

165), which selectively inhibits ErbB2 phosphorylation [117]. Previously, Mubritinib was found to be a potential new treatment for bladder, kidney and androgen-independent prostate cancer due to significant decrease in tumor growth in in vivo xenograft models [117]. A profound affect was seen on cell cycle progression and additionally the inhibitor significantly altered cell proliferation, differentiation, and apoptosis. Most strikingly was the lack of affect of the inhibitor on HL60 cells, which do not have decreased miR-125a expression suggesting that inhibition of the ErbB pathway would be specific for low miR-125a AML.

Several recent studies have additionally demonstrated that inhibition of the ErbB pathway may be a potential new therapeutic for leukemia. Irwin et al recently found that small molecular ErbB inhibitors may be an effective new therapeutic in BCR-ABL acute lymphoblastic leukemia due to increased apoptosis and decreased proliferation with ErbB inhibitors [143]. Martin-Subero et al discovered that ErbB2 was amplified within a Myelodysplatic Syndrome (MDS) patient who developed AML[144]. Further studies by Nordigården et al demonstrate that canertinib, a pan-ERBB inhibitor is effective in both primary samples and within a murine model for treatment of FMS-like tyrosine kinase 3 (FLT3) in patients with acute myeloid leukemia (AML) [145].

In closing, from profiling results and literature, I developed a hypothesized model for how ectopic miR-125a is altering NB4 cells function. By suppressing the ErbB pathway, there are significant alterations in several downstream effectors leading to altered cell cycle progression, proliferation, apoptosis and differentiation. Increased expression of p27 leads to inhibition of cell cycle

progression since p27 binds to cyclin-CDK complexes inhibiting their ability to promote cell cycle progression[146]. Inhibition of CAMKII in myeloid leukemia is presently being study as a potential new therapeutic since inhibition results in decreased proliferation of myeloid leukemia cells [147,148]. Through inhibition of STAT5, apoptosis [149,150] is induced and proliferation is inhibited [149-151]. Inhibition of myc within AML has shown to result in increased differentiation and apoptosis in addition to inhibition of cell cycle progression [152]. Lastly, promotion of CEBPα is known to result in differentiation of myeloid cells [56]. Confirmation of this hypothesized model will be characterized in future studies. (Figure 5.1.)

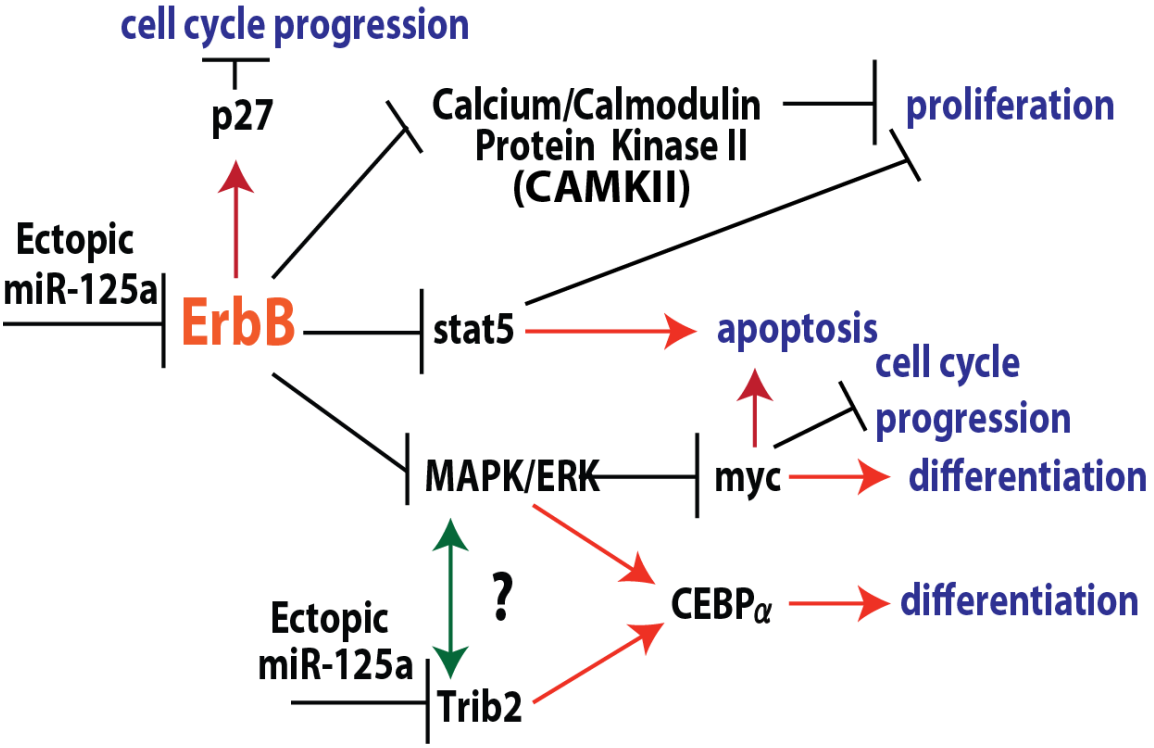

Figure 5.1. Hypothesized mechanism of action for ectopic miR-125a in NB4 cells. Black lines represent expression inhibition and red arrows represent promotion of expression. By inhibiting the ErbB pathway, miR-125a is altering p27, CAMKII, STAT5, myc, and CEBPα resulting in inhibition of cell cycle progression, proliferation while enhancing apoptosis and differentiation. Through inhibition of Trib2, miR-125a promotes CEBPα expression further enhancing differentiation.

5.2.3. Future Directions

With each insight gained when characterizing miR-125a regulation in AML and molecular pathways, new questions are raised. Though it was determined that miR-125a was epigenetically silenced by methylation, its expression was not sustained beyond 24 hours with decitabine. Treatment with decitabine aided in discovery of miR-125a suppression but could potentially be as a therapeutic if the treatment was optimized. The addition with other epigenetic modulators may yield better results as well. Since decitabine does de-methylate globally it would not specifically target miR-125a and potentially result in expression of many off targets, which is why this treatment was specifically used to determine if miR-125a was methylated.

From profiling NB4 cells ectopically expressing miR-125a in comparison to the control transduced NB4 cells, 812 genes were significantly differentially expressed. Trib2 was identified as a target due to it being a predicted target and significantly decreased. Though Trib2 was proven to be a target, it function within AML with low miR-125a was not characterized. To confirm that there is an inverse correlation of miR-125a and Trib2, the level of expression should be analyzed in both leukemic cell lines and clinical samples. Therefore in order to implicate if Trib2 could lead to the pathogenesis of miR-125a low AML, Trib2 effects on cell cycle progression, proliferation, apoptosis, and differentiation on leukemic blasts should be determined. Ectopically expressing and silencing Trib2 could establish its role in these cellular pathways. If the hypothesis of elevated Trib2 due to silenced miR-125a leads to the pathogenesis of AML, then silencing

Trib2 should decrease proliferation and cell cycle progression and potentially lead to enhanced apoptosis and differentiation. Lastly, an in vivo model should be utilized to conclude if decreased Trib2 could be a potential therapeutic for low miR-125a similar to the design suggested in Aim 1.

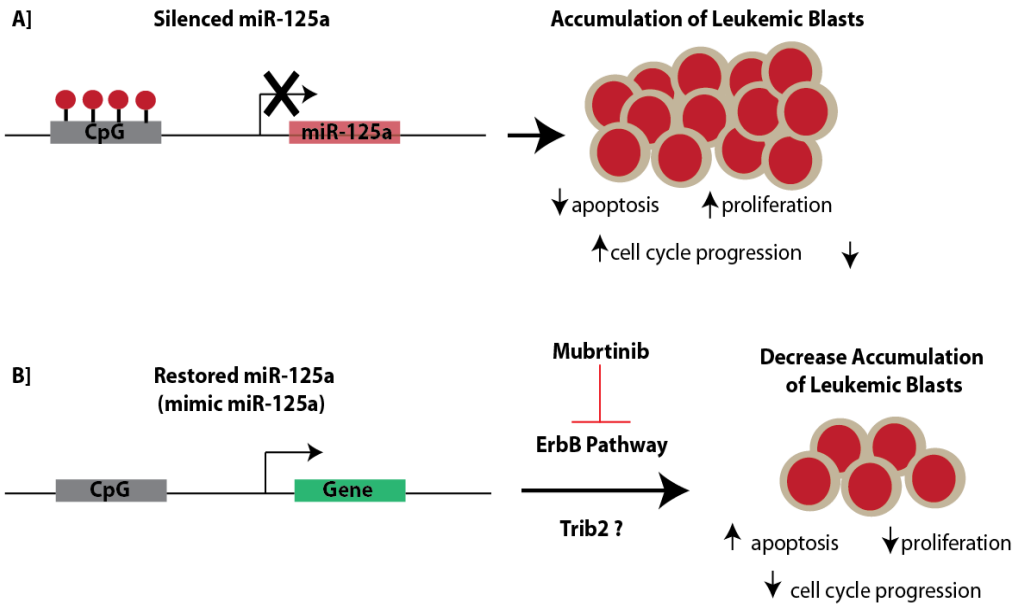

Figure 5.2. Hypothesized Model for miR-125a functional role in AML. A] Within AML, miR-125a is epigenetically suppressed by methylation leading to enhanced cell cycle progression, proliferation, and survival B] By ectopically expressing miR-125a via mimic miR-125a / epigenetic modulators or by inhibiting its aberrant pathways (ErbB by Mubritinib), leukemic blasts have decreased proliferation, cell cycle progression, and survival.

5.3. Overall Significance of Studies

As a result of these novel findings, several insights have been gained (Figure 5.2.). First, decreased miR-125a within AML may give leukemic blasts an advantage. Secondly, for the first time Trib2 is demonstrated to be a target of miR-125a within AML, suggesting it could be playing a role in AML pathogenesis for decreased miR-125a AML. From pathway analysis the systemic affects that miR's can have beyond studying a single target was presented. By utilizing pathway analysis in NB4 cells ectopically expressing miR-125a, a potential new therapeutic target for miR-125a low AML was identified, which could be tested further due to the availability of ErbB pathway inhibitors. Thus, ErbB inhibitors currently being utilized for treating ErbB overexpressing epithelial cancers could be tested in hematopoietic malignancies, such as miR-125a low AML.

REFERENCES

1. Bruce Alberts AJ, Julian Lewis, Martin Raff, Keith Roberts, and Peter Walter. Molecular Biology of the Cell. 4th edition. New York: Garland Science; 2002.

2. Orkin SH, Zon LI. Hematopoiesis: an evolving paradigm for stem cell biology. Cell 2008;132(4):631-44.

3. Park D, Sykes DB, Scadden DT. The hematopoietic stem cell niche. Frontiers in bioscience 2012;17:30-9.

4. Bockamp E, Antunes C, Liebner S, Schmitt S, Cabezas-Wallscheid N, Heck R, Ohnngemach S, Oesch-Bartlomowicz B, Rickert C, Sanchez MJ and others. In vivo fate mapping with SCL regulatory elements identifies progenitors for primitive and definitive hematopoiesis in mice. Mechanisms of development 2009;126(10):863-72.

5. Tavian M, Peault B. Embryonic development of the human hematopoietic system. The International journal of developmental biology 2005;49(2-3):243-50.

6. Wang LD, Wagers AJ. Dynamic niches in the origination and differentiation of haematopoietic stem cells. Nature reviews. Molecular cell biology 2011;12(10):643-55.

7. Sugiyama T, Nagasawa T. Bone marrow niches for hematopoietic stem cells and immune cells. Inflammation & allergy drug targets 2012;11(3):201-6.

8. Seita J, Weissman IL. Hematopoietic stem cell: self-renewal versus differentiation. Wiley interdisciplinary reviews. Systems biology and medicine 2010;2(6):640-53.

9. Wilkinson AC, Gottgens B. Transcriptional regulation of haematopoietic stem cells. Advances in experimental medicine and biology 2013;786:187-212.

10. Yoshiko Matsumoto HI, and Toshio Suda. Maintenance of Adult Stem Cells: Role of the Stem Cell Niche. In: Phinney DG, editor. Adult Stem

Cells: Biology and Methods of Analysis. Tokyo: Springer Science; 2011. p 35-55.

11. Dario-Becker J. Derived Copy of Anataomy & Physiology: A&PII. In: Physiology CAa, editor. Anatomy of the Lymphatic and Immune Systems2013.

12. Systems RD. Hematopoietic Stem Cell & Lineage-Specific Markers. R&D Systems Tools for Cell Biology Research.

13. Spitz F, Furlong EE. Transcription factors: from enhancer binding to developmental control. Nature reviews. Genetics 2012;13(9):613-26.

14. Dinarello CA. Historical insights into cytokines. European journal of immunology 2007;37 Suppl 1:S34-45.

15. Koschmieder S, Rosenbauer F, Steidl U, Owens BM, Tenen DG. Role of transcription factors C/EBPalpha and PU.1 in normal hematopoiesis and leukemia. International journal of hematology 2005;81(5):368-77.

16. Voso MT, Burn TC, Wulf G, Lim B, Leone G, Tenen DG. Inhibition of hematopoiesis by competitive binding of transcription factor PU.1. Proceedings of the National Academy of Sciences of the United States of America 1994;91(17):7932-6.

17. North TE, Stacy T, Matheny CJ, Speck NA, de Bruijn MF. Runx1 is expressed in adult mouse hematopoietic stem cells and differentiating myeloid and lymphoid cells, but not in maturing erythroid cells. Stem cells 2004;22(2):158-68.

18. Okuda T, Nishimura M, Nakao M, Fujita Y. RUNX1/AML1: a central player in hematopoiesis. International journal of hematology 2001;74(3):252-7.

19. Yamagata T, Maki K, Mitani K. Runx1/AML1 in normal and abnormal hematopoiesis. International journal of hematology 2005;82(1):1-8.

20. Kurokawa M, Hirai H. Role of AML1/Runx1 in the pathogenesis of hematological malignancies. Cancer science 2003;94(10):841-6.

21. Cai Z, de Bruijn M, Ma X, Dortland B, Luteijn T, Downing RJ, Dzierzak E. Haploinsufficiency of AML1 affects the temporal and spatial generation of hematopoietic stem cells in the mouse embryo. Immunity 2000;13(4):423-31.

22. Okuda T, van Deursen J, Hiebert SW, Grosveld G, Downing JR. AML1, the target of multiple chromosomal translocations in human leukemia, is essential for normal fetal liver hematopoiesis. Cell 1996;84(2):321-30.

23. Friedman AD. Transcriptional regulation of granulocyte and monocyte development. Oncogene 2002;21(21):3377-90.

24. Bresnick EH, Katsumura KR, Lee HY, Johnson KD, Perkins AS. Master regulatory GATA transcription factors: mechanistic principles and emerging links to hematologic malignancies. Nucleic acids research 2012;40(13):5819-31.

25. Spadaccini A, Tilbrook PA, Sarna MK, Crossley M, Bieker JJ, Klinken SP. Transcription factor erythroid Kruppel-like factor (EKLF) is essential for the erythropoietin-induced hemoglobin production but not for proliferation, viability, or morphological maturation. The Journal of biological chemistry 1998;273(37):23793-8.

26. Perrotti D, Marcucci G, Caligiuri MA. Loss of C/EBP alpha and favorable prognosis of acute myeloid leukemias: a biological paradox. Journal of clinical oncology : official journal of the American Society of Clinical Oncology 2004;22(4):582-4.

27. Zhang CC, Lodish HF. Cytokines regulating hematopoietic stem cell function. Current opinion in hematology 2008;15(4):307-11.

28. Metcalf D. Hematopoietic cytokines. Blood 2008;111(2):485-91.

29. Society LaL. 2012 Fighting Blood Cancers. <http://www.lls.org/content/nationalcontent/resourcecenter/freeeducationmaterials/generalcancer/pdf/facts.pdf%3E.

30. Li AW, Morash B, Hollenberg AN, Ur E, Wilkinson M, Murphy PR. Transcriptional regulation of the leptin gene promoter in rat GH3 pituitary

and C6 glioma cells. Molecular and cellular endocrinology 2001;176(1-2):57-65.

31. WebMD. Leukemia. In Cancer Health Center. <http://www.webmd.com/cancer/tc/leukemia-topic-overview%3E.

32. Alitheen N, S.K. Yeap, N.H. Faujan, W.Y. Ho, B.K. Beh and A.R. Mashitoh. Leukemia and Therapy. American Journal of Immunology 2011;7(4):54-61.

33. Sorbera LaV, C. Therapeutic targets for acute myeloid leukemia (AML). Drugs of the Future, Thomas Reuters 2009;34(1):67.

34. Shieffer K. 2008 Diagnosis of Myelogenous Leukemia. <http://udel.edu/~kschieff/leukemiadiagnosis.html%3E.

35. Vardiman JW, Harris NL, Brunning RD. The World Health Organization (WHO) classification of the myeloid neoplasms. Blood 2002;100(7):2292-302.

36. Dohner H, Estey EH, Amadori S, Appelbaum FR, Buchner T, Burnett AK, Dombret H, Fenaux P, Grimwade D, Larson RA and others. Diagnosis and management of acute myeloid leukemia in adults: recommendations from an international expert panel, on behalf of the European LeukemiaNet. Blood 2010;115(3):453-74.

37. Assouline S. Lecture 31. Clinical Aspects of Acute and Chronic Leukemia.

38. Tonks A, Pearn L, Mills KI, Burnett AK, Darley RL. The sensitivity of human cells expressing RUNX1-RUNX1T1 to chemotherapeutic agents. Leukemia 2006;20(10):1883-5.

39. Licht JD. AML1 and the AML1-ETO fusion protein in the pathogenesis of t(8;21) AML. Oncogene 2001;20(40):5660-79.

40. Hyde RK, Liu PP. RUNX1 repression-independent mechanisms of leukemogenesis by fusion genes CBFB-MYH11 and AML1-ETO (RUNX1-RUNX1T1). Journal of cellular biochemistry 2010;110(5):1039-45.

41. Zelent KPaA. AML1/ETO, a promiscuous fusion oncoprotein. Neoplasia 2007;109(10):4109-4110.

42. Mulloy JC, Cammenga J, MacKenzie KL, Berguido FJ, Moore MA, Nimer SD. The AML1-ETO fusion protein promotes the expansion of human hematopoietic stem cells. Blood 2002;99(1):15-23.

43. Labbaye C, Valtieri M, Grignani F, Puglisi R, Luchetti L, Masella B, Alcalay M, Testa U, Peschle C. Expression and role of PML gene in normal adult hematopoiesis: functional interaction between PML and Rb proteins in erythropoiesis. Oncogene 1999;18(23):3529-40.

44. Collins SJ. The role of retinoids and retinoic acid receptors in normal hematopoiesis. Leukemia 2002;16(10):1896-905.

45. Raelson JV, Nervi C, Rosenauer A, Benedetti L, Monczak Y, Pearson M, Pelicci PG, Miller WH, Jr. The PML/RAR alpha oncoprotein is a direct molecular target of retinoic acid in acute promyelocytic leukemia cells. Blood 1996;88(8):2826-32.

46. Rousselot P, Hardas B, Patel A, Guidez F, Gaken J, Castaigne S, Dejean A, de The H, Degos L, Farzaneh F and others. The PML-RAR alpha gene product of the t(15;17) translocation inhibits retinoic acid-induced granulocytic differentiation and mediated transactivation in human myeloid cells. Oncogene 1994;9(2):545-51.

47. Jing Y. The PML-RARalpha fusion protein and targeted therapy for acute promyelocytic leukemia. Leukemia & lymphoma 2004;45(4):639-48.

48. Hyde RK, Kamikubo Y, Anderson S, Kirby M, Alemu L, Zhao L, Liu PP. Cbfb/Runx1 repression-independent blockage of differentiation and accumulation of Csf2rb-expressing cells by Cbfb-MYH11. Blood 2010;115(7):1433-43.

49. Wells L, Edwards KA, Bernstein SI. Myosin heavy chain isoforms regulate muscle function but not myofibril assembly. The EMBO journal 1996;15(17):4454-9.

50. Castilla LH, Garrett L, Adya N, Orlic D, Dutra A, Anderson S, Owens J, Eckhaus M, Bodine D, Liu PP. The fusion gene Cbfb-MYH11 blocks

myeloid differentiation and predisposes mice to acute myelomonocytic leukaemia. Nature genetics 1999;23(2):144-6.

51. Falini B, Martelli MP, Bolli N, Sportoletti P, Liso A, Tiacci E, Haferlach T. Acute myeloid leukemia with mutated nucleophosmin (NPM1): is it a distinct entity? Blood 2011;117(4):1109-20.

52. Bolli N, Payne EM, Grabher C, Lee JS, Johnston AB, Falini B, Kanki JP, Look AT. Expression of the cytoplasmic NPM1 mutant (NPMc+) causes the expansion of hematopoietic cells in zebrafish. Blood 2010;115(16):3329-40.

53. Argiropoulos B, Humphries RK. Hox genes in hematopoiesis and leukemogenesis. Oncogene 2007;26(47):6766-76.

54. Alharbi RA, Pettengell R, Pandha HS, Morgan R. The role of HOX genes in normal hematopoiesis and acute leukemia. Leukemia 2013;27(5):1000-8.

55. Shih LY, Liang DC, Huang CF, Wu JH, Lin TL, Wang PN, Dunn P, Kuo MC, Tang TC. AML patients with CEBPalpha mutations mostly retain identical mutant patterns but frequently change in allelic distribution at relapse: a comparative analysis on paired diagnosis and relapse samples. Leukemia 2006;20(4):604-9.

56. Paz-Priel I, Friedman A. C/EBPalpha dysregulation in AML and ALL. Critical reviews in oncogenesis 2011;16(1-2):93-102.

57. Ballabio E, Milne TA. Molecular and Epigenetic Mechanisms of MLL in Human Leukemogenesis. Cancers 2012;4(3):904-44.

58. Marschalek R. Mechanisms of leukemogenesis by MLL fusion proteins. British journal of haematology 2011;152(2):141-54.

59. Unnisa Z, Clark JP, Roychoudhury J, Thomas E, Tessarollo L, Copeland NG, Jenkins NA, Grimes HL, Kumar AR. Meis1 preserves hematopoietic stem cells in mice by limiting oxidative stress. Blood 2012;120(25):4973-81.

60. Broxmeyer HE, Mor-Vaknin N, Kappes F, Legendre M, Saha AK, Ou X, O'Leary H, Capitano M, Cooper S, Markovitz DM. Concise review: role of DEK in stem/progenitor cell biology. Stem cells 2013;31(8):1447-53.

61. Koleva RI, Ficarro SB, Radomska HS, Carrasco-Alfonso MJ, Alberta JA, Webber JT, Luckey CJ, Marcucci G, Tenen DG, Marto JA. C/EBPalpha and DEK coordinately regulate myeloid differentiation. Blood 2012;119(21):4878-88.

62. Hutten S, Kehlenbach RH. Nup214 is required for CRM1-dependent nuclear protein export in vivo. Molecular and cellular biology 2006;26(18):6772-85.

63. Sanden C, Ageberg M, Petersson J, Lennartsson A, Gullberg U. Forced expression of the DEK-NUP214 fusion protein promotes proliferation dependent on upregulation of mTOR. BMC cancer 2013;13:440.

64. Gilliland DG, Griffin JD. The roles of FLT3 in hematopoiesis and leukemia. Blood 2002;100(5):1532-42.

65. Kikushige Y, Yoshimoto G, Miyamoto T, Iino T, Mori Y, Iwasaki H, Niiro H, Takenaka K, Nagafuji K, Harada M and others. Human Flt3 is expressed at the hematopoietic stem cell and the granulocyte/macrophage progenitor stages to maintain cell survival. Journal of immunology 2008;180(11):7358-67.

66. Pradeep Singh Chauhan RI, L. C. Singh, Dipendra Kumar Gupta, Vishakha Mittal, and Sujala Kapur. Mutation of NPM1 and FLT3 Genes in Acute Myeloid Leukemia and Their Association with Clinical and Immunophenotypic Features. Disease Markers 2013;35(5):581-588.

67. Thiede C, Koch S, Creutzig E, Steudel C, Illmer T, Schaich M, Ehninger G. Prevalence and prognostic impact of NPM1 mutations in 1485 adult patients with acute myeloid leukemia (AML). Blood 2006;107(10):4011-20.

68. Dupont C, Armant DR, Brenner CA. Epigenetics: definition, mechanisms and clinical perspective. Seminars in reproductive medicine 2009;27(5):351-7.

69. Cheung P, Lau P. Epigenetic regulation by histone methylation and histone variants. Molecular endocrinology 2005;19(3):563-73.

70. Suganuma T, Workman JL. Signals and combinatorial functions of histone modifications. Annual review of biochemistry 2011;80:473-99.

71. Dootz R, Toma AC, Pfohl T. Structural and dynamic properties of linker histone H1 binding to DNA. Biomicrofluidics 2011;5(2):24104.

72. Annunziato AT. DNA Packaging: Nucleosomes and Chromatin. Chromosomes and Cytogenetics, Nature Education 2008.

73. Bannister AJ, Kouzarides T. Regulation of chromatin by histone modifications. Cell research 2011;21(3):381-95.

74. Cohen I, Poreba E, Kamieniarz K, Schneider R. Histone modifiers in cancer: friends or foes? Genes & cancer 2011;2(6):631-47.

75. Sterner DE, Berger SL. Acetylation of histones and transcription-related factors. Microbiology and molecular biology reviews : MMBR 2000;64(2):435-59.

76. Zhang Y. Transcriptional regulation by histone ubiquitination and deubiquitination. Genes & development 2003;17(22):2733-40.

77. Klose RJ, Zhang Y. Regulation of histone methylation by demethylimination and demethylation. Nature reviews. Molecular cell biology 2007;8(4):307-18.

78. Rossetto D, Avvakumov N, Cote J. Histone phosphorylation: a chromatin modification involved in diverse nuclear events. Epigenetics : official journal of the DNA Methylation Society 2012;7(10):1098-108.

79. Biotechnology A. 2013 Nucelosomes and Histone Proteins. <http://www.amsbio.com/Nucleosomes-and-Histone-Proteins.aspx%3E.

80. Rodriguez-Paredes M, Esteller M. Cancer epigenetics reaches mainstream oncology. Nature medicine 2011;17(3):330-9.

81. Deaton AM, Bird A. CpG islands and the regulation of transcription. Genes & development 2011;25(10):1010-22.

82. Illingworth RS, Gruenewald-Schneider U, Webb S, Kerr AR, James KD, Turner DJ, Smith C, Harrison DJ, Andrews R, Bird AP. Orphan CpG islands identify numerous conserved promoters in the mammalian genome. PLoS genetics 2010;6(9):e1001134.

83. Fuks F. DNA methylation and histone modifications: teaming up to silence genes. Current opinion in genetics & development 2005;15(5):490-5.

84. Curradi M, Izzo A, Badaracco G, Landsberger N. Molecular mechanisms of gene silencing mediated by DNA methylation. Molecular and cellular biology 2002;22(9):3157-73.

85. Marcucci G, Haferlach T, Dohner H. Molecular genetics of adult acute myeloid leukemia: prognostic and therapeutic implications. Journal of clinical oncology : official journal of the American Society of Clinical Oncology 2011;29(5):475-86.

86. Plass C, Oakes C, Blum W, Marcucci G. Epigenetics in acute myeloid leukemia. Seminars in oncology 2008;35(4):378-87.

87. Mizuno S, Chijiwa T, Okamura T, Akashi K, Fukumaki Y, Niho Y, Sasaki H. Expression of DNA methyltransferases DNMT1, 3A, and 3B in normal hematopoiesis and in acute and chronic myelogenous leukemia. Blood 2001;97(5):1172-9.

88. Lubbert M, Minden M. Decitabine in acute myeloid leukemia. Seminars in hematology 2005;42(3 Suppl 2):S38-42.

89. Claus R, Lubbert M. Epigenetic targets in hematopoietic malignancies. Oncogene 2003;22(42):6489-96.

90. Bernadette F Rodak GAF, Kathryn Doig. Hematology Clinical Principles and Applications. W.B. Saunders Company; 2007.

91. Sears DW. 2009 Blood Cell Identification by Staining and Morphology.

92. Vance GH, Nickerson C, Sarnat L, Zhang A, Henegariu O, Morichon-Delvallez N, Butler MG, Palmer CG. Molecular cytogenetic analysis of patients with holoprosencephaly and structural rearrangements of 7q. American journal of medical genetics 1998;76(1):51-7.

93. Frohling S, Skelin S, Liebisch C, Scholl C, Schlenk RF, Dohner H, Dohner K. Comparison of cytogenetic and molecular cytogenetic detection of chromosome abnormalities in 240 consecutive adult patients with acute myeloid leukemia. Journal of clinical oncology : official journal of the American Society of Clinical Oncology 2002;20(10):2480-5.

94. Padron E, Fernandez H. Anthracycline dose intensification in young adults with acute myeloid leukemia. Therapeutic advances in hematology 2012;3(1):17-27.

95. Robak T, Wierzbowska A. Current and emerging therapies for acute myeloid leukemia. Clinical therapeutics 2009;31 Pt 2:2349-70.

96. Fathi AT, Grant S, Karp JE. Exploiting cellular pathways to develop new treatment strategies for AML. Cancer treatment reviews 2010;36(2):142-50.

97. Starega-Roslan J, Koscianska E, Kozlowski P, Krzyzosiak WJ. The role of the precursor structure in the biogenesis of microRNA. Cellular and molecular life sciences : CMLS 2011;68(17):2859-71.

98. Francia S, Michelini F, Saxena A, Tang D, de Hoon M, Anelli V, Mione M, Carninci P, d'Adda di Fagagna F. Site-specific DICER and DROSHA RNA products control the DNA-damage response. Nature 2012;488(7410):231-5.

99. Winter J, Jung S, Keller S, Gregory RI, Diederichs S. Many roads to maturity: microRNA biogenesis pathways and their regulation. Nature cell biology 2009;11(3):228-34.

100. Pratt AJ, MacRae IJ. The RNA-induced silencing complex: a versatile gene-silencing machine. The Journal of biological chemistry 2009;284(27):17897-901.

101. Friedman RC, Farh KK, Burge CB, Bartel DP. Most mammalian mRNAs are conserved targets of microRNAs. Genome research 2009;19(1):92-105.

102. miRBase. 2013 In release 20. <http://www.mirbase.org/index.shtml%3E.

103. Kluiver J, Kroesen BJ, Poppema S, van den Berg A. The role of microRNAs in normal hematopoiesis and hematopoietic malignancies. Leukemia : official journal of the Leukemia Society of America, Leukemia Research Fund, U.K 2006;20(11):1931-6.

104. Petriv OI, Kuchenbauer F, Delaney AD, Lecault V, White A, Kent D, Marmolejo L, Heuser M, Berg T, Copley M and others. Comprehensive microRNA expression profiling of the hematopoietic hierarchy. Proceedings of the National Academy of Sciences of the United States of America 2010;107(35):15443-8.

105. Garzon R, Volinia S, Liu CG, Fernandez-Cymering C, Palumbo T, Pichiorri F, Fabbri M, Coombes K, Alder H, Nakamura T and others. MicroRNA signatures associated with cytogenetics and prognosis in acute myeloid leukemia. Blood 2008;111(6):3183-9.

106. Jongen-Lavrencic M, Sun SM, Dijkstra MK, Valk PJ, Lowenberg B. MicroRNA expression profiling in relation to the genetic heterogeneity of acute myeloid leukemia. Blood 2008;111(10):5078-85.

107. Ramsingh G, Koboldt DC, Trissal M, Chiappinelli KB, Wylie T, Koul S, Chang LW, Nagarajan R, Fehniger TA, Goodfellow P and others. Complete characterization of the microRNAome in a patient with acute myeloid leukemia. Blood 2010;116(24):5316-26.

108. Guo S, Lu J, Schlanger R, Zhang H, Wang JY, Fox MC, Purton LE, Fleming HH, Cobb B, Merkenschlager M and others. MicroRNA miR-125a controls hematopoietic stem cell number. Proceedings of the National Academy of Sciences of the United States of America 2010;107(32):14229-34.

109. Gerrits A, Walasek MA, Olthof S, Weersing E, Ritsema M, Zwart E, van Os R, Bystrykh LV, de Haan G. Genetic screen identifies microRNA cluster 99b/let-7e/125a as a regulator of primitive hematopoietic cells. Blood 2012;119(2):377-87.

110. Sun YM, Lin KY, Chen YQ. Diverse functions of miR-125 family in different cell contexts. Journal of hematology & oncology 2013;6:6.

111. Balakrishnan A, Stearns AT, Park PJ, Dreyfuss JM, Ashley SW, Rhoads DB, Tavakkolizadeh A. Upregulation of proapoptotic microRNA mir-125a after massive small bowel resection in rats. Annals of surgery 2012;255(4):747-53.

112. Chen J, Chen Y, Chen Z. MiR-125a/b regulates the activation of cancer stem cells in paclitaxel-resistant colon cancer. Cancer investigation 2013;31(1):17-23.

113. Ferretti E, De Smaele E, Po A, Di Marcotullio L, Tosi E, Espinola MS, Di Rocco C, Riccardi R, Giangaspero F, Farcomeni A and others. MicroRNA profiling in human medulloblastoma. International journal of cancer. Journal international du cancer 2009;124(3):568-77.

114. Nishida N, Mimori K, Fabbri M, Yokobori T, Sudo T, Tanaka F, Shibata K, Ishii H, Doki Y, Mori M. MicroRNA-125a-5p is an independent prognostic factor in gastric cancer and inhibits the proliferation of human gastric cancer cells in combination with trastuzumab. Clinical cancer research : an official journal of the American Association for Cancer Research 2011;17(9):2725-33.

115. Scott GK, Goga A, Bhaumik D, Berger CE, Sullivan CS, Benz CC. Coordinate suppression of ERBB2 and ERBB3 by enforced expression of micro-RNA miR-125a or miR-125b. The Journal of biological chemistry 2007;282(2):1479-86.

116. Hollenbach PW, Nguyen AN, Brady H, Williams M, Ning Y, Richard N, Krushel L, Aukerman SL, Heise C, MacBeth KJ. A comparison of azacitidine and decitabine activities in acute myeloid leukemia cell lines. PloS one 2010;5(2):e9001.

117. Nagasawa J, Mizokami A, Koshida K, Yoshida S, Naito K, Namiki M. Novel HER2 selective tyrosine kinase inhibitor, TAK-165, inhibits bladder, kidney and androgen-independent prostate cancer in vitro and in vivo. International journal of urology : official journal of the Japanese Urological Association 2006;13(5):587-92.

118. Livak KJ, Schmittgen TD. Analysis of relative gene expression data using real-time quantitative PCR and the 2(-Delta Delta C(T)) Method. Methods 2001;25(4):402-8.

119. Gatto S, Della Ragione F, Cimmino A, Strazzullo M, Fabbri M, Mutarelli M, Ferraro L, Weisz A, D'Esposito M, Matarazzo MR. Epigenetic alteration of microRNAs in DNMT3B-mutated patients of ICF syndrome. Epigenetics : official journal of the DNA Methylation Society 2010;5(5):427-43.

120. Duan R, Pak C, Jin P. Single nucleotide polymorphism associated with mature miR-125a alters the processing of pri-miRNA. Human molecular genetics 2007;16(9):1124-31.

121. Krol J, Loedige I, Filipowicz W. The widespread regulation of microRNA biogenesis, function and decay. Nature reviews. Genetics 2010;11(9):597-610.

122. Treiber T, Treiber N, Meister G. Regulation of microRNA biogenesis and function. Thrombosis and haemostasis 2012;107(4):605-10.

123. Schanen BC, Li X. Transcriptional regulation of mammalian miRNA genes. Genomics 2011;97(1):1-6.

124. Obernosterer G, Leuschner PJ, Alenius M, Martinez J. Post-transcriptional regulation of microRNA expression. RNA 2006;12(7):1161-7.

125. Thomson JM, Newman M, Parker JS, Morin-Kensicki EM, Wright T, Hammond SM. Extensive post-transcriptional regulation of microRNAs and its implications for cancer. Genes & development 2006;20(16):2202-7.

126. Keeshan K, He Y, Wouters BJ, Shestova O, Xu L, Sai H, Rodriguez CG, Maillard I, Tobias JW, Valk P and others. Tribbles homolog 2 inactivates C/EBPalpha and causes acute myelogenous leukemia. Cancer cell 2006;10(5):401-11.

127. Keeshan K, Shestova O, Ussin L, Pear WS. Tribbles homolog 2 (Trib2) and HoxA9 cooperate to accelerate acute myelogenous leukemia. Blood cells, molecules & diseases 2008;40(1):119-21.

128. Hynes NE, MacDonald G. ErbB receptors and signaling pathways in cancer. Current opinion in cell biology 2009;21(2):177-84.

129. Jelovac D, Emens LA. HER2-directed therapy for metastatic breast cancer. Oncology 2013;27(3):166-75.

130. Mund C, Hackanson B, Stresemann C, Lubbert M, Lyko F. Characterization of DNA demethylation effects induced by 5-Aza-2'-deoxycytidine in patients with myelodysplastic syndrome. Cancer research 2005;65(16):7086-90.

131. Hagemann S, Heil O, Lyko F, Brueckner B. Azacytidine and decitabine induce gene-specific and non-random DNA demethylation in human cancer cell lines. PloS one 2011;6(3):e17388.

132. Kracmarova A, Cermak J, Brdicka R, Bruchova H. High expression of ERCC1, FLT1, NME4 and PCNA associated with poor prognosis and advanced stages in myelodysplastic syndrome. Leukemia & lymphoma 2008;49(7):1297-305.

133. Bernal T, Moncada-Pazos A, Soria-Valles C, Gutierrez-Fernandez A. Effects of azacitidine on matrix metalloproteinase-9 in acute myeloid leukemia and myelodysplasia. Experimental hematology 2013;41(2):172-9.

134. Testa U, Riccioni R, Militi S, Coccia E, Stellacci E, Samoggia P, Latagliata R, Mariani G, Rossini A, Battistini A and others. Elevated expression of IL-3Ralpha in acute myelogenous leukemia is associated with enhanced blast proliferation, increased cellularity, and poor prognosis. Blood 2002;100(8):2980-8.

135. Tettamanti S, Marin V, Pizzitola I, Magnani CF, Giordano Attianese GM, Cribioli E, Maltese F, Galimberti S, Lopez AF, Biondi A and others. Targeting of acute myeloid leukaemia by cytokine-induced killer cells redirected with a novel CD123-specific chimeric antigen receptor. British journal of haematology 2013;161(3):389-401.

136. Kugler M, Stein C, Kellner C, Mentz K, Saul D, Schwenkert M, Schubert I, Singer H, Oduncu F, Stockmeyer B and others. A recombinant trispecific single-chain Fv derivative directed against CD123 and CD33 mediates

effective elimination of acute myeloid leukaemia cells by dual targeting. British journal of haematology 2010;150(5):574-86.

137. Rao DS, Hyun TS, Kumar PD, Mizukami IF, Rubin MA, Lucas PC, Sanda MG, Ross TS. Huntingtin-interacting protein 1 is overexpressed in prostate and colon cancer and is critical for cellular survival. The Journal of clinical investigation 2002;110(3):351-60.

138. Jin W, Wu K, Li YZ, Yang WT, Zou B, Zhang F, Zhang J, Wang KK. AML1-ETO targets and suppresses cathepsin G, a serine protease, which is able to degrade AML1-ETO in t(8;21) acute myeloid leukemia. Oncogene 2013;32(15):1978-87.

139. Voehringer D, van Rooijen N, Locksley RM. Eosinophils develop in distinct stages and are recruited to peripheral sites by alternatively activated macrophages. Journal of leukocyte biology 2007;81(6):1434-44.

140. DiMartino JF, Lacayo NJ, Varadi M, Li L, Saraiya C, Ravindranath Y, Yu R, Sikic BI, Raimondi SC, Dahl GV. Low or absent SPARC expression in acute myeloid leukemia with MLL rearrangements is associated with sensitivity to growth inhibition by exogenous SPARC protein. Leukemia 2006;20(3):426-32.

141. Giallongo C, La Cava P, Tibullo D, Barbagallo I, Parrinello N, Cupri A, Stagno F, Consoli C, Chiarenza A, Palumbo GA and others. SPARC expression in CML is associated to imatinib treatment and to inhibition of leukemia cell proliferation. BMC cancer 2013;13:60.

142. Keeshan K, Bailis W, Dedhia PH, Vega ME, Shestova O, Xu L, Toscano K, Uljon SN, Blacklow SC, Pear WS. Transformation by Tribbles homolog 2 (Trib2) requires both the Trib2 kinase domain and COP1 binding. Blood 2010;116(23):4948-57.

143. Irwin ME, Nelson LD, Santiago-O'Farrill JM, Knouse PD, Miller CP, Palla SL, Siwak DR, Mills GB, Estrov Z, Li S and others. Small molecule ErbB inhibitors decrease proliferative signaling and promote apoptosis in philadelphia chromosome-positive acute lymphoblastic leukemia. PloS one 2013;8(8):e70608.

144. Martin-Subero JI, Harder L, Gesk S, Schoch R, Novo FJ, Grote W, Calasanz MJ, Schlegelberger B, Siebert R. Amplification of ERBB2,

RARA, and TOP2A genes in a myelodysplastic syndrome transforming to acute myeloid leukemia. Cancer genetics and cytogenetics 2001;127(2):174-6.

145. Nordigarden A, Zetterblad J, Trinks C, Green H, Eliasson P, Druid P, Lotfi K, Ronnstrand L, Walz TM, Jonsson JI. Irreversible pan-ERBB inhibitor canertinib elicits anti-leukaemic effects and induces the regression of FLT3-ITD transformed cells in mice. British journal of haematology 2011;155(2):198-208.

146. Coqueret O. New roles for p21 and p27 cell-cycle inhibitors: a function for each cell compartment? Trends in cell biology 2003;13(2):65-70.

147. Si J, Collins SJ. Activated Ca2+/calmodulin-dependent protein kinase IIgamma is a critical regulator of myeloid leukemia cell proliferation. Cancer research 2008;68(10):3733-42.

148. Gu Y, Chen T, Meng Z, Gan Y, Xu X, Lou G, Li H, Gan X, Zhou H, Tang J and others. CaMKII gamma, a critical regulator of CML stem/progenitor cells, is a target of the natural product berbamine. Blood 2012;120(24):4829-39.

149. Tam WF, Hahnel PS, Schuler A, Lee BH, Okabe R, Zhu N, Pante SV, Raffel G, Mercher T, Wernig G and others. STAT5 is crucial to maintain leukemic stem cells in acute myelogenous leukemias induced by MOZ-TIF2. Cancer research 2013;73(1):373-84.

150. Baskiewicz-Masiuk M, Machalinski B. The role of the STAT5 proteins in the proliferation and apoptosis of the CML and AML cells. European journal of haematology 2004;72(6):420-9.

151. Kaymaz BT, Selvi N, Gunduz C, Aktan C, Dalmizrak A, Saydam G, Kosova B. Repression of STAT3, STAT5A, and STAT5B expressions in chronic myelogenous leukemia cell line K-562 with unmodified or chemically modified siRNAs and induction of apoptosis. Annals of hematology 2013;92(2):151-62.

152. Huang MJ, Cheng YC, Liu CR, Lin S, Liu HE. A small-molecule c-Myc inhibitor, 10058-F4, induces cell-cycle arrest, apoptosis, and myeloid differentiation of human acute myeloid leukemia. Experimental hematology 2006;34(11):1480-9.

APPENDIX A: MIR-125A CLUSTER EXPRESSION IN PARAFFIN EMBEDDED SAMPLES FROM AML PATIENTS

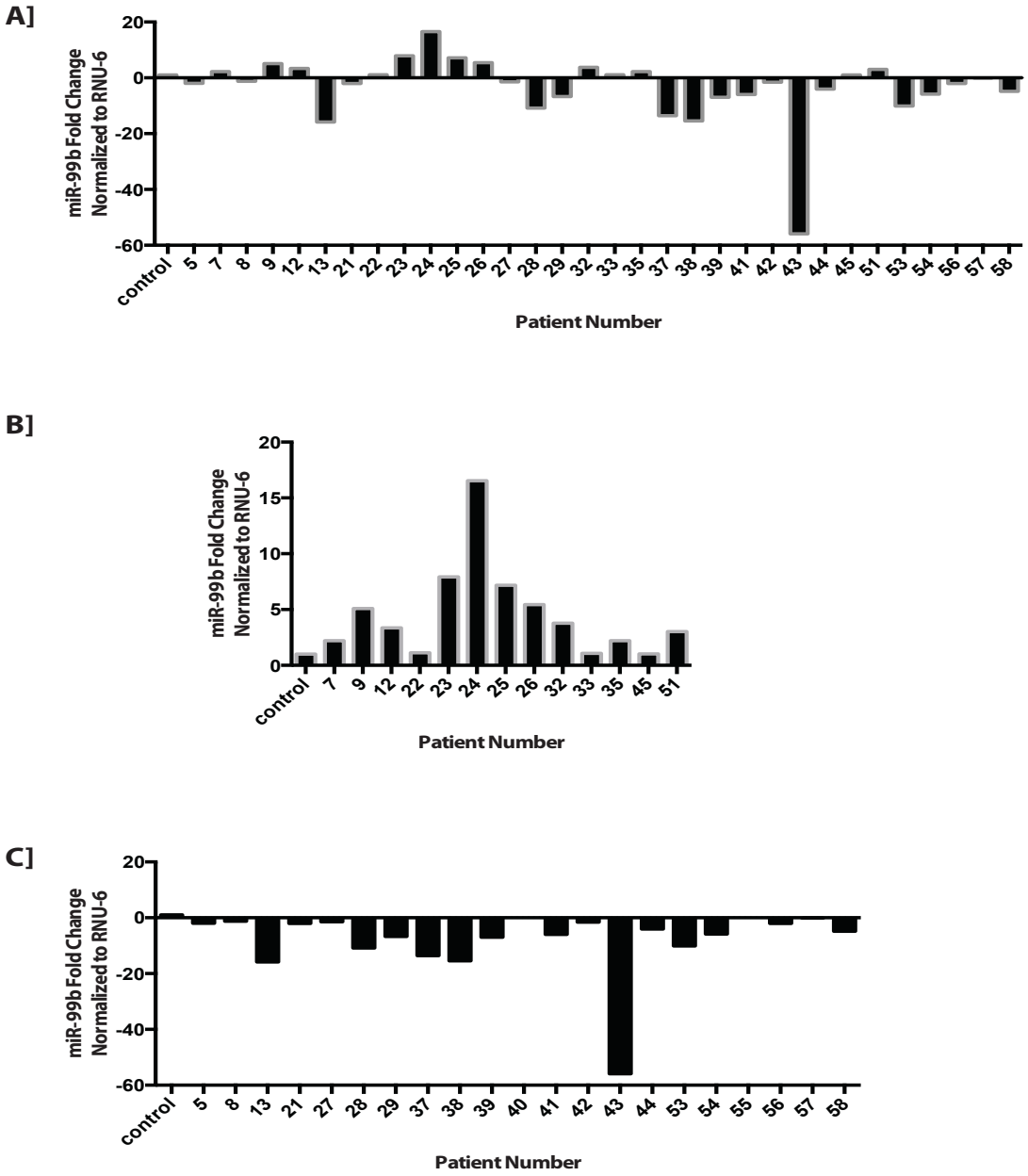

Figure A.1. miR-99b expression is decreased in AML from paraffin embedded bone marrow samples. A] miR-99b expression in paraffin embedded bone marrow samples from AML patients and healthy CD34+ samples B] Patient samples with increased miR-99b expression compared to healthy CD34+ samples C] Patient samples with decreased miR-99b expression compared to healthy CD34+ samples.

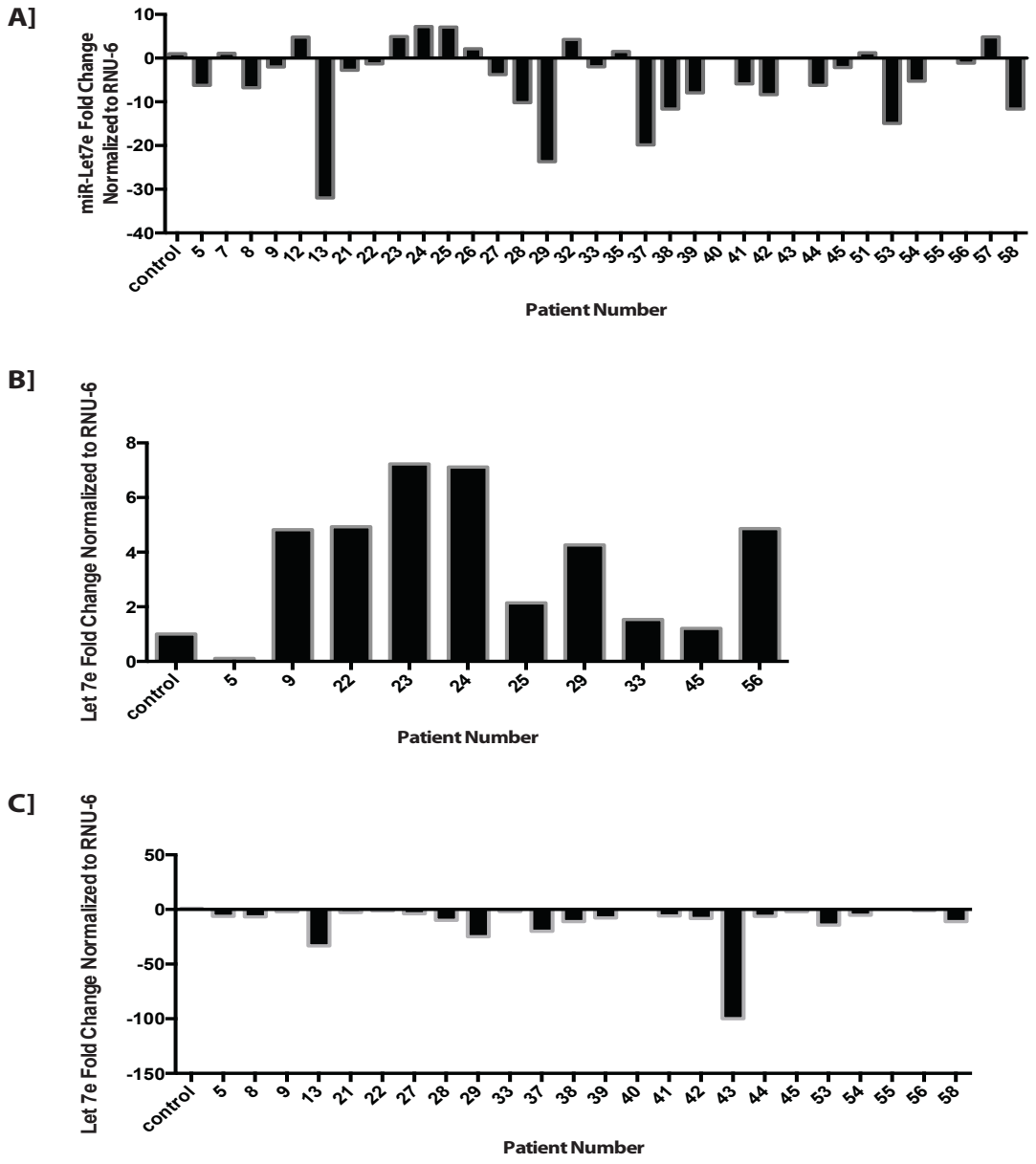

Figure A.2. miR-let7e expression is decreased in AML from paraffin embedded bone marrow samples. A] miR-let7e expression in paraffin embedded bone marrow samples from AML patients and healthy CD34+ samples B] Patient samples with increased miR-let7e expression compared to healthy CD34+ samples C] Patient samples with decreased miR-let7e expression compared to healthy CD34+ samples.

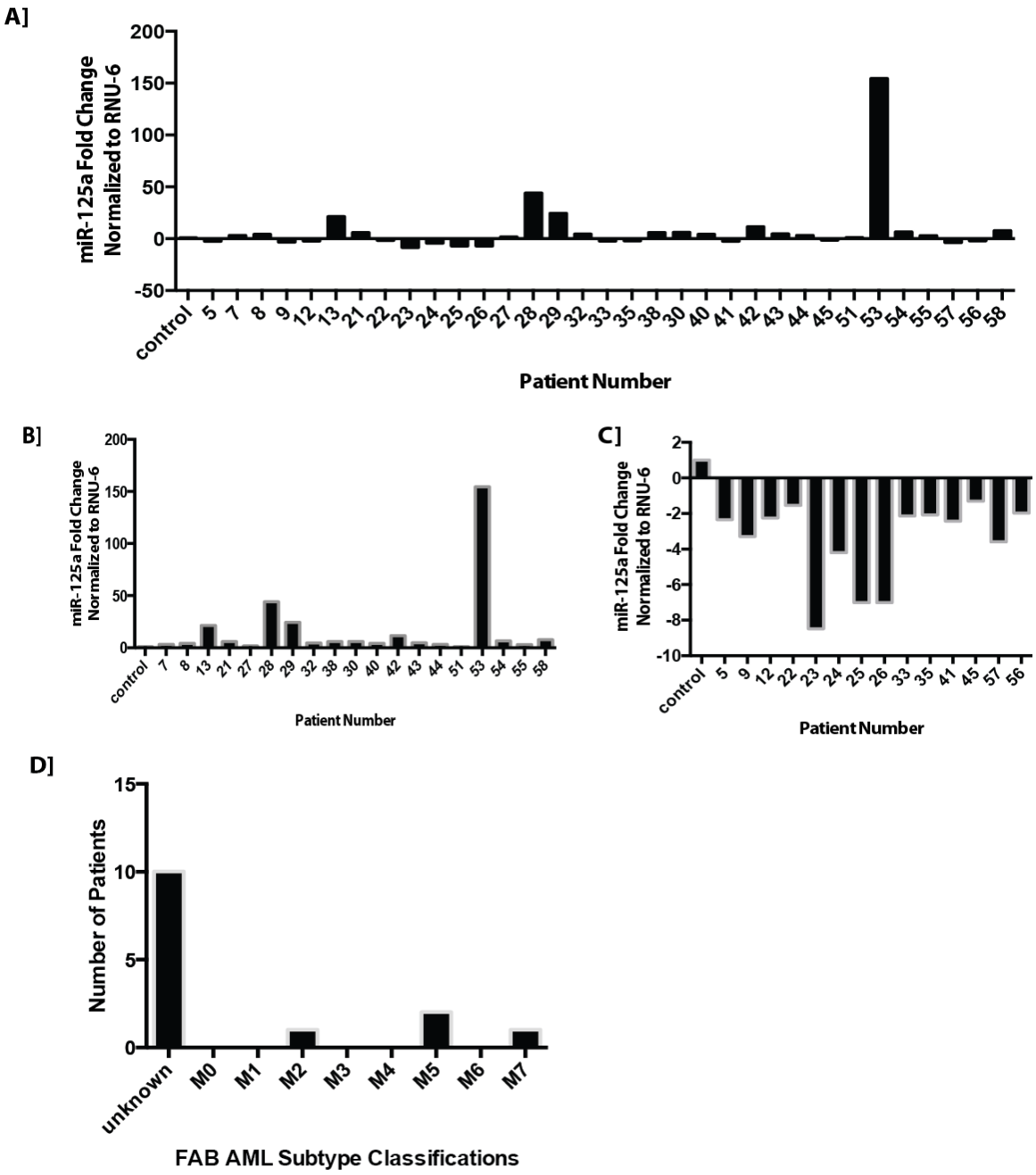

Figure A.3. miR-125a expression is decreased in AML from paraffin embedded bone marrow samples. A] miR-125a expression in paraffin embedded bone marrow samples from AML patients and healthy CD34+ samples B] Patient samples with increased miR-125a expression compared to healthy CD34+ samples C] Patient samples with decreased miR-125a expression compared to healthy CD34+ samples D] miR-125a expression analyzed in random paraffin embedded samples in comparison to healthy CD34+ samples E] French-American-British AML subtype classification of clinical AML samples and their corresponding normalized small RNA sequencing miR-125a-5p expression level.

APPENDIX B: TRANSFECTION OF MIMIC MIR-125A, HAIRPIN INHIBITOR OF MIR-125A AND CONTROL IN NB4 CELLS

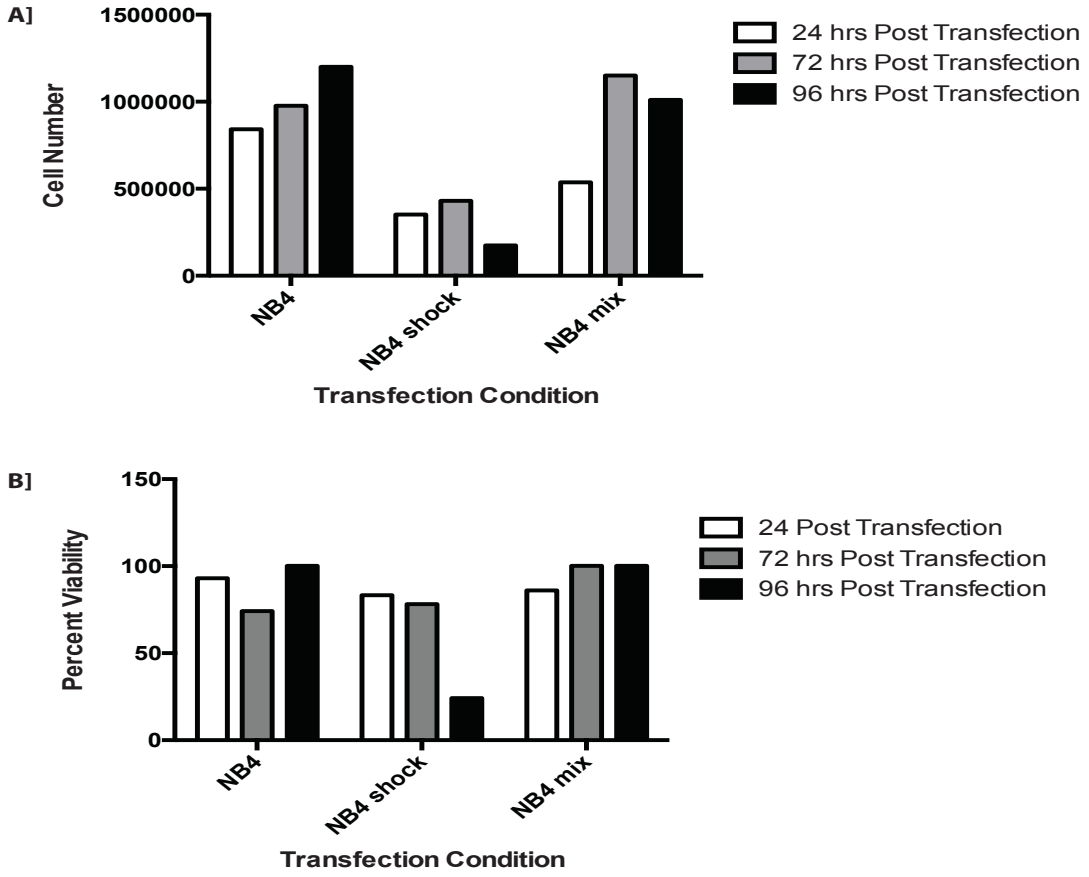

Figure B.1. Effects of transfection on cell number and viability of NB4 cell. A] Cell number post transfection conditions at 24, 48, and 72 hours post condition determined by Moxi B] Cell viability post transfection conditions at 24, 48, and 72 hours post condition determined by Moxi.

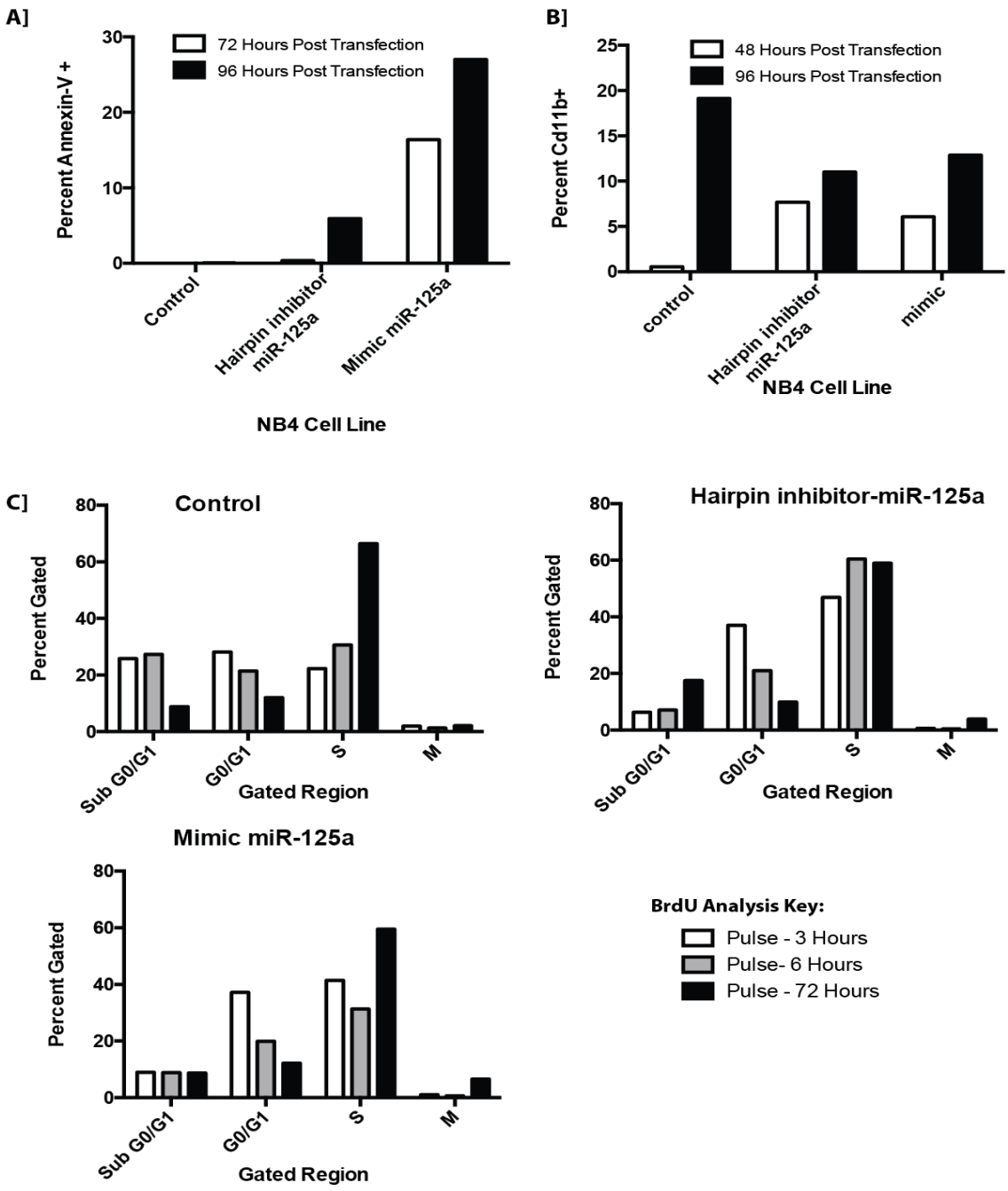

Figure B.2. Transfection of mimic miR-125a leads to altered cellular function of NB4 cells. A] Apoptosis analysis via Annexin-V+ staining of NB4 cells transfected with control, hairpin inhibitor miR-125a and mimic miR-125a B] Differentiation analysis via Cd11b+ staining of NB4 cells transfected with control, hairpin inhibitor miR-125a and mimic miR-125a C] Cell cycle analysis via BrdU incorporation of NB4 cells transfected with control, hairpin inhibitor miR-125a and mimic miR-125a.

APPENDIX C: PROFILING RESULTS

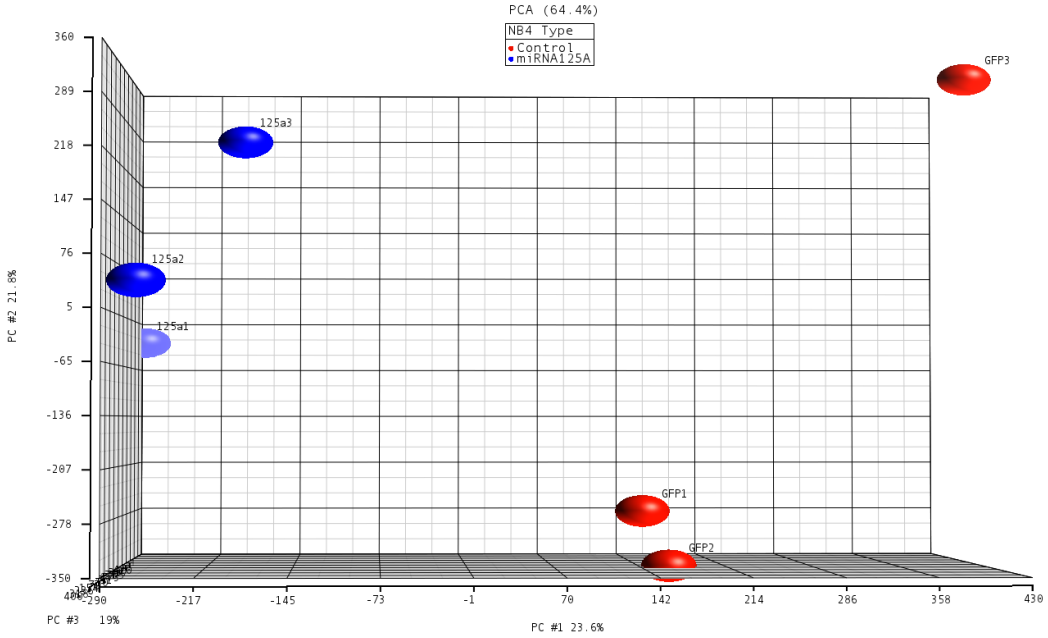

Figure C.1. Principle component analysis. Red represents values for each GFP-NB4 sample and blue represents each miR-125a shMIMIC-NB4 sample.

A] Decreased genes

Gene Symbol	RefSeq	p-value (miRNA125A vs. Control)	Fold-Change (miRNA125A vs. Control)
THBS1	ENST00000260356	5.27E-05	-10.9747
	---	4.17E-05	-10.9382
CCL2	NM_002982	0.000536621	-5.21197
GPX7	NM_015696	4.56E-05	-4.26209
LOC283710	NM_001243538	0.00101942	-3.88959
CYP51A1	NM_000786	6.28E-06	-3.38293
LOC100130876	AK130278	6.15E-05	-3.19698
	---	0.0210288	-3.12791
C15orf54	ENST00000318578	0.00145414	-3.06882
SLC24A3	NM_020689	0.00273443	-2.91811
	---	0.00503588	-2.84281
RN5S496	ENST00000391240	0.00347104	-2.83131
		0.0325195	-2.82142
	---	0.0496001	-2.67222
	---	0.000118335	-2.66747
	---	0.00100138	-2.65801
	---	0.00106834	-2.63649
	---	2.31E-05	-2.61604
		0.0275157	-2.59761
	---	5.45E-05	-2.55932
TSPAN2	NM_005725	0.013072	-2.54781
H1F0	NM_005318	0.00100074	-2.54719
	---	0.0122709	-2.54492
SIGLEC6	NM_001245	7.79E-06	-2.54292
SPATA2	NM_001135773	0.000485145	-2.50221
	---	0.0119872	-2.45323
IL32	ENST00000526464	0.000905322	-2.44802
	---	0.000775358	-2.41801
TTC14	NM_001042601	0.000313101	-2.39381
	---	0.0294158	-2.38359
	---	0.0399722	-2.3784

Table C.1. Significantly differentially expressed genes ($p \leq 0.05$; fold change $\geq |1.5|$) between GFP-NB4 sells and miR-125a shMIMIC-NB4 cells. A] Significantly decreased genes. B] Significantly increased genes.

Table C.1 Continued

Gene Symbol	RefSeq	p-value (miRNA125A vs. Control)	Fold-Change (miRNA125A vs. Control)
	---	0.0032804	-2.37088
		0.0030359	-2.3292
	---	0.00148678	-2.25869
	---	0.00585175	-2.23659
	---	0.032334	-2.23457
	---	0.0160925	-2.22733
	---	0.000915502	-2.22429
PLIN2	NR_038064	4.48E-05	-2.21155
ZDBF2	ENST00000374423	0.00414555	-2.20267
CD69	NM_001781	1.58E-05	-2.20052
	---	0.0202425	-2.19276
MIER2	AB033019	0.000484588	-2.17826
IL8	NM_000584	0.000375739	-2.15253
	---	0.000572294	-2.14925
	---	0.0216294	-2.14335
KLHL6-AS1	ENST00000491676	0.00414538	-2.14268
	---	0.00345686	-2.14004
	---	0.0117602	-2.12488
FLT1	NM_002019	0.00010717	-2.11953
	---	0.000365178	-2.10039
	---	5.86E-05	-2.08639
	---	0.00736682	-2.08529
		0.000849314	-2.06488
	---	0.048215	-2.04822
	---	0.0264679	-2.04582
		0.00195972	-2.03623
SNORD89	NR_003070	0.0019161	-2.03616
MIR148A	NR_029597	0.0375202	-2.02153
	---	0.00228091	-2.01776
	---	0.0331247	-2.01756
TULP3	ENST00000540184	0.0345289	-2.01242
	---	0.0204415	-2.0108
	---	0.0442727	-2.00046
ANXA2P3	NR_001446	0.00893331	-1.99236
	---	0.00391569	-1.99183

Table C.1 Continued

Gene Symbol	RefSeq	p-value (miRNA125A vs. Control)	Fold-Change (miRNA125A vs. Control)
	---	0.0114884	-1.98933
	---	0.0079296	-1.98782
CRISPLD2	NM_031476	0.0027699	-1.98587
LINC00599	NR_024281	0.00372651	-1.9857
	---	0.0035916	-1.9836
	---	0.0396673	-1.98065
VLDLR	NM_003383	1.62E-05	-1.97832
ANGPTL6	NM_031917	0.00233527	-1.97663
	---	0.0284415	-1.97592
SIGLEC7	NM_014385	0.00484225	-1.97563
	---	0.00563423	-1.96829
RAB27B	NM_004163	0.000390494	-1.96767
	---	0.0348719	-1.9614
MIER2	AB033019	0.000292678	-1.95946
XYLT1	NM_022166	0.00127558	-1.94948
RN5S74	ENST00000363538	0.00232507	-1.94776
	---	0.000334741	-1.93799
RNF149	NM_173647	0.00145911	-1.93737
	---	0.00293604	-1.93035
CCL3L3	ENST00000378354	0.00074056	-1.92603
LOC100505531	XR_108724	0.0360766	-1.91661
	---	0.0023733	-1.91519
RAB31	NM_006868	3.13E-05	-1.90149
IL3RA	NM_002183	0.000373144	-1.90028
	---	0.0145011	-1.89782
	---	0.00201299	-1.89083
	---	0.0400695	-1.89078
	---	0.0112247	-1.89046
TRIB2	NM_021643	0.000271123	-1.88845
	---	0.00213237	-1.8879
MIR4275	NR_036237	0.0473693	-1.88471
EMR1	NM_001256252	0.000113376	-1.88434
IL1A	NM_000575	0.00151727	-1.874
ATL3	ENST00000398868	0.000192958	-1.8692
SLC5A4	NM_014227	0.0360852	-1.86794

Table C.1 Continued

Gene Symbol	RefSeq	p-value (miRNA125A vs. Control)	Fold-Change (miRNA125A vs. Control)
	---	0.0337659	-1.86268
SIGLEC17P	NR_047529	0.00314305	-1.85822
IL3RA	NM_002183	0.00027524	-1.85786
TRDV3	AK301114	0.00441692	-1.85768
GIMAP2	NM_015660	0.00313433	-1.85758
TREM1	NM_018643	0.000414021	-1.85438
RN5S302	ENST00000364896	0.00486746	-1.8527
	---	0.0133401	-1.8516
	---	2.14E-05	-1.84611
	---	0.0122736	-1.84601
	---	0.000660717	-1.83957
	---	0.0323765	-1.83011
MMP9	NM_004994	0.000255111	-1.82861
SLCO3A1	NM_001145044	0.000401421	-1.82663
TRAJ5	ENST00000390532	0.00565565	-1.82506
	---	0.0279878	-1.82418
	---	0.0373035	-1.82414
	---	0.0212914	-1.81992
		0.00321584	-1.81906
SNORA60	NR_002986	0.0118172	-1.81806
	---	0.00188303	-1.81439
	---	0.00168271	-1.80148
	---	0.01647	-1.80009
LOC100130264	ENST00000319682	0.00092263	-1.79568
	---	0.0174906	-1.79321
ZNF506	NM_001099269	0.0319158	-1.79301
TRIB2	NM_021643	0.000773746	-1.78899
IPCEF1	NM_001130699	0.00198382	-1.78054
	---	0.00714309	-1.78025
	---	0.00391308	-1.77968
	---	0.0060317	-1.77916
RNU4ATAC2P	ENST00000408674	0.0338797	-1.77857
	---	0.00200834	-1.77787
	---	0.00788912	-1.77728
	---	0.0162794	-1.77652
SLC24A3	NM_020689	0.000499885	-1.77631

Table C.1 Continued

Gene Symbol	RefSeq	p-value (miRNA125A vs. Control)	Fold-Change (miRNA125A vs. Control)
LOC729296	ENST00000432910	0.00403948	-1.77365
ZNF253	NM_021047	0.00566731	-1.77329
	---	0.000959281	-1.77328
ANXA2	NM_001002857	0.0232968	-1.77265
	---	0.0408392	-1.76952
KLHL6	NM_130446	0.00316622	-1.76885
CYTIP	NM_004288	0.00145301	-1.7652
TPST1	ENST00000304842	2.83E-05	-1.76487
MIER2	AB033019	0.017895	-1.76044
TRBV5-1	ENST00000390381	0.00894025	-1.76035
LOC100288175	BC033949	0.000804308	-1.76017
	---	0.0230994	-1.7598
	---	0.0307023	-1.75965
SYCP2	NM_014258	0.00385796	-1.75604
TP73-AS1	NR_033711	0.00228273	-1.75539
MIR646	NR_030376	0.00596192	-1.74936
	---	0.0201708	-1.74858
RN5S91	ENST00000390902	0.0400838	-1.74389
	---	0.0499197	-1.74317
	---	0.0006199	-1.7415
TNF	NM_000594	2.81E-05	-1.74138
LOC100505875	BC036848	0.0101687	-1.74068
UGT2B28	NM_053039	0.00575952	-1.74019
	---	0.000196538	-1.73998
CD93	NM_012072	0.000588058	-1.73811
RGS16	NM_002928	0.00122525	-1.7377
	---	0.00265348	-1.73703
LOC641367	ENST00000426799	0.014425	-1.73484
	---	0.0291062	-1.73433
RAB27B	NM_004163	0.00339777	-1.73372
ZFAND4	NM_174890	0.000196333	-1.72969
	---	0.0335362	-1.72953
TNF	ENST00000376122	5.13E-05	-1.72766
TNF	ENST00000376122	5.13E-05	-1.72766
TNF	ENST00000376122	5.13E-05	-1.72766
TNF	ENST00000376122	5.13E-05	-1.72766

Table C.1 Continued

Gene Symbol	RefSeq	p-value (miRNA125A vs. Control)	Fold-Change (miRNA125A vs. Control)
TNF	ENST00000376122	5.13E-05	-1.72766
TNF	ENST00000376122	5.13E-05	-1.72766
TNF	ENST00000376122	5.13E-05	-1.72766
OR10G7	NM_001004463	0.0248337	-1.72636
	---	0.00484811	-1.72525
STAB1	NM_015136	0.000150087	-1.72345
LOC100505815	NR_045370	0.00148081	-1.72241
	---	0.0353583	-1.72185
ART3	NM_001130017	0.0065874	-1.72022
PADI4	NM_012387	0.0176414	-1.71748
	---	0.0098097	-1.71672
SLCO3A1	NM_013272	0.00109814	-1.71627
	---	0.0145008	-1.71536
	---	0.0043371	-1.71444
UBE2L6	NM_198183	0.000802874	-1.71146
	---	0.0124827	-1.71104
LOC100507800	ENST00000439237	0.0334749	-1.70995
	---	0.0101642	-1.709
CYP4F12	NM_023944	0.0480118	-1.7083
		0.0472193	-1.70819
	---	0.00717371	-1.70809
	---	0.012839	-1.70765
	---	0.0151223	-1.70616
	---	0.0237629	-1.69832
RN5S398	ENST00000517163	0.0447947	-1.69684
RGS2	NM_002923	0.000100993	-1.69477
ZDHHC21	NM_178566	0.0152353	-1.69393
	---	0.000522898	-1.69339
	---	0.0454167	-1.6922
	---	0.0126242	-1.69171
EBI3	NM_005755	0.00655727	-1.68942
NRP1	ENST00000432372	0.00155542	-1.68607
	---	0.00283463	-1.68464
	---	0.00985469	-1.6843
PECAM1	NM_000442	0.000963162	-1.68176
	---	0.00137696	-1.6806

Table C.1 Continued

Gene Symbol	RefSeq	p-value (miRNA125A vs. Control)	Fold-Change (miRNA125A vs. Control)
	---	0.0191506	-1.68054
LYPD6	NM_001195685	0.0242147	-1.67956
	---	0.042351	-1.6795
ECSCR	NM_001077693	0.00640134	-1.67838
	---	0.0463291	-1.67786
	---	0.0202782	-1.6778
NRP1	NM_003873	0.00769452	-1.6771
TRAF5	NM_004619	0.000337693	-1.6737
	---	0.00315223	-1.67205
FLOT1	NM_005803	4.13E-05	-1.67147
F2RL3	NM_003950	0.0277576	-1.67122
	---	0.0328295	-1.67031
HIP1	NM_005338	0.000102698	-1.66956
LAT	NM_014387	0.00012844	-1.66933
	---	0.0254292	-1.66928
	---	0.0394736	-1.66928
PRDM8	NM_020226	0.00133854	-1.66754
	---	0.0058223	-1.66598
MIR518A1	NR_030210	0.0350356	-1.66522
	---	0.000193456	-1.66293
	---	0.00227249	-1.66242
	---	0.00770127	-1.66052
	---	0.0104163	-1.65961
	---	0.0262369	-1.65573
FLOT1	ENST00000480605	0.00290378	-1.65445
KRT81	NM_002281	0.000119927	-1.64963
	---	0.00401252	-1.64962
	---	0.0308873	-1.64868
	---	0.0239193	-1.64833
	---	0.00061471	-1.6438
TPSAB1	ENST00000461509	0.00921886	-1.64301
	---	0.0226827	-1.64235
OR52D1	NM_001005163	0.00139811	-1.64211
	---	0.00322433	-1.64071
RBMY2FP	NR_002193	0.0421547	-1.63919
	---	0.0330241	-1.63611

Table C.1 Continued

Gene Symbol	RefSeq	p-value (miRNA125A vs. Control)	Fold-Change (miRNA125A vs. Control)
ICAM1	NM_000201	0.00785314	-1.63459
LOC723805	DQ059386	0.0370808	-1.63451
TUBA3FP	NR_003608	0.0137557	-1.63382
	---	0.00188009	-1.63291
NAV3	NM_014903	8.57E-05	-1.63198
FLOT1	NM_005803	0.00100552	-1.63099
10-Sep	NM_144710	0.00455725	-1.62879
	---	0.0371739	-1.62738
	---	0.0193666	-1.62714
	---	0.00498129	-1.6271
PAG1	NM_018440	0.0043795	-1.6243
	---	0.0350603	-1.62369
	---	0.00375904	-1.62273
ANXA2P2	NR_003573	0.0160718	-1.62078
CYTH4	ENST00000248901	0.00128451	-1.62044
	---	0.00738376	-1.62015
	---	0.00514142	-1.61977
PI4KA	ENST00000462210	0.00632406	-1.61959
	---	0.000844639	-1.61795
		0.0354363	-1.61693
MTMR3	NM_153050	0.000513734	-1.61623
PCYT1B	NM_004845	0.00225244	-1.61618
LOC729296	ENST00000458422	0.00194207	-1.61545
NAMPT	NM_005746	0.00525868	-1.61341
TCF20	NM_005650	0.00752769	-1.61058
RGS19	NM_005873	0.00252764	-1.61055
FLOT1	ENST00000436822	0.000872895	-1.61042
MIR3908	NR_037470	0.016075	-1.61033
MSMO1	ENST00000261507	0.00107764	-1.60893
	---	0.0163932	-1.60888
C3	NM_000064	0.00339648	-1.60755
HMGCS1	NM_001098272	0.000261383	-1.60679
DESI1	NM_015704	0.00133265	-1.60608
LOC284757	NR_046099	0.00160944	-1.60577
FLOT1	NM_005803	0.000867622	-1.60524
FLOT1	ENST00000436822	0.000867622	-1.60524

Table C.1 Continued

Gene Symbol	RefSeq	p-value (miRNA125A vs. Control)	Fold-Change (miRNA125A vs. Control)
FLOT1	ENST00000436822	0.000867622	-1.60524
FLOT1	ENST00000436822	0.000867622	-1.60524
	---	0.00117968	-1.60416
	---	0.0238717	-1.60189
RN5S380	ENST00000517190	0.0185044	-1.60069
PRAM1	NM_032152	0.000287235	-1.60018
MGAM	ENST00000549489	0.000370266	-1.59826
VENTX	ENST00000325980	0.000271298	-1.59741
	---	0.0105504	-1.59727
	---	0.00826543	-1.59682
NCF4	NM_013416	0.000135323	-1.59465
MIR4798	NR_039961	0.0220215	-1.59322
	---	0.0135305	-1.59276
TRDV3	AK301114	0.000191414	-1.59248
SNORD93	NR_003075	0.0176823	-1.58833
	---	0.000681521	-1.58804
	---	0.00990321	-1.58769
SREBF2	ENST00000361204	0.000258998	-1.58574
	---	0.017838	-1.58464
PRR14L	NM_173566	0.00384403	-1.58416
TRDJ2	ENST00000390475	0.0131882	-1.5836
KCNMB3	NM_171830	0.00296856	-1.58289
	---	0.00271176	-1.58199
MIR550A1	NR_030319	0.0137833	-1.58003
PI4KAP2	NR_003700	0.0014613	-1.5788
CCL20	NM_004591	0.00102895	-1.57678
		0.0101241	-1.57492
		0.000949311	-1.57486
TAS2R5	NM_018980	0.0111011	-1.57477
	---	0.00261735	-1.57471
KRT86	ENST00000544024	0.0201431	-1.57301
	---	0.00477842	-1.57257
LOC100507244	NR_040076	0.0128933	-1.57137
HDC	ENST00000267845	1.31E-05	-1.56949
IL1B	ENST00000263341	0.0107756	-1.56665
PPP1R12B	AB003062	0.0116569	-1.56513

Table C.1 Continued

Gene Symbol	RefSeq	p-value (miRNA125A vs. Control)	Fold-Change (miRNA125A vs. Control)
	---	0.012837	-1.56483
LOC729296	ENST00000427820	0.0183905	-1.56467
	---	0.0124764	-1.56366
	---	0.0293807	-1.56218
DHCR7	ENST00000355527	2.66E-05	-1.56175
OSBPL3	NM_015550	0.00230844	-1.5615
MIR30C2	NR_029598	0.0428924	-1.56051
		0.000323013	-1.56023
LINC00599	AK091593	0.0159465	-1.55998
TLR9	NM_017442	0.00796946	-1.55943
	---	0.00170333	-1.55678
	---	0.0016596	-1.55593
	---	0.0152797	-1.5557
	---	0.0131818	-1.55564
PAQR9	NM_198504	0.0358313	-1.55559
	---	0.0120161	-1.55556
	---	0.0246731	-1.55534
SLCO4A1	NM_016354	0.0111881	-1.55425
HABP4	NM_014282	0.00269962	-1.55375
		0.0268302	-1.55348
LGALS3	NR_003225	0.00244407	-1.55335
GFI1B	ENST00000339463	0.000574175	-1.55214
ZNRF3-IT1	ENST00000412798	0.0378608	-1.55199
MAFB	NM_005461	0.00162143	-1.55155
LOC100505644	ENST00000415399	0.00234186	-1.55118
LOC100506714	NR_038956	0.018849	-1.55099
PI4KAP1	AK002141	0.000241232	-1.55036
TPSB2	NM_024164	0.00336835	-1.54989
	---	0.0461243	-1.54881
	---	0.00928132	-1.54829
	---	0.00997497	-1.54777
CDK14	NM_012395	0.00147524	-1.5472
ADORA3	NM_020683	0.00214028	-1.54696
MPST	NM_001130517	0.0072777	-1.5467
C9orf72	NM_001256054	0.00568	-1.54503
	---	0.0337838	-1.54479

Table C.1 Continued

Gene Symbol	RefSeq	p-value (miRNA125A vs. Control)	Fold-Change (miRNA125A vs. Control)
MIR128-2	NR_029824	0.0018818	-1.54451
LOC729296	ENST00000426753	0.00665609	-1.54449
DKFZP586I1420	NR_002186	0.0110784	-1.5438
SLCO4C1	NM_180991	0.00515416	-1.54286
PI4KA	NM_058004	8.61E-05	-1.54266
TMC8	NM_152468	0.000496095	-1.54143
	---	0.00084882	-1.54085
MIR223	NR_029637	0.000316138	-1.53864
SNORD13P2	X58060	0.0130567	-1.53864
	---	0.0477994	-1.53794
	---	0.0281312	-1.53767
DOCK10	NM_014689	0.00596831	-1.53754
DESI1	NM_015704	0.000708721	-1.53752
ZNF558	NM_144693	0.000135812	-1.53682
LACTB	NM_032857	0.0128348	-1.53569
	---	0.0445885	-1.53417
CPEB2	NM_182485	0.000378549	-1.53337
	---	0.00442516	-1.53289
EGFLAM-AS2	AK093278	0.039742	-1.53271
FLOT1	NM_005803	0.000494004	-1.53244
MGC24103	AK021795	0.0182325	-1.53242
	---	0.00922803	-1.52952
LOC729296	ENST00000426753	0.0125897	-1.5288
ASAP1	NM_018482	0.00472516	-1.5284
		0.0022801	-1.5271
RAC2	NM_002872	0.00127635	-1.52682
	---	0.0058091	-1.52598
VN1R108P	ENST00000431580	0.00923193	-1.5251
	---	0.00924231	-1.5234
	---	0.0179777	-1.52303
SLC9A7P1	NR_033801	0.0234467	-1.52243
	---	0.0181279	-1.52096
	---	0.00580971	-1.52091
CBR3	NM_001236	0.00276278	-1.52087
IL17RA	NM_014339	0.000371443	-1.5208
EPN2-AS1	NR_048576	0.0111293	-1.52079

Table C.1 Continued

Gene Symbol	RefSeq	p-value (miRNA125A vs. Control)	Fold-Change (miRNA125A vs. Control)
	---	0.0406527	-1.5207
LOC729296	ENST00000427691	0.00229445	-1.52063
LIMS1	NM_001193484	0.00632366	-1.52012
RN5S324	ENST00000365177	0.0370355	-1.51993
	---	0.019821	-1.51951
DGCR14	NM_022719	0.0271936	-1.51926
	---	0.0320164	-1.51867
	---	0.030485	-1.51823
MIR532	NR_030241	0.0105214	-1.51822
AHR	NM_001621	0.00131912	-1.51813
MKL1	NM_020831	0.000898563	-1.51806
	---	0.0306775	-1.51747
TRDV2	ENST00000390469	0.0323839	-1.51682
	---	0.000290858	-1.51566
LYPD6B	NM_177964	0.0264482	-1.51508
LOC100128364	AK096229	0.00303206	-1.51413
		0.0073743	-1.51391
	---	0.0185821	-1.51329
	---	6.13E-05	-1.51267
	---	0.0381497	-1.51248
	---	0.0193911	-1.51168
		0.0056573	-1.51071
	---	0.0225837	-1.51043
NAMPT	NM_005746	0.0023477	-1.51021
ITGAX	NM_000887	0.00185628	-1.50935
IL10	NM_000572	0.0361046	-1.50893
	---	0.000237396	-1.50777
	---	0.0446009	-1.50765
KCTD7	NM_153033	0.00074614	-1.50693
KIF21B	NM_001252100	0.0010995	-1.50672
	---	0.000282561	-1.50666
PI4KAP2	NR_003700	0.00213321	-1.5063
MIR222	NR_029636	0.00902525	-1.5058
PIK3C2B	NM_002646	0.000295237	-1.5044
PI4KAP2	AK126860	0.0043758	-1.50276
		0.0485583	-1.50229

Table C.1 Continued

Gene Symbol	RefSeq	p-value (miRNA125A vs. Control)	Fold-Change (miRNA125A vs. Control)
MIR3686	NR_037457	0.0369532	-1.50222
INSIG1	NM_005542	0.000136201	-1.50126
OGFR	NM_007346	0.0120337	-1.50046

B] Increased genes

Gene Symbol	RefSeq	p-value (miRNA125A vs. Control)	Fold-Change (miRNA125A vs. Control)
CCNB1	NM_031966	0.000198227	1.50039
	---	7.14E-05	1.50181
MT2A	ENST00000245185	0.000391649	1.50211
LOC100287628	ENST00000562396	0.0100796	1.50211
	---	0.00951727	1.50233
	---	0.0474056	1.5027
ZNF443	NM_005815	0.0229003	1.50656
C20orf187	ENST00000378252	0.00975036	1.50663
	---	0.046215	1.50738
MARVELD1	NM_031484	0.0073029	1.5077
	---	0.00988543	1.50816
	---	0.00988543	1.50816
RNASE2	NM_002934	0.000582771	1.50888
	---	0.00634653	1.51
RN5S35	ENST00000391257	0.0104609	1.51143
IL1RN	NM_173842	0.0130114	1.51177
BCL11A	NM_022893	0.000332106	1.51241
		0.00378434	1.51242
FLJ41278	NR_033988	0.0290867	1.51273
VIT	NM_053276	0.0301716	1.51275
	---	0.0320562	1.51297
	---	0.00411514	1.51309
CAPN3	ENST00000356316	0.0211779	1.51472
	---	0.00612007	1.51495
ULK4P3	NR_026859	0.00578307	1.51757
	---	0.00371337	1.51797
FAM66C	ENST00000541558	0.0323367	1.51853

Table C.1 Continued

Gene Symbol	RefSeq	p-value (miRNA125A vs. Control)	Fold-Change (miRNA125A vs. Control)
		0.0340836	1.5189
		0.0153314	1.51928
	---	0.0393133	1.51955
LOC100288637	NR_038254	0.047791	1.52135
	---	0.00232839	1.5219
		0.00953921	1.52292
FKTN	NM_001079802	0.00815478	1.52308
	---	0.022931	1.52313
LOC100507282	XR_109045	0.0323525	1.5238
TRAJ16	ENST00000390521	0.0393711	1.52452
RAPGEF2	NM_014247	0.0125776	1.52464
HIST1H2BC	ENST00000377733	0.0193744	1.52627
MIR4452	NR_039657	0.0223893	1.52685
	---	0.00679112	1.52745
	---	0.0413459	1.52893
	---	0.00090075	1.53039
C11orf49	NM_001003676	0.0425717	1.53148
	---	0.00123396	1.53199
HCP5	NR_040662	0.0231551	1.53467
	---	0.0416453	1.53636
	---	0.00305134	1.5379
HSPB1	AB020027	3.15E-05	1.5383
PTPRS	NM_002850	0.000176745	1.54057
XAF1	NM_017523	0.0234061	1.54063
CLECL1	NM_001253750	0.0041693	1.54153
HSPB1	BC073768	3.88E-05	1.54157
COQ3	ENST00000254759	0.00166399	1.54167
CPA3	NM_001870	0.00751193	1.5428
PBK	ENST00000301905	0.0195559	1.54464
RPS14	ENST00000519690	0.00240003	1.5448
	---	0.00329702	1.54497
PLEKHA5	NM_001256470	0.00465246	1.54569
FAM106A	NR_026809	0.0109962	1.5457
	---	0.00022026	1.54603
	---	0.0468395	1.54674
		0.0199485	1.5469

Table C.1 Continued

Gene Symbol	RefSeq	p-value (miRNA125A vs. Control)	Fold-Change (miRNA125A vs. Control)
	---	0.0319208	1.54713
	---	0.00840429	1.54754
		0.0129101	1.54846
	---	0.0225744	1.55094
IL13RA1	NM_001560	0.000607453	1.55096
PLK1	ENST00000300093	0.000285998	1.55128
	---	0.00686818	1.55167
	---	0.0171927	1.55172
MIR125A	NR_029693	0.00739508	1.55198
	---	0.0290178	1.5528
MAP1B	ENST00000296755	0.027418	1.55474
	---	0.0456191	1.55722
	---	0.0456191	1.55722
RN5S363	ENST00000365072	0.00242831	1.5584
PRTN3	NM_002777	0.000306585	1.55974
	---	0.00895577	1.56019
ULK4P2	NR_027470	0.0135805	1.56072
CNOT10-AS1	ENST00000475395	0.0361304	1.56087
	---	0.0445725	1.56113
	---	0.0445725	1.56113
	---	0.0445725	1.56113
	---	0.0445725	1.56113
	---	0.0445725	1.56113
	---	0.038954	1.56189
EPHX4	NM_173567	0.00249501	1.56594
TMEM45A	ENST00000403410	0.00394491	1.56798
EIF4A2	AK296279	0.0125213	1.56872
TRANK1	ENST00000463764	0.00580078	1.56937
CDKN2C	ENST00000262662	0.00278119	1.56959
	---	0.0248684	1.56962
LOC100287562	XR_111692	0.000227806	1.56976
	---	0.0399638	1.57001
ABCC4	NM_005845	9.55E-05	1.57026
SH3BGRL	NM_003022	0.00402107	1.57036
PRG2	Z26248	0.0232611	1.57237
	---	0.04007	1.57324

Table C.1 Continued

Gene Symbol	RefSeq	p-value (miRNA125A vs. Control)	Fold-Change (miRNA125A vs. Control)
	---	0.0163329	1.57528
LRP11	NM_032832	0.022346	1.57772
SNORD70	NR_003058	0.0267986	1.57873
CDC20	ENST00000372462	0.0041869	1.58009
LRRCC1	NM_033402	0.0110678	1.5804
		0.0207437	1.58055
ACTBL2	NM_001017992	0.021173	1.58089
RASA4	NM_006989	0.000101194	1.58101
	---	0.0292043	1.5815
IGFBP2	NM_000597	0.00226849	1.58312
RASA4B	ENST00000488284	0.044311	1.58343
	---	0.0487873	1.58353
SRGAP3	NM_014850	0.0412453	1.58417
PLSCR1	NM_021105	0.000391867	1.58642
	---	0.00988515	1.58668
HS3ST3B1	ENST00000360954	0.000156279	1.58918
SNORA58	NR_002985	0.0421792	1.59123
RASGRF1	NM_002891	0.0031066	1.59338
	---	0.0312834	1.59348
FLJ38723	AK096042	0.00117858	1.59751
	---	0.0202304	1.59757
ACBD7	NM_001039844	0.019397	1.59784
INPP4B	NM_003866	0.00757959	1.59925
RAB38	NM_022337	0.00096457	1.59986
UPK3A	NM_006953	0.00661975	1.6014
	---	0.0488162	1.6014
	---	0.0295164	1.60348
	---	0.0243227	1.60411
GDAP1	ENST00000220822	0.00273505	1.60573
LGALS3BP	NM_005567	0.00116206	1.60827
PPM1H	ENST00000228705	0.00907987	1.60929
FAM115A	NM_001206938	0.00357327	1.61004
		0.0476863	1.61034
	---	0.0146057	1.61045
	---	0.0169123	1.61142
MIR4295	NR_036177	0.0266609	1.61212

Table C.1 Continued

Gene Symbol	RefSeq	p-value (miRNA125A vs. Control)	Fold-Change (miRNA125A vs. Control)
ZNF618	NM_133374	0.0164625	1.61517
	---	0.0267672	1.61635
OASL	NM_003733	0.00298968	1.61891
	---	0.0038357	1.62064
	---	0.044794	1.62088
		0.0378621	1.62105
	---	0.000184689	1.62204
	---	0.0176229	1.62422
	---	0.0134613	1.62579
	---	0.00113163	1.63075
IFIH1	ENST00000263642	0.0236582	1.63835
	---	0.0436344	1.64402
IFIT3	NM_001031683	0.0289097	1.64744
	---	0.0417885	1.64908
PPFIBP1	ENST00000228425	0.0037454	1.65268
RNU7-2P	ENST00000516096	0.0498244	1.65581
KIAA0895	NM_001199706	0.0115314	1.65769
ASPHD1	ENST00000566693	0.000377061	1.65958
MIR3137	NR_036089	0.013062	1.66116
MIR3137	NR_036089	0.013062	1.66116
		0.00537589	1.66349
TRANK1	NM_014831	0.015721	1.66455
	---	0.0344279	1.6648
VWDE	NM_001135924	0.0060231	1.66485
HN1	NM_016185	0.000712872	1.67016
SPANXN3	NM_001009609	0.0433352	1.67104
CLEC12A	NM_138337	0.00939232	1.67453
CD59	NM_001127223	7.21E-05	1.67613
LINC00422	ENST00000434601	0.00251262	1.6778
	---	0.0134276	1.6784
MIR942	NR_030640	0.00242704	1.68042
	---	0.00238644	1.6811
SLC27A2	NM_003645	7.43E-05	1.68231
SESN3	ENST00000536441	5.12E-05	1.68233
TRAJ53	ENST00000390485	0.0273023	1.68841
	---	0.0437873	1.69347
STAP1	NM_012108	0.0103296	1.6977

Table C.1 Continued

Gene Symbol	RefSeq	p-value (miRNA125A vs. Control)	Fold-Change (miRNA125A vs. Control)
C19orf59	ENST00000333598	0.000878955	1.69985
SNORA13	NR_002922	0.00658367	1.70081
		0.00355108	1.70225
		0.000448451	1.70389
IFI6	ENST00000361157	0.00120695	1.71043
	---	0.0120578	1.71261
DEFB1	ENST00000297439	0.000201753	1.71391
O3FAR1	NM_181745	0.00249302	1.71833
ATF5	NM_001193646	2.26E-05	1.71848
	---	0.000617143	1.72034
PPFIBP1	ENST00000545381	0.00544292	1.72291
	---	0.0191576	1.72399
	---	0.015745	1.72886
DLGAP5	NM_014750	0.000789624	1.73484
	---	0.0127638	1.73777
RPS14	ENST00000519690	0.000186361	1.73859
LOC100505801	XR_110042	0.00591209	1.73908
	---	0.0455949	1.73909
PCDHB3	NM_018937	0.00243695	1.74376
PPFIBP1	NM_003622	0.000191051	1.74588
	---	0.00456751	1.7517
MIR548L	NR_031630	0.0113148	1.75759
TMEM65	NM_194291	0.0282841	1.75843
KIAA0125	NR_026800	0.0079527	1.75968
HERC5	NM_016323	0.000805556	1.76067
	---	0.0307132	1.76203
	---	0.003184	1.76634
	---	0.0366778	1.76648
MAP2K6	NM_002758	0.023549	1.76772
	---	0.0134646	1.76858
EPB41L2	NM_001431	0.00176824	1.7713
	---	0.0159671	1.77168
	---	0.0427098	1.77322
	---	0.00509151	1.77381
	---	0.00618107	1.77446
NEO1	ENST00000339362	0.00404012	1.77473

Table C.1 Continued

Gene Symbol	RefSeq	p-value (miRNA125A vs. Control)	Fold-Change (miRNA125A vs. Control)
KRTAP5-3	NM_001012708	0.00823532	1.77922
TRANK1	NM_014831	0.00496302	1.77942
	---	0.00354255	1.78171
	---	0.00471009	1.78389
TRANK1	ENST00000429976	0.00177341	1.78904
SPTLC2	NM_004863	8.27E-05	1.79276
SNAR-F	NR_004384	0.000118045	1.7951
CD59	NM_203330	0.00156589	1.79613
	---	0.00333059	1.79696
COL5A1	NM_000093	0.045752	1.80539
KIF20A	NM_005733	0.00776684	1.80695
DEFA4	ENST00000297435	0.00531406	1.807
KYNU	NM_001199241	1.43E-05	1.80979
ZNF30	NR_024018	0.0153121	1.81155
ATF5	AB021663	3.64E-05	1.81217
PLA2G4A	NM_024420	0.000923744	1.81314
		0.0414839	1.82422
SPACA5	NM_205856	0.0228815	1.82655
CCND1	ENST00000227507	0.000247652	1.82767
	---	0.0348201	1.82806
ECRP	NR_033909	0.00213244	1.82961
	---	0.00825015	1.8327
		0.00421698	1.83435
MT1CP	ENST00000379816	0.00205742	1.83539
KIF16B	NM_024704	0.00538037	1.84355
PPFIBP1	NM_003622	0.00108678	1.84549
	---	0.0366383	1.84786
	---	0.00552806	1.84926
HP	NM_005143	0.0176726	1.85025
		0.034572	1.85584
	---	0.0338274	1.85681
RAVER2	NM_018211	3.83E-05	1.86243
C11orf67	CR457332	0.000344934	1.86528
	---	0.00960577	1.86962
S100B	NM_006272	0.00827567	1.87016
	---	0.0362337	1.87825

Table C.1 Continued

Gene Symbol	RefSeq	p-value (miRNA125A vs. Control)	Fold-Change (miRNA125A vs. Control)
PCDHB2	ENST00000194155	0.00439308	1.88957
		0.0124975	1.89303
HFM1	NM_001017975	0.00183916	1.89616
	---	0.00669573	1.89979
TNNT1	NM_003283	0.00224519	1.90648
HLA-DRB3	ENST00000383126	0.00185835	1.90654
KLF12	ENST00000377666	0.00719863	1.90695
	---	0.0475179	1.9112
LGR4	NM_018490	0.000635345	1.91247
	---	0.000374096	1.92294
CD2	ENST00000369478	0.00724333	1.9323
	---	0.0155786	1.95125
	---	0.0026727	1.96175
	---	0.00582307	1.9653
SNORD14E	NR_003125	0.00136213	1.97368
HOXB9	ENST00000311177	0.00119358	1.97558
MYO6	NM_004999	0.013912	1.98886
		0.00037612	1.9961
	---	0.0496587	1.99661
ARHGAP5	NM_001030055	0.00957038	2.00488
NEDD4	NM_006154	0.00474424	2.00753
SNORD114-17	NR_003210	0.00476461	2.01063
LAPTM4B	ENST00000445593	0.00577655	2.02221
RNASE3	NM_002935	0.000392379	2.03723
	---	0.0446006	2.04888
PJA1	NM_145119	0.00227297	2.06834
HMGN5	NM_030763	0.00230742	2.06848
LINC00478	NR_027790	0.00718477	2.08755
AFAP1-AS1	NR_026892	0.000514537	2.09302
	---	0.00195747	2.11242
		0.000256229	2.11853
		0.00692531	2.12948
IFIT2	NM_001547	0.0028959	2.14943
SNORD14D	ENST00000524552	0.00344801	2.15718
YPEL3	NM_031477	0.00601428	2.17552
IL5RA	NM_000564	0.000353884	2.18522

Table C.1 Continued

Gene Symbol	RefSeq	p-value (miRNA125A vs. Control)	Fold-Change (miRNA125A vs. Control)
KIAA1383	NM_019090	0.00420346	2.2363
SYNPO2	NM_001128933	0.0130134	2.24121
	---	0.0456817	2.25453
OAS1	ENST00000202917	3.59E-05	2.27116
	---	0.0475702	2.29274
IKZF2	NM_001079526	0.000454732	2.30109
RNU5A-8P	ENST00000364102	0.00576096	2.32354
		0.000774331	2.32699
LOXL1-AS1	NR_040067	0.0106524	2.33516
SPARC	NM_003118	0.00148476	2.3492
VCX3A	NM_016379	0.000110085	2.37874
CD3D	ENST00000300692	0.000245038	2.38397
		0.0250939	2.40727
	---	0.000154602	2.41078
LGALS9	AB006782	3.16E-05	2.42949
TRANK1	ENST00000505962	0.00269333	2.43109
LGALS9	AB003517	3.20E-05	2.44407
	---	0.0345027	2.47266
	---	0.046828	2.47407
	---	0.036543	2.47993
PHKA1	NM_002637	3.43E-05	2.49562
	---	0.031883	2.49799
	---	0.0161113	2.4986
	---	0.00312132	2.52358
	---	0.00851876	2.53175
		0.0187122	2.54435
LOC100128437	AK126077	0.020213	2.58339
		0.0233748	2.60021
MYO1D	NM_015194	4.27E-06	2.67954
	---	0.00616995	2.76857
	---	0.000278189	2.87635
	---	0.000278189	2.87635
C11orf74	AK290833	3.73E-05	2.92035
		0.000819158	2.93808
		0.00220533	3.06548
IFIT1	NM_001548	0.0051168	3.09057

Table C.1 Continued

Gene Symbol	RefSeq	p-value (miRNA125A vs. Control)	Fold-Change (miRNA125A vs. Control)
EPX	NM_000502	0.000114058	3.10132
	---	0.00694715	3.18329
KIF21A	NM_001173464	9.85E-05	3.24879
LOC100506914	ENST00000515455	0.00136614	3.28536
MNS1	ENST00000260453	4.90E-05	3.31049
	---	0.00776735	3.51517
	---	0.00269814	3.59917
DEFA3	NM_005217	0.0120522	3.60378
PARP14	ENST00000474629	0.00182271	3.81291
DOCK7	NM_033407	1.48E-09	3.98998
	---	0.00141713	4.04757
		0.0315606	4.75878
CTSG	NM_001911	1.38E-06	5.108
T1560	BC040611	0.000149998	5.68313
DEFA1	NM_004084	7.45E-05	6.71886
DEFA3	NM_005217	7.57E-05	6.79864
CA2	NM_000067	1.97E-06	7.28779
ITM2A	NM_004867	1.71E-06	7.81979
MIR196A2	NR_029617	5.92E-06	26.9789

Table C.2. Significant (P<0.05) alternatively spliced and differentially expressed genes. A] Significantly decreased genes. B] Significantly increased genes.

A]

# of markers	Transcript Cluster ID	seqname	start	stop	Gene Symbol		
23	16799315	chr15	39873280	39891667	THBS1		E5
4	16833204	chr17	32582296	32584222	CCL2		N
13	16806624	chr15	31514042	31523050	LOC283710		N
5	16664748	chr1	53068043	53074723	GPX7		N
3	16929920	chr22	38201114	38203443	H1F0		N
13	16911804	chr20	19193290	19703545	SLC24A3		N
15	17059628	chr7	91741463	91772266	CYP51A1		N
9	16691314	chr1	115590632	115632121	TSPAN2		N
21	16948366	chr3	180319918	180335616	TTC14		N
9	16874890	chr19	52022779	52035110	SIGLEC6		N
7	16889958	chr2	207139387	207179148	ZDBF2		E2
11	16815355	chr16	3115298	3131908	IL32		E6
5	16990542	chr5	142985193	143208337			--
4	17005018	chr6	14431958	14463629			--
17	16807233	chr15	39156696	39719396			--
14	16901200	chr2	101887684	101925178	RNF149		N
16	16821541	chr16	84853537	84943116	CRISPLD2		N

Table C.2. continued

# of markers	Transcript Cluster ID	seqname	start	stop	Gene Symbol
19	17092712	chr9	19108373	19149288	PLIN2
2	16807254	chr15	39480639	39486510	
2	17094296	chr9	43184023	43189411	
10	16824352	chr16	17196181	17564738	XYLT1
2	17040899	chr6_ssto_hap7	3184281	3184574	EHMT2
2	17030853	chr6_dbb_hap3	3137120	3137413	EHMT2
2	17026350	chr6_apd_hap1	3166292	3166585	EHMT2
2	17006908	chr6	31851538	31851831	EHMT2-AS
2	17035616	chr6_mcf_hap5	3231411	3231704	EHMT2
2	17028043	chr6_cox_hap2	3361292	3361585	EHMT2
2	17038348	chr6_qbl_hap6	3145329	3145622	EHMT2
2	16883942	chr2	107159393	107160753	
9	16850923	chr18	9708228	9862553	RAB31
4	16992508	chr5	172841038	172878553	
16	16739763	chr11	63391559	63439393	ATL3
7	16868556	chr19	10203013	10213425	ANGPTL6
12	17115868	chrY	1405509	1451582	IL3RA
7	16799281	chr15	39459940	39472231	
2	16917855	chr20	23046042	23052105	

Table C.2. continued

# of markers	Transcript Cluster ID	seqname	start	stop	Gene Symbol
34	16754471	chr12	78224685	78606790	NAV3
2	17102647	chrX	39681271	39681758	
4	17015794	chr6	14391462	14393519	
7	17019056	chr6	41242999	41254457	TREM1
3	16990548	chr5	143191726	143200284	HMHB1
17	16914395	chr20	44637547	44645200	MMP9
3	17096812	chr9	109879740	109883986	
22	16805161	chr15	92396925	92715665	SLCO3A1
22	17025018	chr6	154475618	154677926	IPCEF1
7	16953024	chr3	46899357	46923659	MYL3
22	16929741	chr22	37678068	37711389	CYTH4
15	16968314	chr4	81105033	81125483	PRDM8
9	16877297	chr2	12856998	12882860	TRIB2
10	17053892	chr7	155089486	155101945	INSIG1
6	16917859	chr20	23059986	23066977	CD93
16	16962085	chr3	183205319	183273499	KLHL6
11	16915091	chr20	55204358	55214339	TFAP2C
19	16664802	chr1	53392901	53517375	SCP2
15	17109832	chrX	24576204	24690979	PCYT1B
5	16764817	chr12	52679697	52685318	KRT81

Table C.2. continued

# of markers	Transcript Cluster ID	seqname	start	stop	Gene Symbol
9	16858137	chr19	10381517	10397291	ICAM1
13	17036388	chr6_mcf_hap5	2077369	2091199	FLOT1
2	16932702	chr22	21362492	21368576	TUBA3FP
2	16734491	chr11	2949503	2950685	PHLDA2
3	16919242	chr20	39314488	39317880	MAFB
14	17062955	chr7	130626519	130794935	FLJ43663
22	17057381	chr7	45002260	45018704	MYO1G
5	16798866	chr15	31507884	31516648	
3	16883756	chr2	103055173	103056935	
4	16979782	chr4	132925965	133045186	
4	17100888	chrUn	102510	109743	
8	16738544	chr11	57319128	57335803	UBE2L6
5	16710900	chr10	135051175	135055433	VENTX
11	16846901	chr17	54869274	54916134	C17orf67
16	16915609	chr20	60758081	60778624	GTPBP5
2	16658525	chr1	7429003	7430331	CAMTA1-I
4	17079946	chr8	104145191	104153703	C8orf56
5	16961749	chr3	177919838	178103205	
4	17029082	chr6_cox_hap2	3057948	3059915	LTB
4	17041863	chr6_ssto_hap7	2879133	2881100	LTB

Table C.2. continued

# of markers	Transcript Cluster ID	seqname	start	stop	Gene Symbol
4	17031867	chr6_dbb_hap3	2833873	2835840	LTB
4	17034339	chr6_mann_hap4	2891216	2893183	LTB
4	17036587	chr6_mcf_hap5	2928038	2930005	LTB
4	17026762	chr6_apd_hap1	2863050	2865017	LTB
4	17039380	chr6_qbl_hap6	2841972	2843939	LTB
10	17005077	chr6	16129317	16148479	MYLIP
39	17058978	chr7	76940068	77046115	PION
7	16867088	chr19	3594504	3606831	TBXA2R
16	16756804	chr12	110011060	110035071	MVK
2	16839796	chr17	3608266	3608812	
4	16965467	chr4	21583719	21615351	
27	16813206	chr15	90328120	90358633	ANPEP
3	16930256	chr22	39828165	39833133	LOC10050
33	16697750	chr1	200938514	200992828	KIF21B
16	16759324	chr12	132312938	132336328	MMP17
15	16883733	chr2	103035149	103069025	IL18RAP
16	16935455	chr22	41972890	41985894	PMM1
2	16963894	chr4	1031541	1045258	
14	16812087	chr15	78396948	78423886	CIB2
3	17079329	chr8	96083960	96100152	

Table C.2. continued

# of markers	Transcript Cluster ID	seqname	start	stop	Gene Symbol
8	16815528	chr16	4524719	4560348	HMOX2
2	17051071	chr7	126990182	126991577	
6	16935593	chr22	42556019	42739622	TCF20
20	16787597	chr14	92980118	93155339	RIN3
4	16886461	chr2	150443710	150704747	
11	16916130	chr20	62496581	62522898	TPD52L2
17	16818272	chr16	31366509	31394318	ITGAX
7	16700798	chr1	235710985	235814054	GNG4
20	16928212	chr22	24666786	24813708	SPECC1L
18	16915570	chr20	60697517	60710434	LSM14B
4	17097700	chr9	117881818	117900688	
13	16690388	chr1	108677442	108742974	SLC25A24
24	16934583	chr22	36906897	36925483	EIF3D
7	16993235	chr5	177540444	177553107	N4BP3
7	17046664	chr7	66093868	66108216	KCTD7
19	16741501	chr11	71139239	71163914	DHCR7
16	16811638	chr15	74701630	74726300	SEMA7A
31	17022422	chr6	109765265	109787171	MICAL1
17	16931770	chr22	51021455	51038732	LOC10014
12	16920776	chr20	57600522	57617964	SLMO2

Table C.2. continued

# of markers	Transcript Cluster ID	seqname	start	stop	Gene Symbol
16	16901699	chr2	111195880	111230652	LIMS3
15	16933171	chr22	24936406	24951903	C22orf13
9	16866650	chr19	1397088	1401552	GAMT
22	16868219	chr19	8645126	8675588	ADAMTS1
8	17081027	chr8	128128656	128215467	
18	16753641	chr12	66217911	66360075	HMGA2
16	16730540	chr11	102217942	102249401	BIRC2
15	16854185	chr18	19109262	19180845	ESCO1
2	16711723	chr10	11210885	11213339	
19	16745113	chr11	118764584	118796317	BCL9L
13	16819563	chr16	57702157	57723975	GPR97
3	17061582	chr7	1062977211	106301634	CCDC71L
8	17057026	chr7	42948872	42952151	C7orf25
14	17063930	chr7	1430500493	143059863	FAM131B
2	16772237	chr12	125666413	125668887	
16	16927082	chr22	19701987	19712297	SEPT5-GP
18	16664782	chr1	53308183	53360670	ZYG11A
22	16677944	chr1	2246222362	224928251	CNIH3
21	16931435	chr22	46971909	47075688	GRAMD4
15	17049366	chr7	1001366834	100165843	AGFG2

Table C.2. continued

# of markers	Transcript Cluster ID	seqname	start	stop	Gene Symbol
7	17054923	chr7	6012870	6048756	PMS2
2	16667793	chr1	103817769	103828355	
2	16667796	chr1	103957501	103968087	
19	17050202	chr7	107203929	107218968	DUS4L
20	16927198	chr22	20103461	20114878	RANBP1
4	16984932	chr5	55290989	55299477	FLJ31104
43	16915262	chr20	57226309	57294294	STX16-NP
12	17045542	chr7	43622357	43666978	STK17A
24	16933314	chr22	26839389	26879820	HPS4
7	16930897	chr22	42834029	42846772	
4	16996612	chr5	60497136	60560756	
6	16756822	chr12	110152033	110208312	FAM222A
19	17058557	chr7	73113535	73134017	STX1A
17	16914147	chr20	43595115	43708618	STK4
8	16932914	chr22	22838767	22863505	ZNF280B
24	16659102	chr1	11866207	11903201	CLCN6
3	16698980	chr1	211744910	211752099	SLC30A1
5	16693421	chr1	153409471	153412503	S100A7L2
11	16921036	chr20	60963686	60982341	CABLES2
2	17048027	chr7	87845975	87848541	

Table C.2. continued

# of markers	Transcript Cluster ID	seqname	start	stop	Gene Symbol
11	16958844	chr3	128198265	128212030	GATA2
20	16918694	chr20	33890369	33999945	UQCC
8	16949759	chr3	193853931	193856521	HES1
2	17083229	chr9	2840592	2844073	
12	16858451	chr19	11466062	11476374	LPPR2
2	17004447	chr6	4135657	4146287	
12	16803018	chr15	74833518	74890472	ARID3B
4	16968488	chr4	85887538	85932430	WDFY3-AS
11	17114038	chrX	129198849	129244691	ELF4
11	17045144	chr7	35840542	35946715	
4	16863629	chr19	47987539	48004854	NAPA-AS1
4	16912052	chr20	23331373	23335414	NXT1
12	16820849	chr16	71392616	71424341	CALB2
6	16935553	chr22	42481529	42486959	NDUFA6
17	17110322	chrX	44007128	44202923	EFHC2
2	16854816	chr18	39766366	39805980	
12	17088408	chr9	117373486	117408703	C9orf91
10	16819871	chr16	66878282	66888056	CA7
8	16928680	chr22	29168662	29185698	CCDC117
5	16945224	chr3	128182437	128191160	DNAJB8-A

Table C.2. continued

# of markers	Transcript Cluster ID	seqname	start	stop	Gene Symbol
4	17112963	chrX	102528618	102531800	TCEAL5
30	16894740	chr2	17845079	17981509	SMC6
15	16933502	chr22	29083731	29138410	CHEK2
14	17052823	chr7	143078173	143088204	ZYX
6	16795424	chr14	82071691	82089405	
39	17103451	chrX	48659784	48683392	HDAC6
19	16929509	chr22	35653445	35691800	HMGXB4
2	16760079	chr12	3592878	3601985	LOC10012
11	16931647	chr22	50624344	50638027	TRABD
24	16724633	chr11	48002110	48192486	PTPRJ
16	17063047	chr7	132469623	132766848	CHCHD3
24	16931463	chr22	47158518	47571342	TBC1D22A
18	16935648	chr22	42979727	43010968	POLDIP3
46	16894614	chr2	15307032	15701454	NBAS
23	16861604	chr19	38397861	38699012	SIPA1L3
3	17070578	chr8	87719775	87777251	
13	16747402	chr12	6881670	6887621	LAG3
7	16867766	chr19	6583135	6591163	CD70
25	16929782	chr22	38004481	38029571	GGA1
11	17048984	chr7	99156029	99174076	ZNF655

Table C.2. continued

# of markers	Transcript Cluster ID	seqname	start	stop	Gene Symbol
3	17071086	chr8	96145949	96168913	PLEKHF2
6	16856834	chr19	2841433	2860472	ZNF555
21	16697245	chr1	185265218	185286461	IVNS1ABP
23	17091356	chr9	139702374	139735639	RABL6
13	16968680	chr4	88896802	88904563	SPP1
51	17082982	chr9	214854	465259	DOCK8
8	16716008	chr10	81697496	81742370	SFTPD
49	17064603	chr7	151832010	152133090	MLL3
28	16712879	chr10	29746267	30025710	SVIL
9	17054823	chr7	5566779	5603415	ACTB
34	17095587	chr9	91975702	92113045	SEMA4D
5	16900022	chr2	88326724	88355248	KRCC1
3	16901493	chr2	107138359	107154535	
27	16933630	chr22	29901868	29951205	THOC5
12	17012946	chr6	138188351	138204449	TNFAIP3
8	17031616	chr6_dbb_hap3	1937828	1949334	PPP1R18
8	17026687	chr6_apd_hap1	1955812	1967318	PPP1R18
19	16918569	chr20	33432523	33460663	GGT7
16	16732296	chr11	119076752	119178859	CBL
2	17052603	chr7	142028121	142028610	TRBV6-1

Table C.2. continued

# of markers	Transcript Cluster ID	seqname	start	stop	Gene Symbol
2	17061876	chr7	110364215	110365881	IMMP2L-IT
16	16731492	chr11	114310108	114321001	REXO2
2	17118287	chr7	45117402	45119839	LOC10012
23	16921134	chr20	61509090	61569304	DIDO1
8	16875612	chr19	55663135	55669100	TNNI3
13	16863667	chr19	48248793	48260323	GLTSCR2
25	16760760	chr12	7499281	7596781	CD163L1
32	16942103	chr3	57994127	58157982	FLNB
3	17045320	chr7	38381178	38418238	LOC10050
13	16804062	chr15	83776159	83806111	TM6SF1
15	16663033	chr1	40810522	40888998	SMAP2
2	17064264	chr7	150076943	150080973	
22	16931197	chr22	45704849	45737836	FAM118A
12	16929925	chr22	38203912	38213183	GCAT
31	17083855	chr9	19288622	19374275	DENND4C
40	16807342	chr15	40570377	40600174	PLCB2
16	17043418	chr7	6617065	6629005	ZDHHC4
11	17108407	chrX	153672473	153679002	FAM50A
21	16897637	chr2	55199325	55339757	RTN4
9	17028837	chr6_cox_hap2	2156239	2167745	PPP1R18

Table C.2. continued

# of markers	Transcript Cluster ID	seqname	start	stop	Gene Symbol
2	16916126	chr20	62492566	62494341	ABHD16B
2	17099720	chr9	138096568	138129443	
20	16881687	chr2	74648805	74652882	WDR54
9	17034070	chr6_mann_hap4	1992229	2003768	PPP1R18
9	17016946	chr6	30644133	30655672	PPP1R18
9	17036337	chr6_mcf_hap5	2026018	2037557	PPP1R18
13	17099799	chr9	138824815	138853226	UBAC1
25	16704516	chr10	47740330	47770876	ANXA8L2
11	16915676	chr20	60962105	60963576	RPS21
7	16918455	chr20	32290550	32308136	PXMP4
4	17004374	chr6	3849620	3851551	FAM50B
21	16897973	chr2	61167548	61245389	PUS10
2	17091207	chr9	138900082	138901544	NACC2
29	17064984	chr7	158523686	158622944	ESYT2
17	16751750	chr12	53689075	53693234	PFDN5
18	17055804	chr7	22980439	23053770	FAM126A
32	16965942	chr4	37892705	38140796	TBC1D1
21	16681408	chr1	9095166	9148537	SLC2A5
10	16827687	chr16	69775770	69788829	NOB1
19	16908338	chr2	219138915	219157309	TMBIM1

Table C.2. continued

# of markers	Transcript Cluster ID	seqname	start	stop	Gene Symbol
23	17003291	chr5	176910395	176924607	PDLIM7
19	16790592	chr14	23415437	23451467	HAUS4
13	16808066	chr15	43524793	43559055	TGM5
2	17056845	chr7	38393316	38394118	TARP
2	16847395	chr17	58498569	58499698	LOC10050
2	16740997	chr11	67202981	67205538	PTPRCAP
12	16920910	chr20	60711791	60718496	PSMA7
7	16929056	chr22	31365262	31375381	TUG1
20	17049939	chr7	102937869	102969958	PMPCB
13	16907604	chr2	207602487	207630271	MDH1B
19	16755465	chr12	97825431	97958813	RMST
7	17057413	chr7	45022627	45026259	SNHG15
18	17068642	chr8	42995556	43057998	HGSNAT
64	16730845	chr11	108093211	108239829	ATM
9	16916104	chr20	62371211	62375403	SLC2A4R
20	16881838	chr2	75059782	75120486	HK2
27	17003815	chr5	179289066	179334859	TBC1D9B
30	16741442	chr11	70313961	70963623	SHANK2
16	16966563	chr4	48343339	48428215	SLAIN2
18	16913143	chr20	34129770	34145405	ERGIC3

Table C.2. continued

# of markers	Transcript Cluster ID	seqname	start	stop	Gene Symbol
12	16877048	chr2	10443015	10567743	HPCAL1
14	17075426	chr8	22877646	22926700	TNFRSF1(
14	16827546	chr16	68021293	68034489	DPEP2
18	16964906	chr4	8437867	8495258	TRMT44
23	17044568	chr7	27778950	27880938	TAX1BP1
46	17014364	chr6	160390131	160534539	IGF2R
3	16926913	chr22	18257668	18262240	
14	16954669	chr3	52002526	52017425	ABHD14B
31	17021341	chr6	86215214	86303874	SNX14
6	16963375	chr3	196281056	196295545	WDR53
14	16836333	chr17	55055468	55084533	SCPEP1
8	17050736	chr7	117824086	117844093	NAA38
6	16707534	chr10	94821021	94828454	CYP26C1
2	16941049	chr3	50378537	50383128	
33	16880122	chr2	54683422	54898583	SPTBN1
2	16781116	chr13	112849403	112850190	
8	17042936	chr7	2281857	2290781	NUDT1
5	16918296	chr20	30780306	30795594	PLAGL2
13	16659054	chr1	11796141	11814859	AGTRAP
23	17063168	chr7	135046547	135194875	CNOT4

Table C.2. continued

# of markers	Transcript Cluster ID	seqname	start	stop	Gene Symbol
8	16770789	chr12	117153593	117175875	C12orf49
6	16895666	chr2	27359715	27362332	C2orf53
2	17026780	chr6_apd_hap1	3046838	3048116	SAPCD1
2	17032039	chr6_dbb_hap3	3017669	3018947	SAPCD1
2	17029254	chr6_cox_hap2	3241673	3242952	SAPCD1
2	17036757	chr6_mcf_hap5	3111784	3113062	SAPCD1
2	17017400	chr6	31732087	31733365	SAPCD1-A
14	17077525	chr8	61099906	61193971	CA8
14	16958649	chr3	126156444	126194762	ZXDC
22	17000532	chr5	138282409	138629246	SIL1
16	17066791	chr8	22844930	22877712	RHOBTB2
19	16899335	chr2	74753772	74757066	AUP1
18	16931361	chr22	46663858	46690279	TTC38
12	17053051	chr7	148823508	148880134	ZNF398
21	16839769	chr17	3566187	3599698	P2RX5-TA
15	17017126	chr6	31236526	31239913	HLA-C
15	17040719	chr6_ssto_hap7	2884703	2887488	LST1
8	16918064	chr20	25121425	25129894	LOC28479
28	16747623	chr12	7055631	7070479	PTPN6
18	16737645	chr11	45931214	45940363	PEX16

Table C.2. continued

# of markers	Transcript Cluster ID	seqname	start	stop	Gene Symbol
3	16928861	chr22	30163352	30166402	UQCR10
9	16974096	chr4	7060633	7069924	GRPEL1
19	17066302	chr8	20054704	20084330	ATP6V1B2
8	17043214	chr7	5085452	5112854	RBAK
16	16918496	chr20	32822646	32899608	AHCY
20	16914509	chr20	46130601	46285621	NCOA3
16	16715667	chr10	75572259	75634349	CAMK2G
18	16855491	chr18	55267891	55289177	NARS
8	16834179	chr17	39845127	39848920	EIF1
4	16782452	chr14	24505710	24520580	DHRS4L1
4	17093117	chr9	32540542	32552626	TOPORS
28	16943681	chr3	108308337	108413693	DZIP3
2	16951859	chr3	30553387	30567941	
18	16705474	chr10	70715884	70744829	DDX21
6	16769770	chr12	109015671	109027735	SELPLG
22	16892750	chr2	235860617	235964358	SH3BP4
6	16838094	chr17	74553846	74561430	LOC10050
20	16816833	chr16	22308730	22346424	POLR3E
5	17046845	chr7	72349936	72421979	POM121
5	16999011	chr5	114856608	114880591	FEM1C

Table C.2. continued

# of markers	Transcript Cluster ID	seqname	start	stop	Gene Symbol
25	16774690	chr13	48877883	49056122	RB1
14	17064810	chr7	155592680	155604967	SHH
38	16785952	chr14	71374122	71582099	PCNX
27	16943184	chr3	98451080	98540045	ST3GAL6
19	17048142	chr7	89964537	90020769	GTPBP10
16	16919673	chr20	44470360	44486048	ACOT8
42	16795826	chr14	91737667	91884188	CCDC88C
20	16956661	chr3	98216756	98241910	CLDND1
71	16810376	chr15	63900817	64126147	HERC1
20	17103160	chrX	47420516	47431320	ARAF
13	16880682	chr2	64751439	64820139	AFTPH
12	17092737	chr9	19375713	19380252	RPS6
19	17114520	chrX	135747706	135864247	ARHGEF6
20	17066601	chr8	22224762	22291642	SLC39A14
6	16910759	chr20	2187141	2238703	
2	16736679	chr11	20065392	20070849	NAV2-AS2
38	16707409	chr10	93683736	93790082	BTAF1
10	16918485	chr20	32676104	32700138	EIF2S2
14	17049557	chr7	100464760	100471076	TRIP6
57	17030467	chr6_dbb_hap3	2170073	2188361	VARS2

Table C.2. continued

B]

# of markers	Transcript Cluster ID	seqname	start	stop	Gene Sy
2	16822889	chr16	2012061	2012271	RPS2
12	16851121	chr18	12947983	12987535	SEH1L
7	16773583	chr13	29233141	29253094	POMP
9	16752223	chr12	56211703	56215663	ORMDL2
17	16820537	chr16	69166418	69202937	CIRH1A
18	16760329	chr12	6437923	6451283	TNFRSF1A
16	16898498	chr2	68350068	68384826	WDR92
15	17036038	chr6_mcf_hap5	4713557	4718061	RPS18
15	17031289	chr6_dbb_hap3	4521109	4525609	RPS18
15	17007426	chr6	33239787	33244287	RPS18
15	17038759	chr6_qbl_hap6	4472023	4476526	RPS18
15	17028475	chr6_cox_hap2	4683597	4688097	RPS18
14	16741643	chr11	71796941	71814433	LAMTOR1

Table C.2. continued

# of markers	Transcript Cluster ID	seqname	start	stop	Gene Symbol
9	16957095	chr3	107761941	107809935	CD47
18	16947235	chr3	155588325	155658457	GMPS
14	16814693	chr16	1401900	1413352	GNPTG
3	16882142	chr2	85132749	85133799	TMSB10
24	16785869	chr14	70193617	70238722	SRSF5
21	16764348	chr12	49950327	49961936	MCRS1
37	16735801	chr11	10818593	10830657	EIF4G2
4	17008534	chr6	41755181	41757879	TOMM6
23	16790493	chr14	23242431	23299029	SLC7A7
11	17048613	chr7	95107756	95169544	ASB4
18	17024394	chr6	144261437	144385735	PLAGL1
5	17106546	chrX	118370211	118378429	PGRMC1
37	16898110	chr2	61704984	61765761	XPO1
9	16858624	chr19	12273872	12300064	ZNF136
7	16847087	chr17	56422539	56429563	SUPT4H1
22	17079918	chr8	103838536	103906092	AZIN1
4	17098177	chr9	125677845	125693779	ZBTB26
9	16673945	chr1	173446405	173457946	PRDX6
5	16983268	chr5	12574969	12805295	TAG
19	16892321	chr2	233414762	233448354	EIF4E2

Table C.2. continued

# of markers	Transcript Cluster ID	seqname	start	stop	Gene Symbol
45	16897560	chr2	54091204	54197977	PSME4
25	16937252	chr3	9691117	9744078	MTMR14
14	16673822	chr1	171750761	171783163	METTL13
12	17040735	chr6_ssto_hap7	2913768	2915605	AIF1
12	17006683	chr6	31582961	31584798	AIF1
12	17027817	chr6_cox_hap2	3092579	3094416	AIF1
12	17038140	chr6_qbl_hap6	2876602	2878439	AIF1
24	16893449	chr2	242254515	242293442	
57	16908037	chr2	216225163	216300895	FN1
31	16751709	chr12	53662083	53687427	ESPL1
11	16956952	chr3	101399934	101405626	RPL24
10	16833708	chr17	37026112	37078023	LASP1
9	16822001	chr16	89627056	89633237	RPL13
6	16821882	chr16	88923494	88929094	TRAPPC2I
7	17019516	chr6	43638934	43655549	MRPS18A
11	17030643	chr6_dbb_hap3	2868536	2870373	AIF1
25	16983800	chr5	33440802	33469644	TARS
3	16670383	chr1	149822628	149823191	HIST2H2A
15	16923555	chr21	45705721	45718531	AIRE
12	16819640	chr16	58035277	58055527	C16orf57

Table C.2. continued

# of markers	Transcript Cluster ID	seqname	start	stop	Gene Symbol
13	16876670	chr2	3642422	3692234	COLEC11
22	16771430	chr12	121675133	121736111	CAMKK2
33	16990631	chr5	145826873	145891524	TCERG1
21	16892153	chr2	232646381	232674093	COPS7B
19	16956260	chr3	72798428	72911065	SHQ1
7	16822466	chr16	684429	686347	C16orf13
15	16838336	chr17	76183398	76203782	AFMID
33	16760465	chr12	6679248	6716642	CHD4
27	16901830	chr2	112523848	112642267	ANAPC1
26	16745525	chr11	122928197	122933938	HSPA8
6	17019070	chr6	41462591	41516359	LOC10050
6	16720085	chr11	313506	315272	IFITM1
4	16838330	chr17	76164671	76169009	SYNGR2
16	17025070	chr6	155574273	155635627	TFB1M
15	16859583	chr19	17666460	17693965	GLT25D1
22	16709512	chr10	116581503	116659591	FAM160B1
23	16907458	chr2	203745323	203879521	WDR12
2	16657680	chr1	1167629	1170421	B3GALT6
2	16692982	chr1	151120885	151123810	
36	16955887	chr3	65339906	66024509	MAGI1

Table C.2. continued

# of markers	Transcript Cluster ID	seqname	start	stop	Gene Symbol
24	16692892	chr1	150933059	150947479	CERS2
8	16838917	chr17	79849599	79858363	ANAPC11
6	17094028	chr9	37582643	37592639	TOMM5
4	17005564	chr6	26124373	26139336	HIST1H2A
17	16866456	chr19	617223	633568	POLRMT
14	16863974	chr19	49588465	49611870	SNRNP70
6	16869653	chr19	14625582	14640049	DNAJB1
22	16722412	chr11	17229700	17371521	NUCB2
11	16687467	chr1	54387234	54411975	HSPB11
5	16857047	chr19	3762665	3767563	MRPL54
23	16716846	chr10	97365686	97416567	ALDH18A1
10	16840902	chr17	8108049	8113936	AURKB
17	16661589	chr1	28832455	28865708	RCC1
14	16901957	chr2	113493930	113522254	CKAP2L
14	16862408	chr19	41620337	41634281	CYP2F1
11	16876797	chr2	7561392	7590385	LOC10050
11	16777856	chr13	31032877	31191734	HMGB1
11	17038297	chr6_qbl_hap6	3076888	3079370	HSPA1B
18	16996722	chr5	64813593	64858998	CENPK
12	16888786	chr2	190744335	191068210	C2orf88

Table C.2. continued

# of markers	Transcript Cluster ID	seqname	start	stop	Gene Symbol
32	17088320	chr9	116917840	117074791	COL27A1
53	16732584	chr11	121322912	121504471	SORL1
9	16666437	chr1	78444859	78483648	DNAJB4
12	17030820	chr6_dbb_hap3	3068828	3071310	HSPA1B
12	17026318	chr6_apd_hap1	3098002	3100484	HSPA1B
12	17027994	chr6_cox_hap2	3292821	3295303	HSPA1B
10	16864675	chr19	51728320	51743274	CD33
5	16837298	chr17	66244145	66253305	AMZ2
6	17004872	chr6	11934223	11961218	
20	16987046	chr5	87564699	87732860	TMEM161I
15	16751993	chr12	54673977	54680872	HNRNPA1
11	16981588	chr4	175157809	175205415	FBXO8
23	16992096	chr5	169010638	169031782	CCDC99
11	16792369	chr14	45584339	45604522	FKBP3
2	16926066	chr21	44019390	44035168	
18	16838509	chr17	78075355	78093679	GAA
20	16751438	chr12	52416616	52453291	NR4A1
4	16917867	chr20	23105705	23113273	LOC20026
18	16681103	chr1	6324332	6454451	ACOT7
2	17001458	chr5	148727679	148737205	

Table C.2. continued

# of markers	Transcript Cluster ID	seqname	start	stop	Gene Symbol
2	16763011	chr12	32257051	32260462	
30	16779546	chr13	60239717	60738119	DIAPH3
3	17005569	chr6	26156559	26157343	HIST1H1E
11	16775421	chr13	76123619	76180085	UCHL3
3	16960434	chr3	149563574	149569444	ANKUB1
27	16793190	chr14	55405656	55493823	WDHD1
16	17012350	chr6	126307576	126360937	TRMT11
22	16798624	chr15	29129629	29410518	APBA2
29	16960647	chr3	153990335	154042286	DHX36
3	17071485	chr8	102299673	102306011	
9	16673466	chr1	168148171	168171352	TIPRL
17	16764068	chr12	49297286	49351334	ARF3
5	17102532	chrX	37545012	37591383	XK
2	17045589	chr7	44059560	44065967	
2	16664482	chr1	48671637	48672515	
27	16891922	chr2	231280657	231410317	SP100
11	16998892	chr5	112212081	112258236	REEP5
9	16891820	chr2	230787018	230877825	FBXO36
13	16978184	chr4	100044808	100078949	ADH4
10	16722143	chr11	12297627	12380691	MICALCL

Table C.2. continued

# of markers	Transcript Cluster ID	seqname	start	stop	Gene Symbol
32	16951601	chr3	25639475	25706398	TOP2B
2	16698460	chr1	205202949	205205995	
3	16990294	chr5	140571942	140575215	PCDHB9
9	16705074	chr10	60144782	60158981	TFAM
12	16955565	chr3	58549844	58613401	FAM107A
21	17055140	chr7	7395834	7575484	COL28A1
22	16716870	chr10	97423153	97454712	TCTN3
12	16668772	chr1	112938800	113006078	CTTNBP2I
6	16830182	chr17	6544078	6547920	TXNDC17
8	16704125	chr10	43277954	43330385	BMS1
2	16902276	chr2	121895708	121896762	
28	17080749	chr8	124332090	124428590	ATAD2
7	17087498	chr9	101984346	101992901	SEC61B
6	16718747	chr10	118888032	118897812	VAX1
18	16765744	chr12	56119107	56123491	CD63
6	17085093	chr9	38620471	38624987	FAM201A
27	16720268	chr11	694438	727727	EPS8L2
18	16677789	chr1	222885895	222908538	BROX
14	16809123	chr15	50792759	50838905	USP50
4	17005573	chr6	26158349	26171577	HIST1H2B

Table C.2. continued

# of markers	Transcript Cluster ID	seqname	start	stop	Gene Symbol
8	16787869	chr14	95027428	95036250	SERPINA4
11	16850464	chr18	596998	650334	CLUL1
29	16752061	chr12	54891495	54937726	NCKAP1L
10	16971573	chr4	154265801	154336270	MND1
11	16700385	chr1	230838269	230931238	AGT
6	16700147	chr1	228106357	228135676	WNT9A
2	16701579	chr1	247835320	247836365	OR13G1
15	16961806	chr3	179113876	179169378	GNB4
14	16791044	chr14	24608174	24610797	EMC9
8	16867583	chr19	5891287	5904025	NDUFA11
27	16879441	chr2	42721709	42984087	MTA3
15	16957106	chr3	107879659	107941417	IFT57
23	16750761	chr12	49716971	49725514	TROAP
10	17005904	chr6	28109716	28125236	ZNF192
19	17090296	chr9	133320094	133376661	ASS1
2	16702605	chr10	13570516	13572262	
8	16994588	chr5	16451628	16465901	ZNF622
2	16695727	chr1	161607438	161608218	
9	16797694	chr15	22278010	22413497	OR4M1
7	16837029	chr17	61904770	61909387	PSMC5

Table C.2. continued

# of markers	Transcript Cluster ID	seqname	start	stop	Gene Symbol
6	16917939	chr20	23608534	23619110	CST3
2	16803613	chr15	79271231	79278268	
7	16870828	chr19	21987752	22034830	ZNF43
19	16690036	chr1	100174259	100232187	FRRS1
6	16873647	chr19	47341423	47354203	AP2S1
5	16867057	chr19	3474405	3480540	C19orf77
6	16676873	chr1	207818458	207911761	CR1L
20	16993752	chr5	7104700	851101	ZDHHC11
4	16985089	chr5	60457897	60527867	
15	16847034	chr17	56347217	56358296	MPO
4	16851810	chr18	29671818	29711524	RNF138
22	16952383	chr3	39138091	39149854	GORASP1
13	17084549	chr9	34957484	34984679	KIAA1045
12	17013554	chr6	149068271	149398308	UST
7	16810564	chr15	64979773	64995462	OAZ2
3	17074301	chr8	6782215	6783598	DEFA6
36	16995409	chr5	37288239	37371283	NUP155
17	16740828	chr11	66330934	66336312	CTSF
24	16896442	chr2	37326353	37384208	EIF2AK2
30	16665717	chr1	65886131	66107242	LEPR

Table C.2. continued

# of markers	Transcript Cluster ID	seqname	start	stop	Gene Symbol
3	17099454	chr9	136080664	136084630	OBP2B
11	16744125	chr11	108342832	108369159	KDELC2
8	17039914	chr6_qbl_hap6	3784600	3815217	HLA-DRB1
8	17029712	chr6_cox_hap2	3998151	4028758	HLA-DRB1
9	16941648	chr3	52568029	52613253	C3orf78
22	16987531	chr5	96211643	96255420	ERAP2
2	16885232	chr2	123643945	123644599	
12	16881441	chr2	73143176	73162020	EMX1
3	16877555	chr2	20646835	20649206	RHOB
16	17001927	chr5	151040657	151066726	SPARC
19	16970536	chr4	128702976	128755226	HSPA4L
2	16860664	chr19	34286903	34287633	
5	16937930	chr3	14219858	14242619	LSM3
2	17004536	chr6	6725119	6730139	
14	16760621	chr12	6953963	6961230	CDCA3
10	16890675	chr2	217497551	217529159	IGFBP2
9	16823636	chr16	4846969	4852951	ROGDI
22	16987798	chr5	108083523	108532542	FER
9	16904780	chr2	169690642	169769881	SPC25
2	16959311	chr3	132733848	132755896	

Table C.2. continued

# of markers	Transcript Cluster ID	seqname	start	stop	Gene Symbol
2	17016457	chr6	27106072	27114637	HIST1H2B
2	16850316	chr17	81168296	81174267	
7	16995705	chr5	40825364	40835437	RPL37
15	16730313	chr11	94883703	94967568	
16	17069087	chr8	57124245	57131357	CHCHD7
10	17111883	chrX	70323739	70326638	CXorf65
16	17066278	chr8	19759228	19824770	LPL
5	16834091	chr17	38599676	38613983	IGFBP4
18	16801305	chr15	56536207	56738195	TEX9
2	17014619	chr6	166650457	166657197	
30	16984492	chr5	43602791	43707507	NNT
2	17002529	chr5	163546104	163661103	
13	16958974	chr3	129120164	129147494	C3orf25
8	16691155	chr1	114466622	114472114	
8	16930954	chr22	43547520	43559248	TSPO
18	17087836	chr9	108320411	108403399	FKTN
8	16727351	chr11	66036004	66044963	RAB1B
9	16689869	chr1	94994732	95007413	F3
10	17077171	chr8	54138276	54164257	OPRK1
45	16978568	chr4	104026963	104119566	CENPE

Table C.2. continued

# of markers	Transcript Cluster ID	seqname	start	stop	Gene Symbol
6	16842403	chr17	20352708	20372296	LGALS9B
9	17063981	chr7	143548450	143599291	FAM115A
23	16847050	chr17	56378592	56406152	BZRAP1
4	16866031	chr19	57922529	57933307	ZNF17
4	16864925	chr19	53837002	53858122	ZNF845
3	16679816	chr1	248684916	248685964	OR2G6
7	16921258	chr20	62119366	62130505	EEF1A2
5	16871031	chr19	28477699	28491271	
2	17019916	chr6	49936390	49937338	DEFB113
16	17064299	chr7	150642044	150675403	KCNH2
5	16831306	chr17	14204400	14252721	HS3ST3B1
2	16951406	chr3	18243623	18264275	LOC10050
10	16784498	chr14	56584532	56768244	PELI2
6	17104186	chrX	56755677	56844813	LOC55064
6	16933885	chr22	30884889	30901698	SEC14L4
19	16904365	chr2	163123589	163175213	IFIH1
3	17092394	chr9	11143876	11194381	
9	17075553	chr8	23699428	23712320	STC1
7	17080853	chr8	125323159	125384940	TMEM65
29	16971995	chr4	160025330	160281321	RAPGEF2

Table C.2. continued

# of markers	Transcript Cluster ID	seqname	start	stop	Gene Symbol
3	16936643	chr22	50989541	51001334	SYCE3
3	17048068	chr7	89748714	89754914	DPY19L2P
11	16756431	chr12	107349497	107372556	C12orf23
4	16789785	chr14	106355942	106362435	
20	16879094	chr2	36923833	37041937	VIT
28	16812274	chr15	79252289	79383215	RASGRF1
2	16678486	chr1	228454507	228455299	
7	16864393	chr19	50431959	50437515	ATF5
8	16826586	chr16	54317212	54320675	IRX3
21	16881031	chr2	69240276	69476459	ANTXR1
3	17065842	chr8	11946847	11973025	ZNF705D
6	16712035	chr10	15117474	15130775	ACBD7
15	17088300	chr9	116638562	116818875	ZNF618
32	16950470	chr3	9022275	9404987	SRGAP3
11	16998097	chr5	92745065	92921354	FLJ42709
11	16830202	chr17	6659156	6678966	XAF1
21	16825561	chr16	29882379	29910585	SEZ6L2
10	16802903	chr15	74218789	74244478	LOXL1
4	17074305	chr8	6793344	6795860	DEFA4
31	16802795	chr15	73344051	73597547	NEO1

Table C.2. continued

# of markers	Transcript Cluster ID	seqname	start	stop	Gene Symbol
28	16763783	chr12	48366748	48398285	COL2A1
6	16935188	chr22	39214456	39240017	NPTXR
6	17039907	chr6_qbl_hap6	3720954	3734041	HLA-DRB3
19	16796829	chr14	102547075	102606086	HSP90AA1
21	16989636	chr5	137514408	137523404	KIF20A
29	17055295	chr7	12370509	12443852	VWDE
11	17094088	chr9	38540566	38620657	ANKRD18A
4	16864751	chr19	52264183	52273779	FPR2
2	16723447	chr11	33730981	33731568	
13	16985950	chr5	71403061	71505851	MAP1B
3	16955044	chr3	53112200	53120488	
8	16669169	chr1	117297007	117311851	CD2
5	16707567	chr10	95326422	95349829	O3FAR1
3	16890404	chr2	213660045	213683988	
14	16743432	chr11	94898704	94965705	SESN3
4	16704475	chr10	47379720	47421238	FAM35B2
44	16980160	chr4	142944313	143768585	INPP4B
6	16926754	chr21	48018531	48025121	S100B
14	16766923	chr12	63037762	63328817	PPM1H
2	16923802	chr21	47013568	47017005	

Table C.2. continued

# of markers	Transcript Cluster ID	seqname	start	stop	Gene Symbol
13	16872648	chr19	42470734	42498384	ATP1A3
8	16875599	chr19	55644161	55660606	TNNT1
16	16795192	chr14	77972340	78083116	SPTLC2
2	16963669	chr4	206389	249774	ZNF876P
2	17117467	chr10	99609995	99631337	GOLGA7B
4	17074296	chr8	6728097	6735544	DEFB1
10	17111769	chrX	68380581	68385365	PJA1
5	17004843	chr6	11173685	11259332	
11	16728261	chr11	69455855	69469242	CCND1
9	16736726	chr11	22835345	22851845	SVIP
26	16809687	chr15	56119120	56285835	NEDD4
32	17010461	chr6	76458909	76629254	MYO6
37	16689490	chr1	91726323	91870426	HFM1
8	17112426	chrX	80369200	80457441	HMGN5
4	16890058	chr2	208104374	208110611	
11	16921627	chr21	17442842	17982094	LINC00478
9	17071208	chr8	98787285	98865241	LAPTM4B
7	17108914	chrX	6451659	6453159	VCX3A
18	16950216	chr3	3108008	3168297	IL5RA
12	16946744	chr3	148583043	148614983	CPA3

Table C.2. continued

# of markers	Transcript Cluster ID	seqname	start	stop	Gene Symbol
3	17038059	chr6_qbl_hap6	26610 07	2677562	MICA
21	16907912	chr2	21386 4408	214017151	IKZF2
20	16757324	chr12	11334 4582	113369991	OAS1
9	16745016	chr11	11820 9669	118213459	CD3D
6	16825638	chr16	30103 635	30107537	YPEL3
3	16678824	chr1	23294 0638	232946092	KIAA1383
12	16783215	chr14	32543 521	32628934	ARHGAP5
2	16888216	chr2	17964 1653	179644690	
5	16707196	chr10	91152 303	91163745	IFIT1
2	16801700	chr15	62548 375	62552162	LOC10012
12	16723748	chr11	36616 051	36694823	C11orf74
27	17112060	chrX	71798 664	71934167	PHKA1
3	17068932	chr8	54090 131	54155243	
25	16843241	chr17	30819 628	31203902	MYO1D
33	16763138	chr12	39687 030	39837192	KIF21A
13	16836416	chr17	56270 089	56282535	EPX
11	16809748	chr15	56720 929	56757335	MNS1
18	16944695	chr3	12239 9465	122449775	PARP14
52	16688024	chr1	62920 397	63153969	DOCK7
3	16691755	chr1	12148 4057	121485434	

Table C.2. continued

# of markers	Transcript Cluster ID	seqname	start	stop	Gene Symbol
2	16817821	chr16	30107751	30116841	
7	16791427	chr14	25042724	25045466	CTSG
3	17069173	chr8	58890917	58896685	T1560
11	17112364	chrX	78615881	78623164	ITM2A
11	17070456	chr8	86376081	86393721	CA2

BIOGRAPHY OF AUTHOR

Melanie Ufkin was born in Riverside, CA where she was raised until age 9 until relocating to Portland, ME and lastly New Gloucester, ME. She graduated from Gray-New Gloucester High School in 2002. Following high school, Melanie attended and graduated from Lawrence University in 2006 with a Bachelor of Arts Degree in Biochemistry and an Interdisciplinary Degree in Neuroscience. Upon graduation, Melanie worked as a laboratory technician in the biophysics department at the Medical College of Wisconsin. In 2007, Melanie joined the Graduate School of Biomedical Science at the Medical College of Wisconsin where she attended until transferring to the University of Maine's Graduate School of Biomedical Science and Engineering Program in 2009. Upon joining the University of Maine's graduate program, she joined Dr. Pradeep Sathyanarayana where she has been characterizing microRNA miR-125a's role in the pathogenesis of acute myeloid leukemia. Melanie has one co-author manuscript published from collaboration. Currently, she has a manuscript under review and is working on two additional manuscripts for submission. Melanie is a candidate for the Doctor of Philosophy degree in Biomedical Sciences from the University of Maine in December 2013.